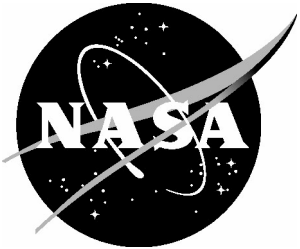


NASA/TM-2005-213541



Aerodynamics of an Axisymmetric Missile Concept Having Cruciform Strakes and In-Line Tail Fins From Mach 0.60 to 4.63

Jerry M. Allen
Langley Research Center, Hampton, Virginia

The NASA STI Program Office . . . in Profile

Since its founding, NASA has been dedicated to the advancement of aeronautics and space science. The NASA Scientific and Technical Information (STI) Program Office plays a key part in helping NASA maintain this important role.

The NASA STI Program Office is operated by Langley Research Center, the lead center for NASA's scientific and technical information. The NASA STI Program Office provides access to the NASA STI Database, the largest collection of aeronautical and space science STI in the world. The Program Office is also NASA's institutional mechanism for disseminating the results of its research and development activities. These results are published by NASA in the NASA STI Report Series, which includes the following report types:

- **TECHNICAL PUBLICATION.** Reports of completed research or a major significant phase of research that present the results of NASA programs and include extensive data or theoretical analysis. Includes compilations of significant scientific and technical data and information deemed to be of continuing reference value. NASA counterpart of peer-reviewed formal professional papers, but having less stringent limitations on manuscript length and extent of graphic presentations.
- **TECHNICAL MEMORANDUM.** Scientific and technical findings that are preliminary or of specialized interest, e.g., quick release reports, working papers, and bibliographies that contain minimal annotation. Does not contain extensive analysis.
- **CONTRACTOR REPORT.** Scientific and technical findings by NASA-sponsored contractors and grantees.

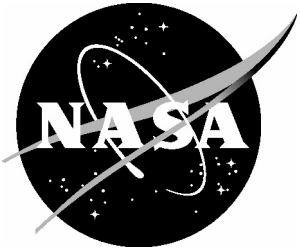
- **CONFERENCE PUBLICATION.** Collected papers from scientific and technical conferences, symposia, seminars, or other meetings sponsored or co-sponsored by NASA.
- **SPECIAL PUBLICATION.** Scientific, technical, or historical information from NASA programs, projects, and missions, often concerned with subjects having substantial public interest.
- **TECHNICAL TRANSLATION.** English-language translations of foreign scientific and technical material pertinent to NASA's mission.

Specialized services that complement the STI Program Office's diverse offerings include creating custom thesauri, building customized databases, organizing and publishing research results ... even providing videos.

For more information about the NASA STI Program Office, see the following:

- Access the NASA STI Program Home Page at <http://www.sti.nasa.gov>
- E-mail your question via the Internet to help@sti.nasa.gov
- Fax your question to the NASA STI Help Desk at (301) 621-0134
- Phone the NASA STI Help Desk at (301) 621-0390
- Write to:
NASA STI Help Desk
NASA Center for AeroSpace Information
7121 Standard Drive
Hanover, MD 21076-1320

NASA/TM-2005-213541



Aerodynamics of an Axisymmetric Missile Concept Having Cruciform Strakes and In-Line Tail Fins From Mach 0.60 to 4.63

Jerry M. Allen
Langley Research Center, Hampton, Virginia

National Aeronautics and
Space Administration

Langley Research Center
Hampton, Virginia 23681-2199

March 2005

Available from:

NASA Center for AeroSpace Information (CASI)
7121 Standard Drive
Hanover, MD 21076-1320
(301) 621-0390

National Technical Information Service (NTIS)
5285 Port Royal Road
Springfield, VA 22161-2171
(703) 605-6000

Introduction

Reliable control laws on missile configurations depend on accurate modeling of control fin loads over the missile's operating envelope. This modeling requires a large amount of basic control fin information, and therefore often comes from experimental data. Most data sets designed to provide this basic control fin information are obtained from body-tail configurations (refs. 1 through 4), or in some cases fin-alone studies (ref. 5). Such data do not contain control fin data in the presence of upstream strakes or fins; thus, they do not account for fin-on-fin interference effects.

The current project was undertaken to produce a set of data that would contain these interference effects for one class of missile: a cruciform tail-control missile with upstream in-line strakes. Although the test model is a generic configuration, it was intended to represent a class of missiles similar to the Nation's Standard Missile (ref. 6).

Because a large volume of data was needed for this task, the existing core model of reference 7 was used where control fin deflection angles could be set remotely while the tunnel was in operation. In addition, this model had the capability of remotely setting the configuration roll angle, thereby allowing the data to be obtained in a reasonable time frame. The aerodynamic surface in this project was actually a shell wrapped around this remote-control model in the same manner that was done in the project reported in references 1 through 4. The data obtained in the current project include both six-component force-and-moment measurements on the entire configuration as well as three-component measurements on all four cruciform tail fins.

The current project was conducted as a cooperative effort between NASA Langley Research Center (LaRC) and several branches of the U.S. Department of Defense (DoD). The DoD provided funding for the aerodynamic model and data acquisition system used in this study and participated in the wind tunnel tests. LaRC fabricated the model and balances, provided the remote-control test equipment and test facilities, and conducted the tests.

The experiments were conducted during three separate tests in the NASA LaRC 8-Foot Transonic Pressure Tunnel (8-Ft TPT), Test 1041, and in both test sections of the LaRC Unitary Plan Wind Tunnel (UPWT), Tests 1670 and 1529. The data cover Mach numbers from 0.6 to 4.63, configuration angles of attack from -2° to 22° , configuration roll angles from -90° to 0° , and fin deflection angles from -30° to 30° . The test unit Reynolds numbers were held constant at about 1.5×10^6 per foot. Geometry variables in this study include configuration buildup, strake length, nose size, and tail fin deflection angles that produced pitch, yaw, or roll control on the configuration.

The primary purpose of this project was to investigate the effects of upstream interference effects on tail fin loads, not to study the control characteristics of a specific missile configuration. A total of 1059 runs are included in this database. Because of the large volume of data involved, it was not practical to include in this paper tabulations or even plots of all the data from this project. Instead, a CD-ROM containing the entire data set in digital electronic form is attached. The data on the CD-ROM are presented in two formats. Plots of much of the data are also included on the CD-ROM to illustrate the effects of the test variables on both the six-component configuration data and the three-component data on all four tail fins. Selected examples from these plotted data have been included to illustrate some of the features and trends found in the data.

Nomenclature

The measurements and calculations in this paper were made in U.S. customary units. The six-component main balance coefficients are presented in the body axis system. The parenthetical expressions among the nomenclature are computer-generated equivalents of symbols that were used to create the electronic data files. The positive directions of all forces, moments, and angles in this report are defined in figure 1.

AF	configuration axial force, lb
A_{ref}	maximum body cross-section area, 0.0541 ft ²
BM_1	tail root-chord bending moment at fin location 1, in-lb
BM_2	tail root-chord bending moment at fin location 2, in-lb
BM_3	tail root-chord bending moment at fin location 3, in-lb
BM_4	tail root-chord bending moment at fin location 4, in-lb
B_{ref}	exposed span of single tail fin, 1.953 in.
C_{AF} (CAFBA)	configuration axial-force coefficient, $AF/(qA_{\text{ref}})$
C_{BM1} (CBM1)	tail bending-moment coefficient at fin location 1, $BM_1/(qB_{\text{ref}}S_{\text{ref}})$
C_{BM2} (CBM2)	tail bending-moment coefficient at fin location 2, $BM_2/(qB_{\text{ref}}S_{\text{ref}})$
C_{BM3} (CBM3)	tail bending-moment coefficient at fin location 3, $BM_3/(qB_{\text{ref}}S_{\text{ref}})$
C_{BM4} (CBM4)	tail bending-moment coefficient at fin location 4, $BM_4/(qB_{\text{ref}}S_{\text{ref}})$
C_{HM1} (CHM1)	tail hinge-moment coefficient at fin location 1, $HM_1/(qC_{\text{ref}}S_{\text{ref}})$
C_{HM2} (CHM2)	tail hinge-moment coefficient at fin location 2, $HM_2/(qC_{\text{ref}}S_{\text{ref}})$
C_{HM3} (CHM3)	tail hinge-moment coefficient at fin location 3, $HM_3/(qC_{\text{ref}}S_{\text{ref}})$
C_{HM4} (CHM4)	tail hinge-moment coefficient at fin location 4, $HM_4/(qC_{\text{ref}}S_{\text{ref}})$
C_{NF} (CNFBA)	configuration normal-force coefficient, $NF/(qA_{\text{ref}})$
C_{NF1} (CNF1)	tail normal-force coefficient at fin location 1, $NF_1/(qS_{\text{ref}})$
C_{NF2} (CNF2)	tail normal-force coefficient at fin location 2, $NF_2/(qS_{\text{ref}})$
C_{NF3} (CNF3)	tail normal-force coefficient at fin location 3, $NF_3/(qS_{\text{ref}})$
C_{NF4} (CNF4)	tail normal-force coefficient at fin location 4, $NF_4/(qS_{\text{ref}})$
C_{PM} (CPMBA)	configuration pitching-moment coefficient, $PM/(qA_{\text{ref}}D)$

C_{ref}		tail fin root chord length, 1.992 in.
C_{RM}	(CRMBA)	configuration rolling-moment coefficient, $RM/(qA_{\text{ref}}D)$
C_{SF}	(CSFBA)	configuration side-force coefficient, $SF/(qA_{\text{ref}}D)$
C_{YM}	(CYMBA)	configuration yawing-moment coefficient, $YM/(qA_{\text{ref}}D)$
Config		configuration
D		body maximum diameter, 3.15 in.
HM_1		tail hinge moment at fin location 1, in-lb
HM_2		tail hinge moment at fin location 2, in-lb
HM_3		tail hinge moment at fin location 3, in-lb
HM_4		tail hinge moment at fin location 4, in-lb
L		body length, 42.528 in.
LN		large nose
LS		long strakes
M	(MACH)	free-stream Mach number
MS		longitudinal station measured from model nose, in.
NF		configuration normal force, lb
NF_1		tail normal force at fin location 1, lb (always normal to fin planform surface)
NF_2		tail normal force at fin location 2, lb (always normal to fin planform surface)
NF_3		tail normal force at fin location 3, lb (always normal to fin planform surface)
NF_4		tail normal force at fin location 4, lb (always normal to fin planform surface)
PM		configuration pitching moment, in-lb
q	(Q)	free-stream dynamic pressure, psf
R/ft	(RNFT)	free-stream unit Reynolds number $\times 10^{-6}$, ft^{-1}
RM		configuration rolling moment, in-lb
SF		configuration side force, lb
SN		small nose

SS		short strakes
S_{ref}		tail fin planform area, 0.0217 ft^2
T		tail
YM		configuration yawing moment, in-lb
α	(ALPHA)	model angle of attack, deg
δ_1	(DEL1)	tail deflection angle at fin location 1, deg
δ_2	(DEL2)	tail deflection angle at fin location 2, deg
δ_3	(DEL3)	tail deflection angle at fin location 3, deg
δ_4	(DEL4)	tail deflection angle at fin location 4, deg
δ_P		pitch control deflection angle (see definitions to follow)
δ_R		roll control deflection angle (see definitions to follow)
δ_Y		yaw control deflection angle (see definitions to follow)
ϕ	(PHI)	model roll angle, deg
	(CONFIG)	configuration number (see definitions to follow)
	(FINSET)	code identifying tail fin deflection angle settings (see definitions to follow)
	(HO)	tunnel stagnation pressure, psf
	(PINF)	free-stream static pressure, psf
	(POINT)	point number
	(RUN)	run number
	(TEST)	test number
	(TT0)	tunnel stagnation temperature, °F

Definitions

Tail fin control deflection

ϕ , deg	δ_P , deg	δ_Y , deg	δ_R , deg
0	$(\delta_2 - \delta_4)/2$	$(\delta_3 - \delta_1)/2$	$(\delta_1 + \delta_2 + \delta_3 + \delta_4)/4$
-45	$(\delta_2 + \delta_3 - \delta_1 - \delta_4)/4$	$(\delta_1 + \delta_2 - \delta_3 - \delta_4)/4$	$(\delta_1 + \delta_2 + \delta_3 + \delta_4)/4$
-90	$(\delta_3 - \delta_1)/2$	$(\delta_4 - \delta_2)/2$	$(\delta_1 + \delta_2 + \delta_3 + \delta_4)/4$

Configuration code

Configuration	Nose	Strakes	Tails	Code
1	Small	Long	On	SN-LS-T
2	Small	Short	On	SN-SS-T
3	Small	Off	On	SN-no S-T
4	Small	Long	Off	SN-LS-no T
5	Small	Short	Off	SN-SS-no T
6	Small	Off	Off	SN-no S-no T
7	Large	Short	On	LN-SS-T

Fin set code

Fin set	δ_1	δ_2	δ_3	δ_4	No. runs	Control setting
0	999.9	999.9	999.9	999.9	65	Tails off
1	0	0	0	0	261	Baseline
2	0	10	0	-10	73	Pitch
3	0	20	0	-20	74	
4	0	30	0	-30	24	
5	0	-10	0	10	72	
6	0	-20	0	20	71	
7	0	-30	0	30	24	
8	5	5	5	5	45	Roll
9	10	10	10	10	32	
10	20	20	20	20	5	
11	0	10	0	10	1	
12	0	20	0	20	4	
13	0	-30	0	-30	2	
14	0	20	20	0	19	
15	10	20	10	0	22	
16	10	0	10	20	10	
17	10	-10	-10	10	17	Pitch-yaw
18	20	-20	-20	20	6	
19	30	-30	-30	30	6	
20	-10	10	10	-10	34	
21	-20	20	20	-20	22	
22	-30	30	30	-30	14	
23	-10	20	10	-20	16	
24	5	15	5	-5	13	Combination
25	5	25	5	-15	16	
26	10	30	10	-10	45	
27	5	-5	5	15	14	
28	5	-15	5	25	14	
29	10	-10	10	30	14	
30	-10	30	30	-10	16	
31	0	30	20	-10	8	

Run total 1059

Wind Tunnels

The experiments reported in this paper cover Mach numbers ranging from 0.60 to 4.63 and were performed in facilities located at NASA Langley Research Center (LaRC). Data Mach numbers from 0.60 to 1.18 were obtained in the LaRC 8-Ft Transonic Pressure Tunnel (TPT) while Mach data from 1.70 to 4.63 were obtained in the LaRC Unitary Plan Wind Tunnel (UPWT).

The 8-Ft TPT is a continuous-flow, variable-pressure, transonic wind tunnel capable of operating over a Mach number range from about 0.2 to 1.3. The tunnel can obtain unit Reynolds numbers from about 0.5 to 6 million per foot. A complete description of this facility can be found in Reference 8. This tunnel has been subsequently closed.

The UPWT is a continuous-flow, variable-pressure, supersonic wind tunnel with two test sections. The nozzles leading to the test sections contain asymmetric sliding blocks that permit continuous variation of Mach number from about 1.5 to 2.9 in the low-speed test section and from about 2.3 to 4.6 in the high-speed section. The tunnel can obtain unit Reynolds numbers from about 1 to 9 million per foot. A complete description of this facility can be found in reference 9.

Test Description

Key test features in this project including using the TPT at Mach 0.6 to 1.18 (test 1041) and the UPWT low-speed test section at Mach 1.70 to 2.10 (test 1670), the UPWT low-speed or high-speed test sections at Mach 2.36 and 2.86 (tests 1670 or 1529), and the UPWT high-speed test section at Mach 3.95 and 4.63 (test 1529). Reynolds number for all tests was 1.5×10^6 per ft. Configuration angle of attack ranged from -2° to 22° , and configuration roll angles were 0° to -90° . Tail fin deflection angle ranged from -30° to 30° . The data acquisition method consisted of angle-of-attack sweeps at a constant model roll angle for a total of 1059 runs.

The balances used in this project to measure tail fin loads were the same as those used in references 1 through 4. Three-component fin loads were measured at all four tail fin locations along with six-component overall configuration loads. These fin balances were located near the base of the fins and measured three components: normal force, hinge moment, and bending moment. The direction of the normal force was always perpendicular to the fin planform regardless of the deflection angle and was not rotated to conform to the body axis system (see fig. 1). Hinge moments were measured about the fin hinge line with no transfer distance being applied. The measured bending moments were transferred during data reduction from the center of the fin balance gauges to the fin root chord.

Each fin balance was located just below the body surface directly underneath the fin to which it was attached. Because of the data transfer previously described, the magnitudes of the fin bending moments contained in this paper are always somewhat smaller than the actual measured bending moments. This reduction results from the fact that the fin spanwise centers of pressure are closer to the fin root chord than they are to the center of the gauges. The bending-moment transfer distance was 0.455 in.

The positive directions of the forces, moments, and angles in this project are illustrated in figure 1(a). It should be emphasized that the tail fin numbering system shown in this figure rotates with roll angle. For example, at $\phi = 0^\circ$, fin 1 is located at the top vertical location, but for $\phi = 90^\circ$, fin 1 would be at the right horizontal location. The positive directions for the deflection angles and tail fin aerodynamic coefficients were chosen so that the parameters would be consistent with each other at all roll angles.

These fin deflection angle definitions, however, lead to some unusual results for specific control settings. For example, at $\phi = 0^\circ$, a deflection setting to give nose-up (positive) pitching moment on the configuration requires leading edge-down deflections on the two horizontal tail fins. Following the angle definitions of figure 1(b), this is achieved by a positive deflection on the right fin and a negative deflection on the left fin, which at low angles of attack yields negative normal force on the right fin and positive normal force on the left fin.

The six-component main balance was located inside the body and measured overall loads on the configuration at the same time that the fin loads were being measured. The configuration data moment center was located on the body centerline 23.387 in. aft of the model nose, or at about 55 percent of the body length. The internal balance moment center was located 29.577 in. aft of the nose. The measured moments were therefore transferred 6.19 in. upstream so that the moment reference center would be closer to the model center of pressure. The internal balance was mounted on a sting that was attached to the permanent tunnel-support mechanism downstream from the model. The model angle of attack was corrected for deflection of the balance and sting due to aerodynamic loads and for test section flow misalignment.

Pressures inside the body base cavity were measured by tubes located near the balance chamber. The body internal diameter was beveled to the outer diameter at the base of the model to allow internal pressures to act over the entire base area and therefore eliminate the need for base pressure measurements. Configuration axial-force data were corrected for the difference between the internal chamber pressure and free-stream static pressure (i.e., axial-force coefficients due to cavity pressures were subtracted from the measured values of the six-component balance axial-force coefficients).

The same data reduction reference quantities were used for all three tests in this project. The reference area and reference length for the configuration data were the body maximum cross-section area and maximum diameter, respectively. The planform area of a single tail fin was used as the reference area for the fin data. The fin hinge-moment and root bending-moment reference lengths were the exposed span and root chord, respectively, of a single fin.

Transition grit was used on the model in this project to establish a turbulent boundary layer near the body nose and near the strake and tail fin leading edges. The method developed in reference 10 was used to determine the grit size and application location. The transition grit application information for the tests in each facility entails (1) grit size #80 in the 8-Ft TPT applied as a one-tenth-in. strip with streamwise locations on the body nose at 1 in., the strake leading edge at 1 in., and the tail leading edge at 1 in.; (2) grit size #50 in the UPWT test section 1 applied as a one-sixteenth-in. strip with streamwise locations on the body nose at 1.2 in., the strake leading edge at 0.4 in., and on the tail leading edge at 0.4 in.; and (3) grit size #35 in the UPWT test section 2 applied as individual particles with streamwise locations on the body nose at 1.2 in., the strake leading edge at 0.4 in., and the tail leading edge at 0.4 in.

Model Description

As mentioned earlier, the test body used in this project was actually a thin shell built around an existing modular model known as the Langley Remote Control Missile Model. As the name implies, this model had the capability of remotely setting the tail fin deflection angles and configuration roll angle. In its original form, however, this model did not have the capability to measure fin loads. A description and the early uses of this Remote Control Missile Model can be found in reference 7.

This modular model was used in the Triservice Missile Project described in reference 1. The modification made to the existing modular model for use in that project was to attach a thin shell around the

body to produce a new aerodynamic surface that was larger in diameter and longer than the original model described in reference 7. The diameter of the original model was 2.5 in., whereas the diameter of the triservice model was 3.0 in. This added thickness allowed space to install fin balances between the fin bases and the fin-attachment surface of the original model.

A similar procedure was used in this project to create the model's outer surface. A new shell was attached around the modular model to produce the current model's aerodynamic surface, and the strakes were attached to this shell. The current model's maximum diameter was 3.15 in., which provided ample space to attach the fin balances to the internal modular model and the fins to the fin balances.

The technique used to assemble the test configuration was to first build up the modular model on the internal balance, add the fin balances, and then add the outer shell to produce the aerodynamic surface. Subsequently, the strakes and tail fins were added as needed to complete the configuration.

A complete description of the modular model used that gives the various body sections and the assembly process can be found in reference 1. The key features of this modular model were the ability to simultaneously (1) set remotely the tail fin deflection and model roll angles and (2) measure three-component fin loads at all four cruciform tail fins along with six-component overall configuration loads. Thus, for a given configuration, all attitude parameters—configuration angle of attack, configuration roll angle, and tail fin deflection angles—could be changed during testing without the need to interrupt the tunnel operation to make model changes. A control computer was used in this project to set the tail fin deflection and model roll angles. Figure 2 is a photograph of this computer along with one of the test configurations.

Figure 3 is taken from reference 1 and shows an exploded view of how the tail fins were mounted to the body. Each part shown in this figure attaches to the ones on either side by stacking the parts together. Thus, the fin balances were positioned between the fin base and the remotely actuated gear mounting surface. Thus, these balances not only isolated the fins from the body to allow fin loads to be measured, but also could be rotated by the gear to allow the fin attitude angles to be set. Figure 4 illustrates where the balances were located between the base of the fin and the body.

The geometry components of the model were combined to form the seven configurations shown in figure 5. The configuration components are identified in the nomenclature. Configuration 1, composed of the small nose, short strake, and tail components, was considered the baseline configuration. The other configurations were designed to investigate the effects of strake length and for configuration buildup effects. A limited number of runs were made with an alternate nose (configuration 7).

Figure 6 shows the major dimensions of the body. The body is shown with the small nose attached. Aft of the nose section, the body is a constant diameter of 3.15 in. except for a small boattail near the downstream end of the body, where the diameter decreases to 3.04 in. at the base. This boattail angle is about 2.3° and covers the last 1.37 in. of the body.

Figure 7 shows the long and short strake dimensions. The strakes were mounted on a small pad, seen in figure 8, before being attached to the body. The same mounting pads were used for both the long and short strakes. For the strakes-off configurations, the pads were removed to produce a clean aerodynamic surface.

Figure 9 shows the dimensions of the tail fin. Also shown is the tail fin hinge-line location, which is defined as the streamwise location about which the fins were rotated to set the deflection angles, and is

the location of the measurement center of the fin balance to which the fin is attached. The corresponding location of the hinge line on the body is identified in figure 6.

The tail fins had a small gap between the fin root chord and the body external surface to prevent fouling of the fin balance gauges. This gap was nominally about 0.020 in. for all fins. A small radius (about 0.005 in.) was included on the nominally sharp leading and trailing edges of all fins.

Figures 10 through 17 are photographs of the model installed in the tunnels. Figure 10 shows an oblique front view of configuration 1 and the tunnel mounting hardware in the 8-Ft TPT. Figures 11 and 12 show front and rear oblique views, respectively, of the same configuration in the same facility. Figure 12 also shows the tail fin balance cables and chamber pressure tubes exiting the model. Figures 13 and 14 show a side view and an oblique rear view, respectively, of the same configuration in the low-speed test section of the UPWT. It can be seen in figure 14 how the internal diameter of the model was beveled to the outside diameter at the base of the model so that only chamber pressure tubes were needed.

Figures 15 and 16 show a side view and an oblique front view, respectively, of configuration 2 in the high-speed test section of the UPWT. Figure 16 also shows the tunnel mounting system used in the UPWT. Figure 17 shows a technician hanging check loads on one of the tail fins on configuration 7 in the UPWT high-speed test section. Check loading of the tail fin balances was performed periodically during this project to ensure that the fin balance gauges were operating properly.

Presentation of Data

The test data, which include six-component overall configuration data and three-component data from all four tail fins, are presented in two electronic tabular formats on the attached CD-ROM. One is a standard ASCII text column tabulation format with headers, which is easy to use for visual examination of the data and for spreadsheet applications. The first two runs in this format are shown in figure 18. Figure 18(a) contains the left side of the tabular listing and figure 18(b) shows the right side of the same page.

The second form is an ASCII SIF (standard interface file) format, which is a standard format for many data-plotting programs. The data in this format are compiled in a list of variable names followed by the data. The variable names comprise up to six characters and are placed at the top of the file in a free-field format with five variable names per line. For each data point the values are written on the file in the same order as the variable names listing at the top of the file. Figure 19 contains the first page of data in this format showing the variable names and the first six data points of the first run. The variable names used in the ASCII SIF data files are identified and defined in the nomenclature.

All data in this project were angle-of-attack sweeps at a constant roll angle and Mach number. As shown in figure 5 and defined in the nomenclature, the geometric variables of this model included long and short strakes, fins on and off, and large and small nose sizes. These variables were combined to produce seven configurations. A summary list of these run number tables is presented in the summary table to identify which set of data is located in each table. Tables 1 through 7, one for each configuration, identify the run numbers for all data in this project.

Because the data contained in these tables came from tests conducted in three different facilities, it was important to ensure that run numbers were not repeated when data from different tests were combined. This was accomplished by adding 500 and 1000, respectively, to the original run numbers of UPWT tests 1670 and 1529 while retaining the original run numbers of the 8-Ft TPT test 1041. This ensured that each run number would be unique.

The summary table also shows that the largest number of runs (about 44 percent) was obtained with configuration 1, which came to be considered the baseline configuration in this study. Strake size was considered as the primary geometric variable in this project, thus the next largest number of runs (almost 34 percent) was obtained on configuration 2. The remaining configurations were obtained by combining the geometric parameters primarily to produce component buildup effects.

Plots from the tabulated data included in the data_plots folder on the attached CD-ROM represent about 46 percent of all runs in this project. Selected samples from these data plots are presented and analyzed subsequently to illustrate the effects of the test variables and to explore some of the aerodynamic effects that can be found there.

The data plots in this report represent only a small part of the entire database; therefore, selecting a baseline set of test conditions is helpful to serve as a common point around which the effects of the individual test variables can be shown. For this purpose, configuration 1 at Mach 2.86, zero roll angle, and no fin deflections was chosen. In general, the effects of the test variables are examined by looking at variations from this baseline condition.

The effects of the test variables are examined in this paper by analyzing plots of the main six-component balance data and the three-component fin balance data from all four tail fins. These data are generally presented in a six-plot format. The first two plots are the configuration longitudinal coefficients (C_{NF} , C_{AF} , and C_{PM}) and lateral-directional coefficients (C_{RM} , C_{YM} , and C_{Sy}). The last four plots are the three tail fin coefficients (C_{NFi} , C_{HMi} , and C_{BMi}) for each of the fins, where i represents tail fins 1 through 4. Each plot also lists the runs plotted on that page and contains a small sketch of the configuration(s) whose data are contained on that page. Shaded parts on the sketch indicate what geometry parts are a variable on that plot.

The plot legends identify the runs, Mach number, roll angle, and deflections (if any) of each of the tail fins. Also included in the legend is a parameter denoting whether the tail fin deflections result in pitch, yaw, or roll control on the configuration. These control angles are defined from the tail fin deflections found in the nomenclature.

Discussion

Data Repeatability

The purpose of figures 20(a) through (e) is to illustrate the consistency of the data presented. This is the only analysis figure that does not follow the plot layout described in the previous section. In this figure, the tail fin data are presented in three plots (one for each fin data parameter) instead of four plots (one for each fin). The plot was arranged in this manner to facilitate comparing data from different fin locations. Because this configuration is symmetric about the horizontal and vertical axes, similar results should be obtained from different fins that are located in the same physical orientation from runs at different roll angles.

Figures 20(a) through (e) show data from Configuration 1 at Mach 2.86 with no fin deflections at three roll angles— 0° , -90° , and $+90^\circ$. Figure 20(a) shows that the overall configuration longitudinal loads are virtually identical for these three roll angles, as would be expected due to model symmetry and no fin deflections. This condition should also result in very small lateral-directional loads, which figure 20(b) confirms. Figures 20(c) through (e) show fin normal force, hinge moment, and bending moment, respectively, for all four fin locations. The fin loads at each location are virtually identical regardless of which

fin was actually producing the measurement at that roll angle. Moreover, the fins in the upper and lower locations show very small loads, as would be expected. The two horizontal fins show similar trends, although the signs of the coefficients on the left and right sides are opposite due to the definition of the positive load directions at each fin location discussed earlier. Note that the hinge moments are small at all fin locations at this Mach number because the tail fin hinge lines were located near the expected center-of-pressure location, which should result in small hinge moments.

For all data in this project, flow angle corrections were made to the overall configuration data but none were made to the fin measurements. The configuration flow angle represents the average flow angle over the length of the body. Therefore, the local flow angle at any one location could be slightly different from this average. Thus, the fin data might be expected to have a small offset. This appears to be the case as seen in figures 20(a) through (e) where the fin data appear to have these offsets. Note, however, that the offsets are virtually the same at each fin location regardless of which fin balance was producing the measurement. This is an indication of the accuracy of the measurements and that the local tunnel flow angles were probably the cause.

Data repeatability results for other test conditions in both wind tunnels, including those for the other symmetric condition (roll angles of $+45^\circ$ and -45°), show similar results as those of figure 20. Plots of these data can be found in the data_repeatability folder on the CD-ROM that is attached to this paper.

Configuration Buildup

Configuration buildup effects can be observed by comparing body-alone, body-tail, and body-strake-tail data. A sample of these buildup effects is shown in figures 21(a) through (e), which compare data from configurations 1, 3, and 6 at Mach 2.86, zero roll angle, and no fin deflections. The effect on the overall longitudinal aerodynamics of adding the strakes (fig. 21(a)) causes a substantial increase in normal force, an increase in configuration stability, and minor changes in axial force. Figure 21(b) shows that all of these configurations had negligible lateral-directional loads, which would be expected due to model symmetry.

Because the data in this figure are for zero roll angle, tail fins 1 and 3 are in the vertical plane and should have very small loads on them. Figures 21(c) and (e) confirm that this is the case. On the other hand, tail fins 2 and 4 are in the horizontal plane and should show increasing loads with angle of attack. Figures 21(d) and (f) show this to be the case. Note that the tail fin loads are greater for the strake-off configuration (configuration 30) than for the strake-on configuration (configuration 1). This result illustrates the shielding effect that the strakes can have on flow over the tail fins. Also note that the right and left tail fins are loaded equally, but their plots are mirror images of each other due to the fin loads direction definition used in this project.

Configuration buildup plots for other Mach numbers, some of which also include strakes-on, tails-off data (configuration 4), can be found in the configuration_buildup folder on the attached CD-ROM.

Roll Angle Effects

Sample effects of varying model roll angle for configuration 1 at Mach 2.86 and zero tail fin deflection angle are shown in figures 22(a) through (f), where data from nine roll angles between -90° and 0° are shown. The configuration loads show that there is no measurable effect of roll angle on the axial force, but a systematic variation occurs in the other five components (figs. 22(a) and (b)). Figures 22(c) and (f) show a generally steady decrease in fin loads as the horizontal fin is rolled to the top vertical position. As

the fin is rolled from the horizontal to the bottom vertical position (figs. 22(d) and (e)), however, the loads stay virtually unchanged through about 20° roll angle before they decrease to zero at the bottom vertical position.

Plots of roll-angle effects at other Mach numbers and for other configurations can be found in the roll_angle folder on the attached CD-ROM.

Mach Number Effects

Sample Mach number effects on configuration 1 at zero roll angle and no fin deflections can be seen in figures 23(a) through (f). In general, figure 23(a) shows that increasing Mach number causes a decrease in both normal-force configuration stability level, especially at angles of attack greater than 2°. All lateral-directional loads are seen to be negligible (fig. 23(b)), as are the loads on the vertical fins (figs. 23(c) and (e)). Large Mach number effects are seen on the horizontal fins (figs. 23(d) and (f)). Note that hinge moment becomes significant at the subsonic and transonic Mach numbers, whereas it was negligible at the supersonic Mach numbers. This effect is due to the expected longitudinal center-of-pressure movement with Mach number.

Plots of the effects of Mach number for the small strakes, no strakes, and body-alone configurations, configurations 2, 3, and 6, respectively, can be found in the mach_number folder on the attached CD-ROM.

Strake Length Effects

A sample of the effects due to the length of the strakes at Mach 2.86, zero roll angle, and no fin deflections can be found in figure 24. In this figure, data from long-strake, short-strake, and no-strake configurations (configurations 1, 2, and 3, respectively) are compared. Figure 24(a) shows a systematic increase in overall normal force and stability level with increasing strake length. Also shown is a small axial-force increase with the addition of the short strake, but no measurable difference between the short and long strakes. For this condition of symmetry about the vertical plane, figure 24(b) shows the expected negligible lateral-directional parameters, and figures 24(c) and (e) show the same for the top and bottom fins. Figures 24(d) and (f), however, show an increase in the shielding effect on the horizontal fins with strake length. The results from the horizontal fins are again mirror images of each other because of the load direction definitions.

Plots of the effects of strake length at other Mach numbers can be found in the strake_length folder on the attached CD-ROM.

Two-Fin Pitch Control Deflection Effects

Thus far, all effects described in this paper have been for undeflected tail fins. Beginning in this section several tail fin deflection conditions will be examined.

Figures 25(a) through (f) show an example of the effects of pitch-control deflections of the two horizontal tail fins for configuration 1 at Mach 2.86 and zero roll angle. The nomenclature contains the definitions of all fin deflection angles used in this study. Of relevance here, pitchup control deflection angles are positive on the right fin and negative on the left fin. In these figures, the two horizontal tail fins are deflected to provide both pitchup and pitchdown control effects. The pitching moments seen in figure 25(a) show almost linear changes with deflection angle over the entire angle-of-attack range.

There appears to be no loss of control effectiveness even at the largest deflection angles. This linear variation with deflection angle is not present in the subsonic data plots contained in the attached CD-ROM. There are also systematic changes in normal force in figure 25(a) with both deflection angle and angle of attack, but there is some nonlinearity in axial force at the larger deflection angles.

Because these deflections are symmetric about the vertical axis, no influence on the lateral coefficients would be expected, and figure 25(b) shows that this is the case. Also, the undeflected top and bottom fins show no effects from the horizontal fin deflections (figs. 25(c) and (e)). The deflected horizontal fins, however show a large dependence on deflection angle (figs. 25(d) and (f)). Effects on the normal force and bending moments are almost linear and virtually constant over the angle-of-attack range, and the coefficients are mirror images between the left and right fins, as would be expected.

Plots of pitch control effects at zero roll angle for all tails-on configurations (configurations 1, 2, 3, and 7) at all test Mach numbers can be found in the two-fin-pitch-control folder on the attached CD-ROM.

Four-Fin Pitch Control Deflection Effects

As illustrated in the previous section at zero roll angle, pure pitch control is achieved by deflection of the two horizontal tail fins. Another pure pitch control situation arises when the model is rolled 45° and uses all four tail fins. For these deflections, supersonic data on configuration 1 were not obtained, so figures 26(a) through (e) show this four-fin pitch control at Mach 0.60. The roll angle is -45° and the pitch control deflections vary from 30° pitchup to 30° pitchdown.

Interestingly, the configuration longitudinal data indicates that the normal force and pitching moment do not vary linearly with deflection angle (fig. 26(a)). In fact, the 30° deflection results are at about the same level as the 20° results. This nonlinear effect was not seen in the supersonic two-fin deflection data shown earlier, but it was contained in the two-fin Mach 0.60 data contained in the plots on the CD-ROM. Comparing the Mach 0.60, two-fin, and four-fin results also shows that for a given deflection angle the longitudinal coefficients of the four-fin data are always larger because all the fins are being deflected. Because of symmetry, there are no large effects seen in the lateral-directional parameters of figure 26(b).

The fin data of figure 26(c) through (e) show that the 30° deflection loads are also about the same as those of the 20° deflections. This means that effects seen on the configuration longitudinal parameters result from the loads on the fins. Also note that there are substantial hinge moments on the fins, which were not present in the supersonic results of figures 25(a) through (e).

Figures 26(a) through (e) contain data from only three tail fins. For this set of runs, the balance at the fin 4 location was not functioning properly, so data from this balance were excluded. In this project, whenever a fin balance was not operating properly, the coefficients for that fin were artificially set to a value of 9.9999 for the affected runs. This permitted the “bad” data to be eliminated while allowing data from the main balance and the other fins to be retained in the data set. Thus, all tail fin data in the tabulated data on the attached CD-ROM that have values of 9.9999 should be assumed to be “bad” and therefore ignored.

Plots of four-fin pitch control data for other Mach numbers and configurations can be found in the four-fin-pitch-control folder on the attached CD-ROM.

Yaw Control Deflection Effects

Yaw control deflections were not included in the original data matrix for this project; however, yaw control results can be obtained from the two-fin pitch control runs where the configuration was rolled 90°. This orientation puts the deflected fins in the vertical plane and results in a pure yaw control situation. Figures 27(a) through (e) show a sample of these yaw control results for configuration 1 at the transonic Mach number of 1.18 at a roll angle of -90° for yaw deflections from 20° nose left to 20° nose right. Figure 27(a) shows that the configuration normal force and pitching moment are virtually unaffected by the yaw control deflections, and that the magnitude of the axial force reflects the increments caused by increasing deflection angles.

Figure 27(b), however, shows large effects of the deflections on the yawing moment and side force. The effects are approximately linear with deflection angle, except for an unexpected variation in both parameters at zero deflection angle. The tail fin data from the upper and lower fins (figs. 27(c) and (e)) do not show any behavior that would explain the yawing-moment and side-force results. The rolling moment is seen to be negligible over the entire angle-of-attack range.

Note that because the roll angle of these data is -90°, the fins in the horizontal plane are tail fins 1 and 3. Data from these fins show very little effect of the yaw deflections except for some variation in hinge moment (figs. 27(c) and (e)). Note that data for the left and right fins are virtual mirror images of each other.

The data from the top and bottom fins, figures 27(d) and (f), respectively, show approximately linear variations of normal force and bending moment with deflection angle and almost no variation with angle of attack. Moreover, there is very little difference between the top and bottom fin data, indicating that the body and strake shielding effects on the top fin seen earlier in supersonic Mach number data are not very strong at this transonic Mach number. Because there is very little variation on either fin with angle of attack, the variation in the configuration side force seen in figure 27(b) did not come from the tail fins.

A plot of the effects of yaw control deflections for other Mach numbers and configurations can be found in the `yaw_control` folder on the attached CD-ROM.

Combination Pitch and Yaw Control Deflection Effects

Several runs were made in this project wherein both pitch control deflections were made on the horizontal fins and yaw control deflections were made on the vertical fins. The deflection angle for both the pitch and yaw controls was always the same.

Figures 28(a) through (f) show an example of these combination effects on configuration 1 at Mach 2.86, zero roll angle, and deflection angles up to 30°. Comparing the configuration longitudinal loads (fig. 28(a)) with the corresponding pitch-only deflection data of figure 25(a) shows that they have very similar normal-force and pitching-moment trends. The axial force for the pitch/yaw combination deflections is larger because all the fins were deflected. In addition, the data from the horizontal fins (figs. 28(d) and (f)) are very similar to the corresponding pitch control data of figures 25(d) and (f). Thus, it appears that the addition of the yaw control has very little effect on the longitudinal configuration loads or the horizontal tail fin loads.

Because pure yaw control data at this Mach number were not obtained in this project, no direct comparisons with pitch/yaw data can be made. The most noticeable yaw control effect in figures 28(a)

through (e) is the dramatic decrease in normal force and bending moment on the top vertical fin (fig. 28(c)) at the higher angles of attack. The decrease is caused by shielding of this fin from the flow by the body and strakes as angle of attack increases and results in a loss of yaw control authority on this fin. Note, however, that the configuration yawing moment and side force in fig. 28(b) show almost no variation with angle of attack, that is, no loss of yaw control on the configuration. The reason for this apparent contradiction can be found in the lower fin data of figure 28(e) where the fin normal force and bending moment are seen to increase (in the negative direction) with angle of attack. This increase counteracts the decrease seen in the top fin to produce approximately the same yawing moment and side force on the configuration as angle of attack increases. This uneven loading on the two vertical fins does, however, produce some induced rolling moment on the configuration as seen in figure 28(b).

This loss of control authority on the top vertical fin was not present in the Mach 1.18 yaw control data shown earlier in figure 27. Plots of pitch/yaw combination results for other Mach numbers and configurations can be found in the pitch/yaw_control folder on the attached CD-ROM. In examining these results over the Mach number range, it appears that this loss of control authority on the top fin was not present in the configuration 1 data at Mach 1.70, but was present at Mach 2.36. Thus, this effect appears to begin somewhere between these two supersonic Mach numbers and becomes more pronounced with increasing Mach number. Also, the effect appears to be there but somewhat diminished in the short strake data of configuration 2 at the same Mach numbers. This indicates that the shielding effect is a function of strake size.

Roll Control Deflection Effects

Figures 29(a) through (f) show a sample of the effects of roll control deflections on configuration 1 at Mach 1.18 and zero roll angle at roll control angles of 5° and 10° . Note that from the fin deflection definitions in the nomenclature, all four fins were used to produce the roll control effects. Figures 29(a) and 29(b) show that for the overall configuration aerodynamics the roll control deflections affect primarily the rolling moment and axial force with very little effect on other parameters. Moreover, the configuration rolling moment is almost linear with deflection angle and remains approximately constant over the angle-of-attack range.

Figures 29(c) and (e) show that the loads on the top and bottom fins are virtually unchanged by angle of attack; thus, there is no shielding effect seen at this Mach number. Figures 29(d) and (f) show that although the horizontal fins have about the same loads at zero angle of attack, their trends with angle of attack are opposite because the effective angle of one fin is increasing while it is decreasing on the other fin.

Plots of the effects of roll control deflection at other Mach numbers and all tail-on configurations (configurations 1, 2, 3, and 7) can be found in the roll_control folder on the attached CD-ROM.

Nose Size Effects

As can be seen from the model geometry sketches in figure 5, the nose section of the baseline configuration had a somewhat smaller diameter than the rest of the body, with a cone frustum transitioning between the two diameters. A few runs were made with an alternate nose whose diameter was the same as that of the body, such that no transition section was needed. This alternate nose was tested with the short strakes and tails to produce configuration 7; thus, nose size effects can be examined by comparing data from configurations 7 and 2. All configuration 7 data were inadvertently obtained at Mach 1.75 instead of 1.70, which was one of the Mach numbers of the rest of the project data. This 0.05 difference

in Mach number between the data from configurations 2 and 7, however, should be negligible. Note that, due to main balance limits in this project, runs at low supersonic Mach numbers were generally limited to angles of attack of about 14° , whereas data at other Mach numbers were obtained up to angles of attack of about 22° .

Figures 30(a) through (f) show an example of the nose size effects by comparing data from configurations 2 and 7 at Mach 1.70 and 1.75, respectively, zero roll angle, and no fin deflections. The only effects seen in the overall configuration aerodynamics (figs. 30(a) and (b)) are that the alternate nose shows a small increase in axial force and a decrease in pitching moment. Virtually no difference in the tail fin loads can be seen in figures 30(c) through (f). Similar nose size effects can be found at other roll angles, whose data plots can be found in the nose-size folder on the attached CD-ROM.

Concluding Remarks

An experimental study has been performed to develop a large force and moment aerodynamic data set on a slender axisymmetric missile configuration with cruciform strakes and cruciform in-line tail fins that were used for control. The data include six-component balance measurements of the overall configuration aerodynamics and three-component balance measurements on all four tail fins. The test variables in this project include angle of attack, roll angle, Mach number, model buildup, strake length, nose size, and tail fin deflection angles to provide pitch, yaw, and roll control. The test Mach numbers ranged from 0.60 to 4.63.

The entire data set is presented in two ASCII formats—tabular listing with headers and free-format SIF—on a CD-ROM that is attached to this paper. Also included on the CD-ROM are extensive plots of both the six-component configuration data and the three-component tail fin data. Selected samples of these plots have been presented in this paper to illustrate the features of the data and to investigate the effects of the test variables.

References

1. Allen, Jerry M.: *The Triservice Missile Database*. NASA/TM-2002-211653, 2002.
2. Allen, J. M.; Shaw, D. S.; and Sawyer, W. C.: Analysis of Selected Data From the Triservice Missile Data Base. *J. of Spacecr. & Rockets*, vol. 27, no. 1, Jan.–Feb. 1990, pp. 15–20.
3. Allen, J. M.; Shaw, D. S.; and Sawyer, W. C.: Analysis of Selected Data From the Triservice Missile Data Base. AIAA-89-0478, Jan. 1989.
4. Allen, J. M.; Shaw, D. S.; and Sawyer, W. C.: Remote Control Missile Model Test. Stability and Control of Tactical Missile Systems. AGARD-CP-451, March 1989, pp. 17.1–17.12.
5. Allen, Jerry M.: *Parametric Fin-Body and Fin-Plate Database for a Series of 12 Missile Fins*. NASA/TM-2001-210652, 2001.
6. Jane's Weapons Systems. Jane's Information Group, Inc., Alexandria, VA, 1988–89. p. 723.
7. Corlett, W. A.: Test Technique Development in Interference Free Testing, Flow Visualization, and Remote Control Model Technology at Langley's Unitary Plan Wind Tunnel. 52nd Semi-Annual Meeting of the Supersonic Tunnel Association, Sept. 13–14, 1979.
8. Brooks, Cyler W., Jr.; Harris, Charles D.; and Reagon, Patricia G.: *The NASA Langley 8-Foot Transonic Pressure Tunnel Calibration*. NASA TP-3437, 1994.
9. Jackson, C. M.; Corlett, W. A.; and Monta, W. J.: *Description and Calibration of the Langley Unitary Plan Wind Tunnel*. NASA TP-1905, 1981.
10. Stallings, Robert L., Jr.; and Lamb, Milton: *Effects of Roughness Size on the Position of Boundary-Layer Transition and on the Aerodynamic Characteristics of a 55° Swept Delta Wing at Supersonic Speeds*. NASA TP-1027, 1977.

Tables Supplement: Summary of Data Tables

Table number	Configuration number	Configuration description	Number of runs	Percent of runs
1	1	SN-LS-T	464	43.8
2	2	SN-SS-T	358	33.8
3	3	SN-no S-T	103	9.7
4	4	SN-LS-no T	12	1.1
5	5	SN-SS-no T	9	0.9
6	6	SN-no S-no T	44	4.2
7	7	LN-SS-T	69	6.5
Total			1059	100

Table 1. Configuration 1 Run Matrix

ϕ	δ_1	δ_2	δ_3	δ_4	Run number for Mach—												Fin set
					0.60	0.90	1.18	1.70	1.75	1.90	2.00	2.10	2.36	2.86	3.95	4.63	
0	0	0	0	0	1154	1128	1005	546			510		38	95	170	210	1
-5	0	0	0	0			1020	525					9	82	142		
-12	0	0	0	0	1162	1136	1025	526					10	83	143		
-22.5	0	0	0	0	1163	1137	1036	527					11	84	144		
-33	0	0	0	0			1050										
-40	0	0	0	0			1055	528					12	85	145		
-45	0	0	0	0	1165	1139	1060	529					13	86	146		
-50	0	0	0	0			1079	530					14	87	147		
-57	0	0	0	0			1084										
-67.5	0	0	0	0	1174	1148	1089	531					15	88	148		
-78	0	0	0	0			1103										
-90	0	0	0	0	1175	1149	1112	532					16	89	149		
5	0	0	0	0				524					8	81	141		
12	0	0	0	0				523					7	80	140		
22.5	0	0	0	0	1153	1127	1004	522					6	79	139		
33	0	0	0	0				521					5	78	138		
40	0	0	0	0				520					4	77	137		
45	0	0	0	0	1152	1126	1003	519					3	76	136		
67.5	0	0	0	0	1151	1125	1002	518					2	75	135		
90	0	0	0	0				517					1	74	134		
0	0	10	0	-10	1155	1129	1007	547			511		39	96	171	211	2
-5	0	10	0	-10			1021	558					50	107	182		
-12	0	10	0	-10			1026	562					54	111	186		
-22.5	0	10	0	-10			1038										
-33	0	10	0	-10			1051										
-40	0	10	0	-10			1056										
-45	0	10	0	-10			1062	578					28	127	202		

Table 1. Continued

ϕ	δ_1	δ_2	δ_3	δ_4	Run number for Mach—											Fin set	
					0.60	0.90	1.18	1.70	1.75	1.90	2.00	2.10	2.36	2.86	3.95	4.63	
-50	0	10	0	-10			1080										
-57	0	10	0	-10			1085										
-67.5	0	10	0	-10			1091	584					20	133	208		
-78	0	10	0	-10			1104										
-90	0	10	0	-10			1114										
0	0	20	0	-20	1156	1130	1010	548			512		40	97	172	212	3
-5	0	20	0	-20			1022	559					51	108	183		
-12	0	20	0	-20			1029	563					55	112	187		
-22.5	0	20	0	-20			1041										
-33	0	20	0	-20			1052										
-40	0	20	0	-20			1057	573					64	122	197		
-45	0	20	0	-20			1065	536					27	90	159		
-50	0	20	0	-20			1081	579					69	128	203		
-57	0	20	0	-20			1086										
-67.5	0	20	0	-20			1094										
-78	0	20	0	-20			1106										
-90	0	20	0	-20			1117										
0	0	30	0	-30	1157	1131	1011	549			513		41	98	173	213	4
0	0	-10	0	10	1158	1132	1014	550			514		42	99	174	214	5
-5	0	-10	0	10			1023	560					52	109	184		
-12	0	-10	0	10			1032	564					56	113	188		
-22.5	0	-10	0	10			1044										
-33	0	-10	0	10			1053										
-40	0	-10	0	10			1058	574					65	123	198		
-45	0	-10	0	10			1068										
-50	0	-10	0	10			1082	580					70	129	204		
-57	0	-10	0	10			1087										

Table 1. Continued

ϕ	δ_1	δ_2	δ_3	δ_4	Run number for Mach—												Fin set
					0.60	0.90	1.18	1.70	1.75	1.90	2.00	2.10	2.36	2.86	3.95	4.63	
-67.5	0	-10	0	10			1098										
-78	0	-10	0	10			1108										
-90	0	-10	0	10			1120										
0	0	-20	0	20	1159	1133	1017	551			515		43	100	175	215	6
-5	0	-20	0	20			1024	561					53	110	185		
-12	0	-20	0	20			1034	565					57	114	189		
-22.5	0	-20	0	20			1047										
-33	0	-20	0	20			1054										
-40	0	-20	0	20			1059	575					66	124	199		
-45	0	-20	0	20			1071										
-50	0	-20	0	20			1083	581					71	130	205		
-57	0	-20	0	20			1088										
-67.5	0	-20	0	20			1101										
-78	0	-20	0	20			1110										
-90	0	-20	0	20			1123										
0	0	-30	0	30	1160	1134	1018	552			516		44	101	176	216	7
0	5	5	5	5	1161	1135	1006										8
-22.5	5	5	5	5	1164	1138	1037										
-45	5	5	5	5	1166	1140	1061										
-67.5	5	5	5	5	1173	1147	1090										
-90	5	5	5	5	1176	1150	1113										
0	10	10	10	10			1015						35		168		9
-22.5	10	10	10	10			1045								160		
-45	10	10	10	10			1069								158		
-67.5	10	10	10	10			1099										
-90	10	10	10	10			1121						17		150		
-45	0	10	0	10				538									11

Table 1. Continued

ϕ	δ_1	δ_2	δ_3	δ_4	Run number for Mach—											Fin set	
					0.60	0.90	1.18	1.70	1.75	1.90	2.00	2.10	2.36	2.86	3.95	4.63	
0	0	20	20	0				556					48	105	180		14
-12	0	20	20	0				569					61	118	193		
0	10	20	10	0			1009						36		167		15
-12	10	20	10	0			1028										
-22.5	10	20	10	0			1040						30		161		
-45	10	20	10	0			1064						25		156		
-67.5	10	20	10	0			1093						22		152		
-90	10	20	10	0			1116						18		151		
0	10	0	10	20				545					37	94	169		16
-22.5	10	0	10	20									31		163		
-45	10	0	10	20									26		157		
-67.5	10	0	10	20									23		154		
-45	10	-10	-10	10	1167	1141	1076										17
-45	20	-20	-20	20	1168	1142	1077										18
-45	30	-30	-30	30	1169	1143	1078										19
0	-10	10	10	-10				557					49	106	181		20
12	-10	10	10	-10				571					63	120	195		
40	-10	10	10	-10				577					68	126	201		
-45	-10	10	10	-10	1170	1144	1073										
50	-10	10	10	-10				583					73	132	207		
0	-20	20	20	-20				555					47	104	179		21
12	-20	20	20	-20				568					60	117	192		
40	-20	20	20	-20				576					67	125	200		
-45	-20	20	20	-20	1171	1145	1074										
-50	-20	20	20	-20				582					72	131	206		
0	-30	30	30	-30				542					33	92	165		22
22.5	-30	30	30	-30				541					32	91	164		

Table 1. Continued

ϕ	δ_1	δ_2	δ_3	δ_4	Run number for Mach—											Fin set	
					0.60	0.90	1.18	1.70	1.75	1.90	2.00	2.10	2.36	2.86	3.95	4.63	
-45	-30	30	30	-30	1172	1146	1075										
0	-10	20	10	-20				543									23
-12	-10	20	10	-20				572						121	196		
-22.5	-10	20	10	-20				540									
-45	-10	20	10	-20				537									
0	5	15	5	-5			1008										24
-12	5	15	5	-5			1027										
-22.5	5	15	5	-5			1039										
-45	5	15	5	-5			1063										
-67.5	5	15	5	-5			1092										
-78	5	15	5	-5			1105										
-90	5	15	5	-5			1115										
0	5	25	5	-15			1012										25
-5	5	25	5	-15			1049										
-12	5	25	5	-15			1030										
-22.5	5	25	5	-15			1042										
-45	5	25	5	-15			1066										
-67.5	5	25	5	-15			1095										
-78	5	25	5	-15			1107										
-90	5	25	5	-15			1118										
0	10	30	10	-10			1013	544						34	93	166	
-12	10	30	10	-10			1031	570						62	119	194	
-22.5	10	30	10	-10			1043	539						29		162	
-45	10	30	10	-10			1067	535						24			
50	10	30	10	-10												155	
-67.5	10	30	10	-10			1096	534						21		153	
-90	10	30	10	-10			1119	533						19			

Table 1. Concluded

ϕ	δ_1	δ_2	δ_3	δ_4	Run number for Mach—										Fin set	
					0.60	0.90	1.18	1.70	1.75	1.90	2.00	2.10	2.36	2.86	3.95	
0	5	-5	5	15			1016									27
-12	5	-5	5	15			1033									
-22.5	5	-5	5	15			1046									
-45	5	-5	5	15			1070									
-67.5	5	-5	5	15			1100									
-78	5	-5	5	15			1109									
-90	5	-5	5	15			1122									
0	5	-15	5	25			1019									28
-12	5	-15	5	25			1035									
-22.5	5	-15	5	25			1048									
-45	5	-15	5	25			1072									
-67.5	5	-15	5	25			1102									
-78	5	-15	5	25			1111									
-90	5	-15	5	25			1124									
0	-10	30	30	-10			554					46	103	178		30
-12	-10	30	30	-10			567					59	116	191		
0	0	30	20	-10			553					45	102	177		31
-12	0	30	20	-10			566					58	115	190		

Table 2. Configuration 2 Run Matrix

ϕ	δ_1	δ_2	δ_3	δ_4	Run number for Mach—												Fin set
					0.60	0.90	1.18	1.70	1.75	1.90	2.00	2.10	2.36	2.86	3.95	4.63	
0	0	0	0	0	1344	1318	1182	585			643		275	337	225	234	1
-5	0	0	0	0			1197	586					264/ 267	330	217		
-12	0	0	0	0	1354	1326	1203	587					265/ 268	331	218		
-22.5	0	0	0	0	1355	1327	1214	588					266/ 269	332	219		
-33	0	0	0	0			1227										
-40	0	0	0	0			1232	589					270	333	220		
-45	0	0	0	0	1357	1329	1238	590					271	334	221		
-50	0	0	0	0			1257	591					272	335	222		
-57	0	0	0	0			1262										
-67.5	0	0	0	0	1366	1338	1267	592					273	263	223		
-78	0	0	0	0			1280										
-90	0	0	0	0	1367	1339	1289	593					274	336	224		
22.5	0	0	0	0	1343	1317	1181										
45	0	0	0	0	1342	1316	1180										
67.5	0	0	0	0	1341	1315	1179										
0	0	10	0	-10	1345	1319	1184	594			644		276	338	226	235	2
-5	0	10	0	-10			1199										
-12	0	10	0	-10			1204										
-22.5	0	10	0	-10			1216						292				
-33	0	10	0	-10			1228										
-40	0	10	0	-10			1234						304				
-45	0	10	0	-10			1240						305				
-50	0	10	0	-10			1258						317				
-57	0	10	0	-10			1263										
-67.5	0	10	0	-10			1269						318				
-78	0	10	0	-10			1281										
-90	0	10	0	-10			1291/ 1292						326				

Table 2. Continued

ϕ	δ_1	δ_2	δ_3	δ_4	Run number for Mach—												Fin set
					0.60	0.90	1.18	1.70	1.75	1.90	2.00	2.10	2.36	2.86	3.95	4.63	
0	0	20	0	-20	1346	1320	1187	595			645		277	339	227	236	3
-5	0	20	0	-20			1200										
-12	0	20	0	-20			1207										
-22.5	0	20	0	-20			1219	611					293				
-33	0	20	0	-20			1229										
-40	0	20	0	-20			1235										
-45	0	20	0	-20			1243	622					306				
-50	0	20	0	-20			1259										
-57	0	20	0	-20			1264										
-67.5	0	20	0	-20			1272	633					319				
-78	0	20	0	-20			1283										
-90	0	20	0	-20			1294	640					327				
0	0	30	0	-30	1347	1321	1188	596			646		278	340	228	237	4
0	0	-10	0	10	1348	1322	1191	597			647		279	341	229	238	5
-5	0	-10	0	10			1201										
-12	0	-10	0	10			1210										
-22.5	0	-10	0	10			1222	612					294	354			
-33	0	-10	0	10			1230										
-40	0	-10	0	10			1236										
-45	0	-10	0	10			1246	623					307				
-50	0	-10	0	10			1260										
-57	0	-10	0	10			1265										
-67.5	0	-10	0	10			1275	634					320				
-78	0	-10	0	10			1285										
-90	0	-10	0	10			1297										
0	0	-20	0	20	1349	1323	1194	598			648		280	342	230	239	6
-5	0	-20	0	20			1202										

Table 2. Continued

ϕ	δ_1	δ_2	δ_3	δ_4	Run number for Mach—												Fin set
					0.60	0.90	1.18	1.70	1.75	1.90	2.00	2.10	2.36	2.86	3.95	4.63	
-12	0	-20	0	20			1212										
-22.5	0	-20	0	20			1225	613					295	355			
-33	0	-20	0	20			1231										
-40	0	-20	0	20			1237										
-45	0	-20	0	20			1249	624					308				
-50	0	-20	0	20			1261										
-57	0	-20	0	20			1266										
-67.5	0	-20	0	20			1278						321				
-78	0	-20	0	20			1287										
-90	0	-20	0	20			1300										
0	0	-30	0	30	1351	1324	1195	599			649		281	343	231	240	7
0	5	5	5	5	1353	1325	1183										8
-22.5	5	5	5	5	1356	1328	1215										
-45	5	5	5	5	1358	1330	1239										
-67.5	5	5	5	5	1365	1337	1268										
-90	5	5	5	5	1368	1340	1290										
0	10	10	10	10			1192	603					285	347			9
-22.5	10	10	10	10			1223	617					299				
-45	10	10	10	10			1247	628					312				
-67.5	10	10	10	10			1276	636					322				
-90	10	10	10	10			1298	641					328				
0	20	20	20	20				610					291	353	233		10
0	0	20	0	20				609					290	352	232		12
0	0	-30	0	-30				608									13
0	0	20	20	0				602					284	346			14
-22.5	0	20	20	0				616					298	358			
-45	0	20	20	0				627					311				

Table 2. Continued

ϕ	δ_1	δ_2	δ_3	δ_4	Run number for Mach—											Fin set	
					0.60	0.90	1.18	1.70	1.75	1.90	2.00	2.10	2.36	2.86	3.95	4.63	
0	10	20	10	0			1186										15
-12	10	20	10	0			1206										
-22.5	10	20	10	0			1218										
-45	10	20	10	0			1242										
-67.5	10	20	10	0			1271										
-90	10	20	10	0			1293										
0	10	-10	-10	10				601						283	345		17
-22.5	10	-10	-10	10				615						297	357		
-45	10	-10	-10	10	1359	1331	1254	626						310			
-45	20	-20	-20	20	1360	1332	1255										18
-45	30	-30	-30	30	1361	1333	1256										19
0	-10	10	10	-10				606						288	350		20
-22.5	-10	10	10	-10				620						302			
-45	-10	10	10	-10	1362	1334	1251	631						315			
-67.5	-10	10	10	-10				639						325			
-45	-20	20	20	-20	1363	1335	1252										21
-45	-30	30	30	-30	1364	1336	1253										22
0	-10	20	10	-20				607						289	351		23
-22.5	-10	20	10	-20				621						303			
-45	-10	20	10	-20				632						316			
0	5	15	5	-5			1185										24
-12	5	15	5	-5			1205										
-22.5	5	15	5	-5			1217										
-45	5	15	5	-5			1241										
-67.5	5	15	5	-5			1270										
-78	5	15	5	-5			1282										
0	5	25	5	-15			1189										25

Table 2. Continued

ϕ	δ_1	δ_2	δ_3	δ_4	Run number for Mach—										Fin set	
					0.60	0.90	1.18	1.70	1.75	1.90	2.00	2.10	2.36	2.86	3.95	
-5	5	25	5	-15			1198									
-12	5	25	5	-15			1208									
-22.5	5	25	5	-15			1220									
-45	5	25	5	-15			1244									
-67.5	5	25	5	-15			1273									
-78	5	25	5	-15			1284									
-90	5	25	5	-15			1295									
0	10	30	10	-10			1190	604					286	348		26
-12	10	30	10	-10			1209									
-22.5	10	30	10	-10			1221	618					300			
-45	10	30	10	-10			1245	629					313			
-67.5	10	30	10	-10			1274	637					323			
-90	10	30	10	-10			1296	642					329			
0	5	-5	5	15			1193									27
-12	5	-5	5	15			1211									
-22.5	5	-5	5	15			1224									
-45	5	-5	5	15			1248									
-67.5	5	-5	5	15			1277									
-78	5	-5	5	15			1286									
-90	5	-5	5	15			1299									
0	5	-15	5	25			1196									28
-12	5	-15	5	25			1213									
-22.5	5	-15	5	25			1226									
-45	5	-15	5	25			1250									
-67.5	5	-15	5	25			1279									
-78	5	-15	5	25			1288									
-90	5	-15	5	25			1301									

Table 2. Concluded

ϕ	δ_1	δ_2	δ_3	δ_4	Run number for Mach—											Fin set	
					0.60	0.90	1.18	1.70	1.75	1.90	2.00	2.10	2.36	2.86	3.95	4.63	
0	10	-10	10	30				605					287	349			29
-22.5	10	-10	10	30				619					301				
-45	10	-10	10	30				630					314				
-67.5	10	-10	10	30				638					324				
0	-10	30	30	-10				600					282	344			30
-22.5	-10	30	30	-10				614					296	356			
-45	-10	30	30	-10				625					309				

Table 3. Configuration 3 Run Matrix

ϕ	δ_1	δ_2	δ_3	δ_4	Run number for Mach—												Fin set
					0.60	0.90	1.18	1.70	1.75	1.90	2.00	2.10	2.36	2.86	3.95	4.63	
0	0	0	0	0	1412	1392	1372	655					666	677	251		1
-5	0	0	0	0				656					667	678	246		
-12	0	0	0	0	1420	1400	1380	657					668	679	247		
-22.5	0	0	0	0	1421	1401	1381	658					669	680	248		
-45	0	0	0	0	1423	1403	1383	659					670	681	249		
-67.5	0	0	0	0	1427	1406	1386										
-90	0	0	0	0	1428	1407	1387	660					671	682	250		
5	0	0	0	0				654					665	676	245		
12	0	0	0	0				653					664	675	244		
22.5	0	0	0	0	1411	1391	1371	652					663	674	243		
45	0	0	0	0	1410	1390	1370	651					662	673	242		
67.5	0	0	0	0	1409	1389	1369										
90	0	0	0	0				650					661	672	241		
0	0	10	0	-10	1413	1393	1373										2
0	0	20	0	-20	1414	1394	1374										3
0	0	30	0	-30	1415	1397	1375										4
0	0	-10	0	10	1416		1376										5
0	0	-20	0	20	1417	1396	1377										6
0	0	-30	0	30	1418	1398	1378										7
0	5	5	5	5	1419	1399	1379										8
-22.5	5	5	5	5	1422	1402	1382										
-45	5	5	5	5	1424	1404	1384										
-67.5	5	5	5	5	1425	1405	1385										
-90	5	5	5	5	1429	1408	1388										

Table 4. Configuration 4 Run Matrix

ϕ	δ_1	δ_2	δ_3	δ_4	Run number for Mach—											Fin set	
					0.60	0.90	1.18	1.70	1.75	1.90	2.00	2.10	2.36	2.86	3.95	4.63	
0	Off	Off	Off	Off	1475	1471	1467										0
-12	Off	Off	Off	Off	1476	1472	1468										
-22.5	Off	Off	Off	Off	1477	1473	1469										
-45	Off	Off	Off	Off	1478	1474	1470										

Table 5. Configuration 5 Run Matrix

ϕ	δ_1	δ_2	δ_3	δ_4	Run number for Mach—											Fin set	
					0.60	0.90	1.18	1.70	1.75	1.90	2.00	2.10	2.36	2.86	3.95	4.63	
0	Off	Off	Off	Off			1460										0
-12	Off	Off	Off	Off			1461										
-22.5	Off	Off	Off	Off			1462										
-45	Off	Off	Off	Off			1463										
-67.5	Off	Off	Off	Off			1464										
-90	Off	Off	Off	Off			1465										
22.5	Off	Off	Off	Off			1459										
45	Off	Off	Off	Off			1458										
67.5	Off	Off	Off	Off			1457										

Table 6. Configuration 6 Run Matrix

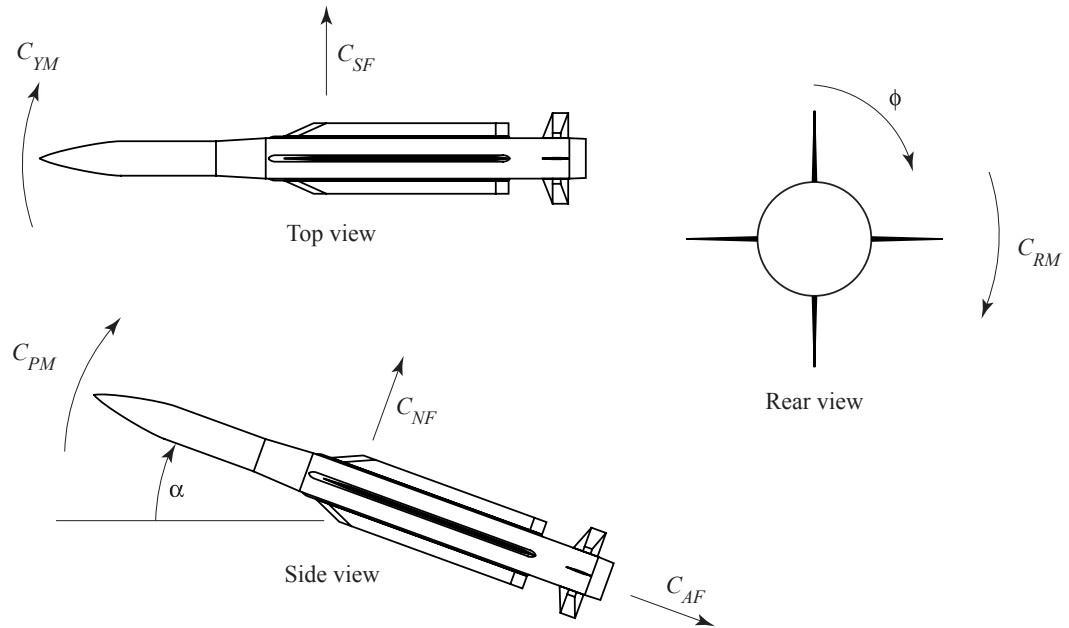
ϕ	δ_1	δ_2	δ_3	δ_4	Run number for Mach—											Fin set	
					0.60	0.90	1.18	1.70	1.75	1.90	2.00	2.10	2.36	2.86	3.95	4.63	
0	Off	Off	Off	Off	1451	1442	1433	683					685	688	262		0
-5	Off	Off	Off	Off													257
-12	Off	Off	Off	Off	1452	1443	1434										258
-22.5	Off	Off	Off	Off	1453	1444	1435										259
-45	Off	Off	Off	Off	1454	1445	1436										260
-67.5	Off	Off	Off	Off	1455	1446	1437										
-90	Off	Off	Off	Off	1456	1447	1438										261
5	Off	Off	Off	Off													256
12	Off	Off	Off	Off													255
22.5	Off	Off	Off	Off	1450	1441	1432										254
45	Off	Off	Off	Off	1449	1440	1431										253
67.5	Off	Off	Off	Off	1448	1439	1430										
90	Off	Off	Off	Off				684					686	687	252		

Table 7. Configuration 7 Run Matrix

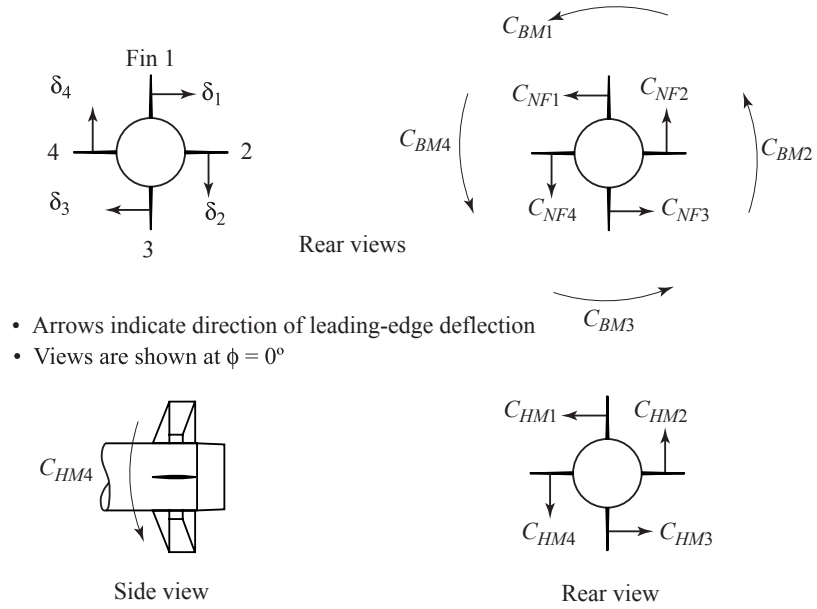
ϕ	δ_1	δ_2	δ_3	δ_4	Run number for Mach—											Fin set	
					0.60	0.90	1.18	1.70	1.75	1.90	2.00	2.10	2.36	2.86	3.95	4.63	
0	0	0	0	0					713	689		697					1
-5	0	0	0	0					705								
-12	0	0	0	0					706								
-22.5	0	0	0	0					707								
-40	0	0	0	0					708								
-45	0	0	0	0					709	696		704					
-50	0	0	0	0					710								
-67.5	0	0	0	0					711								
-90	0	0	0	0					712								
0	0	10	0	-10					714	690		698					2
-22.5	0	10	0	-10					729								
-45	0	10	0	-10					739								
-67.5	0	10	0	-10					750								
-90	0	10	0	-10					755								
0	0	20	0	-20					715	691		699					3
0	0	30	0	-30					716	692		700					4
0	0	-10	0	10					717	693		701					5
-22.5	0	-10	0	10					730								
-45	0	-10	0	10					740								
-67.5	0	-10	0	10					751								
-90	0	-10	0	10					756								
0	0	-20	0	20					718	694		702					6
-22.5	0	-20	0	20					731								
-45	0	-20	0	20					741								
-67.5	0	-20	0	20					752								
0	0	-30	0	30					719	695		703					7
0	10	10	10	10					722								9

Table 7. Concluded

ϕ	δ_1	δ_2	δ_3	δ_4	Run number for Mach—										Fin set	
					0.60	0.90	1.18	1.70	1.75	1.90	2.00	2.10	2.36	2.86	3.95	
-22.5	10	10	10	10					734							
-45	10	10	10	10					744							
-67.5	10	10	10	10					753							
-90	10	10	10	10					757							
0	20	20	20	20					728							10
0	0	-30	0	-30					727							13
0	0	20	20	0					721							14
-22.5	0	20	20	0					733							
-45	0	20	20	0					743							
0	10	-10	-10	10					720							17
-22.5	10	-10	-10	10					732							
-45	10	-10	-10	10					742							
0	-10	10	10	-10					725							20
-22.5	-10	10	10	-10					737							
-45	-10	10	10	-10					748							
0	-10	20	10	-20					726							23
-22.5	-10	20	10	-20					738							
-45	-10	20	10	-20					749							
0	10	30	10	-10					723							26
-22.5	10	30	10	-10					735							
-45	10	30	10	-10					745							
0	10	-10	10	30					724							29
-22.5	10	-10	10	30					736							
-45	10	-10	10	30					746/ 747							
-67.5	10	-10	10	30					754							



(a) Configuration parameters.



(b) Tail fin parameters.

Figure 1. Positive directions of forces, moments, and angles.



Figure 2. Computer control system shown with configuration 2.

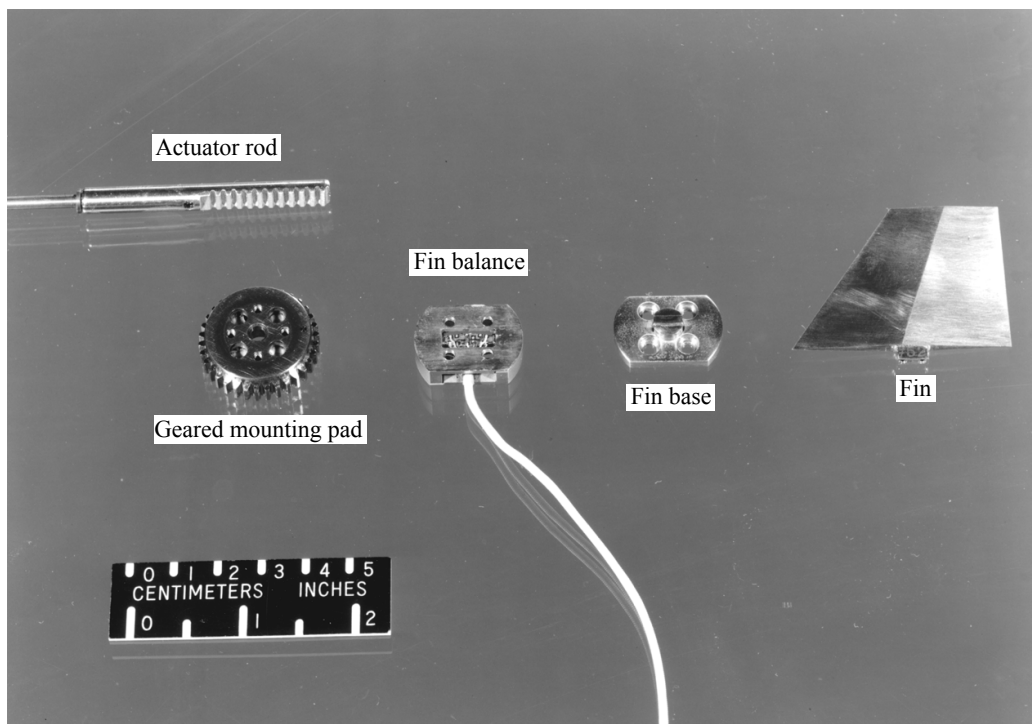


Figure 3. Tail fin mounting system (from ref. 1).

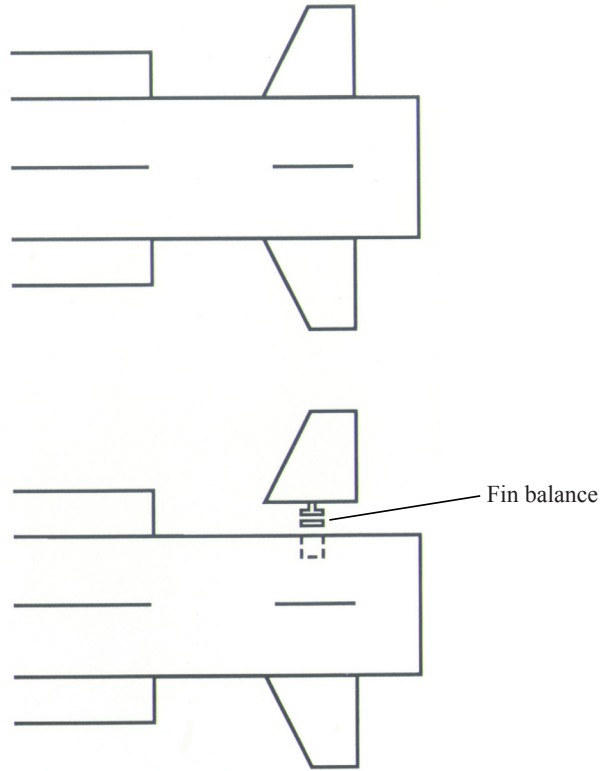


Figure 4. Tail fin balance mounting arrangement.

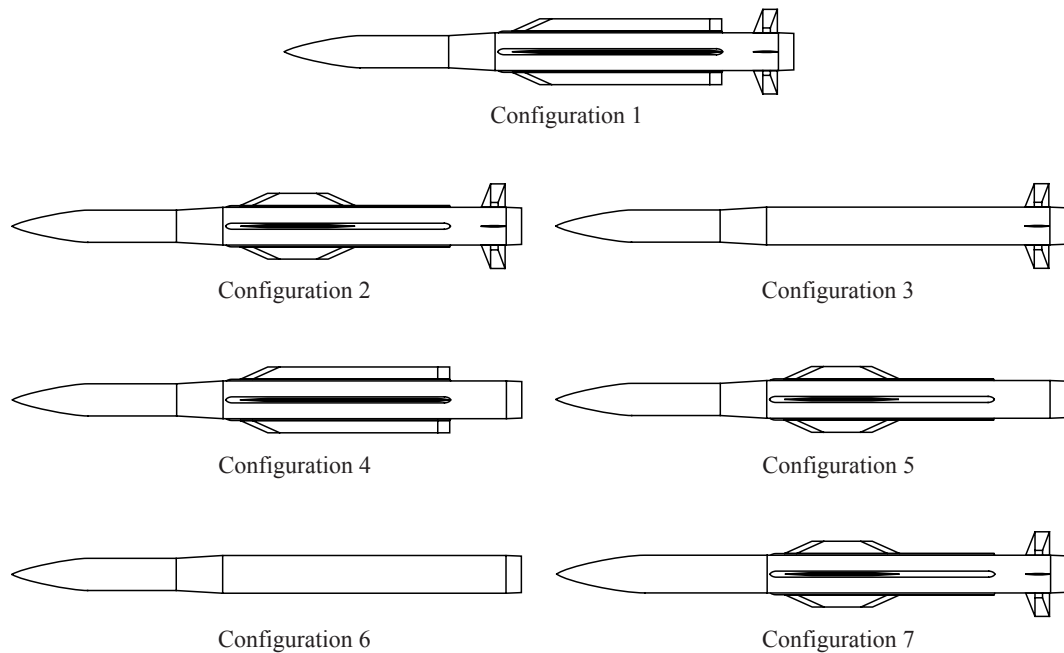


Figure 5. Configurations tested.

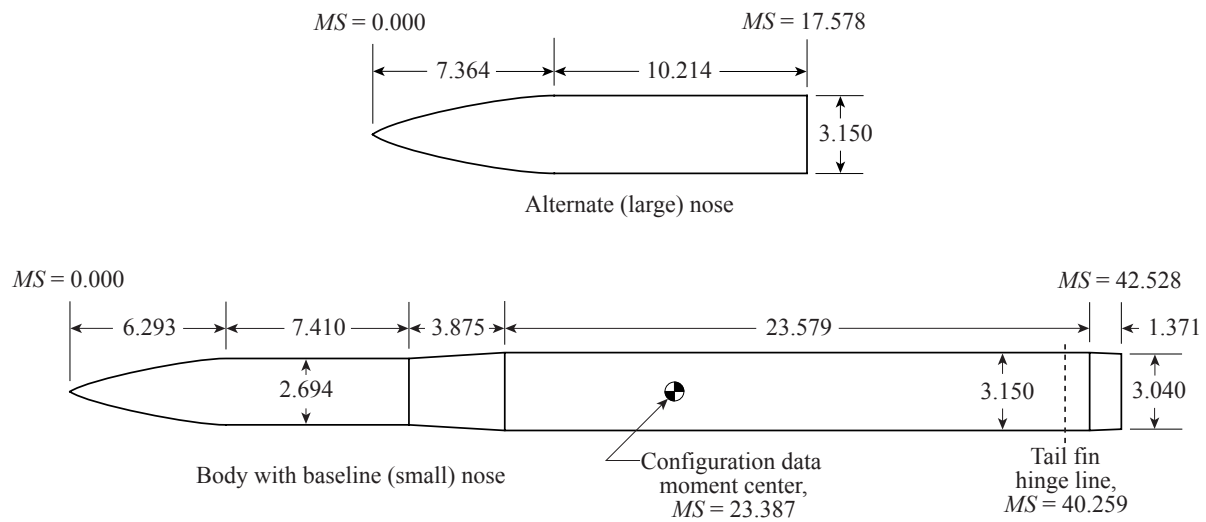


Figure 6. Body with baseline and alternate noses, dimensions in inches.

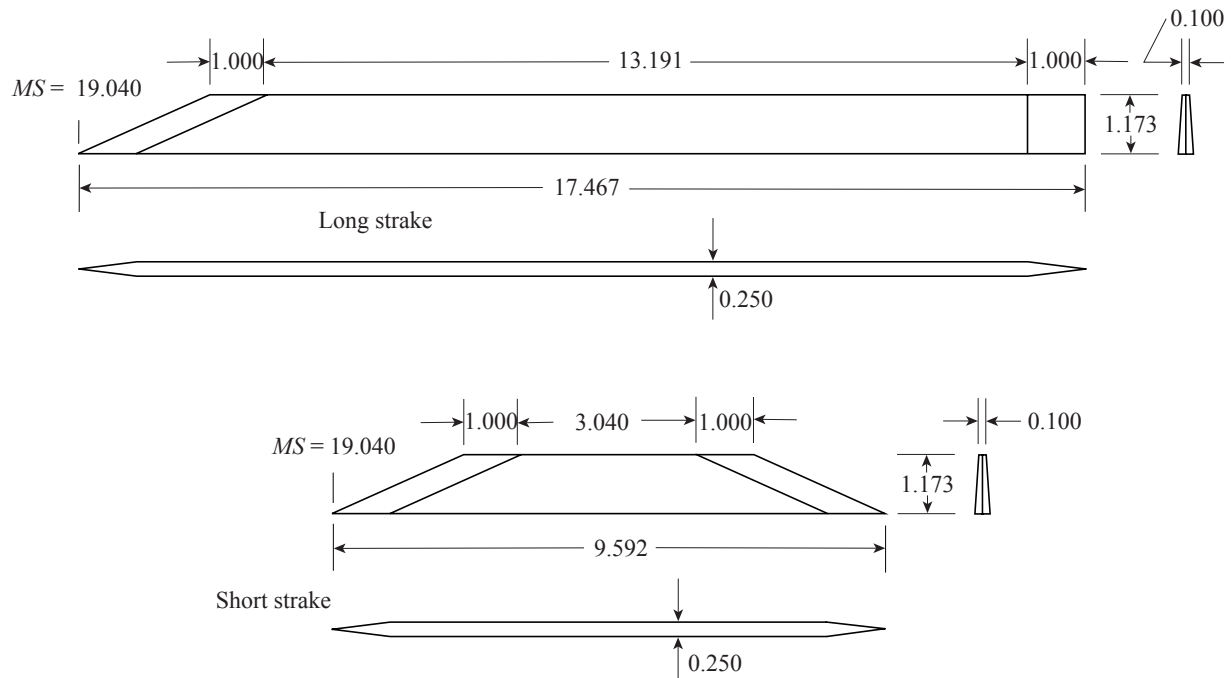


Figure 7. Long and short strakes, dimensions in inches.

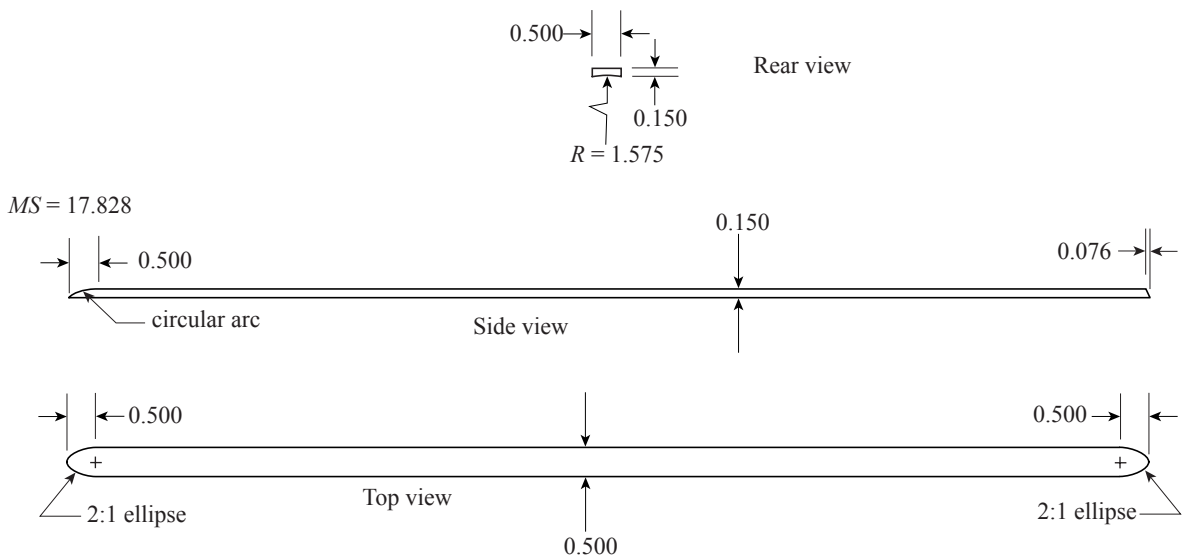


Figure 8. Strake mounting pads, dimensions in inches.

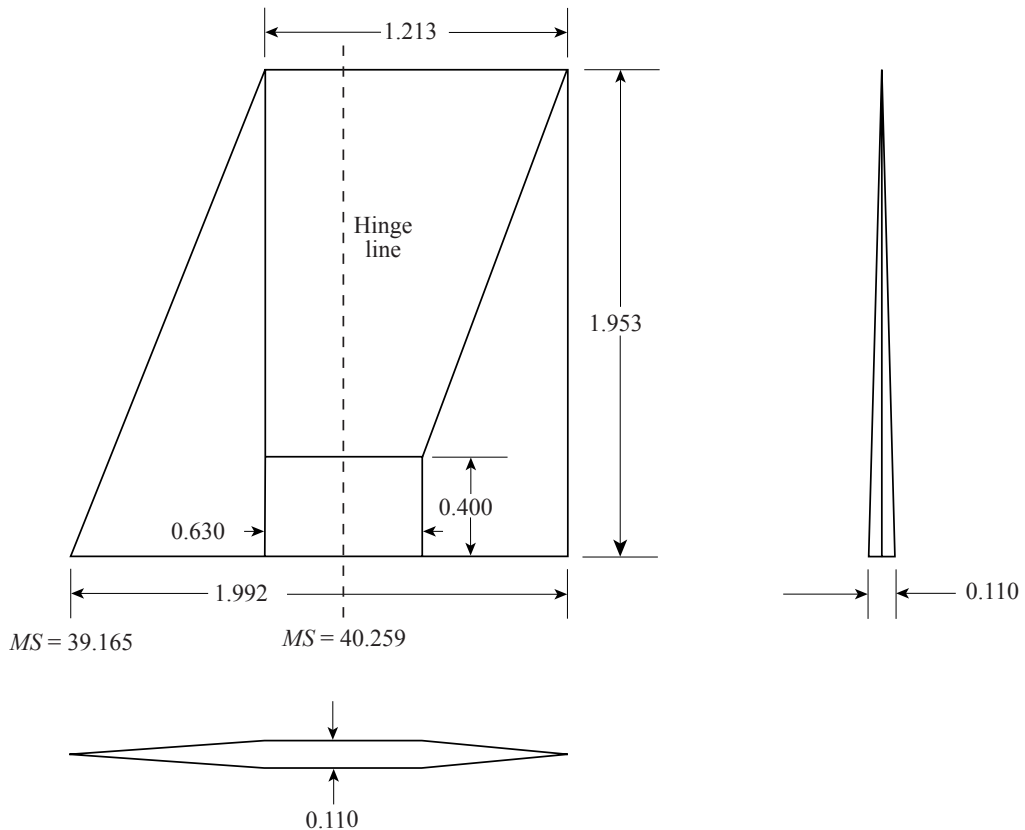


Figure 9. Tail fins, dimensions in inches.

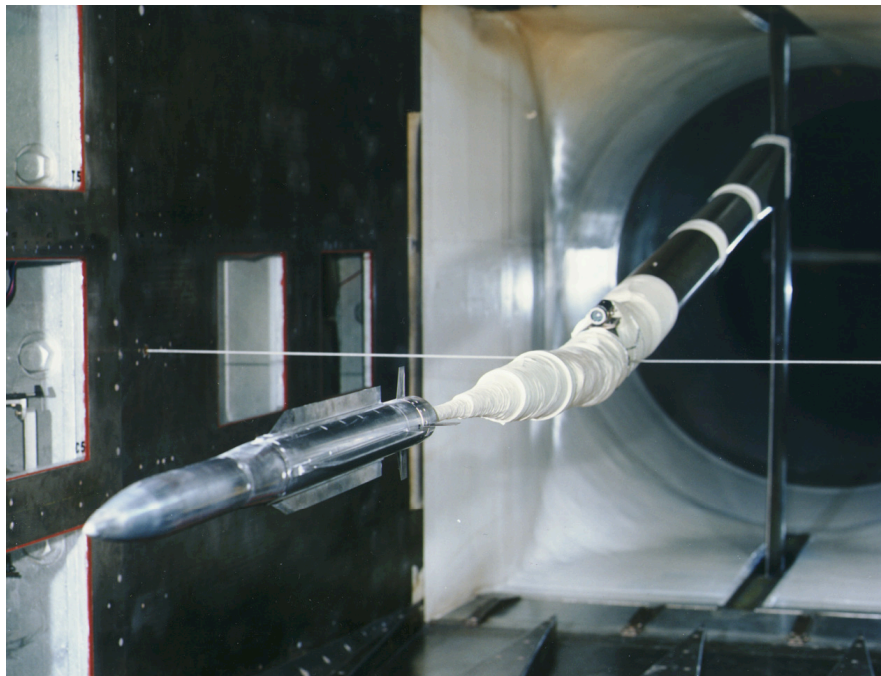


Figure 10. Configuration 1 in 8-Ft TPT showing model mounting setup.

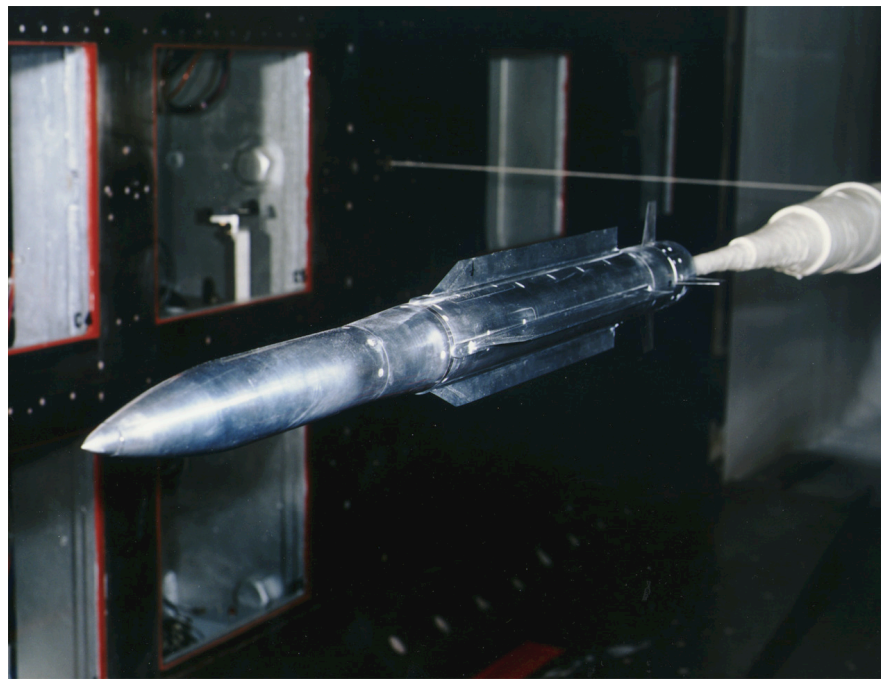


Figure 11. Front view of configuration 1 in 8-Ft TPT.

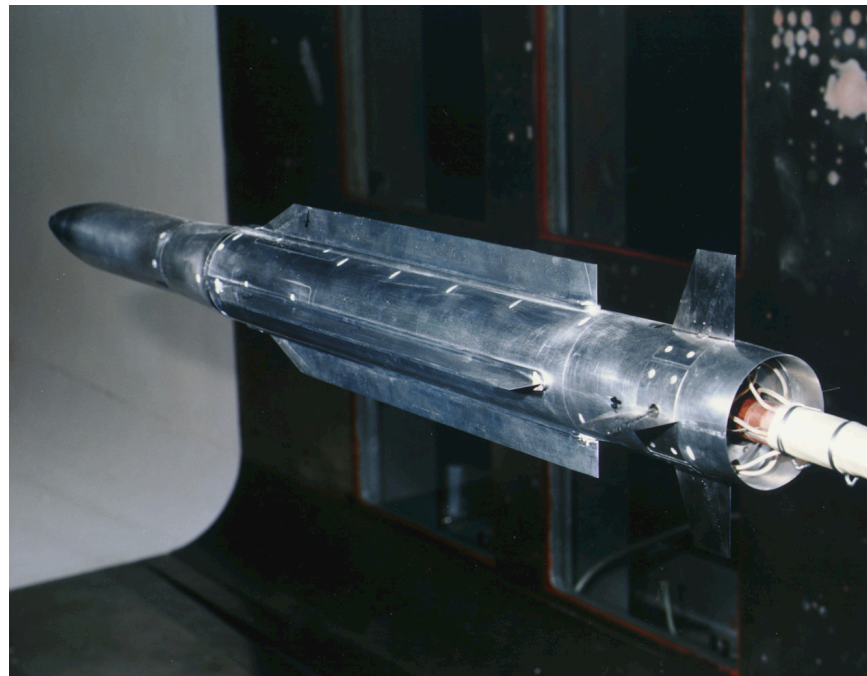


Figure 12. Rear view of configuration 1 in 8-Ft TPT.

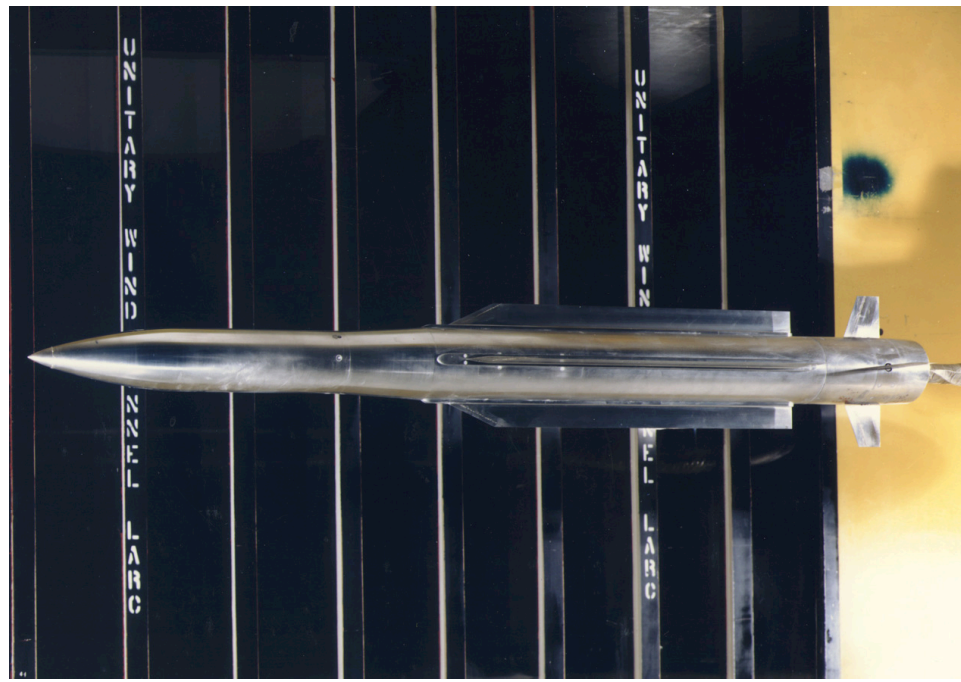


Figure 13. Side view of configuration 1 in test section 1 of UPWT.

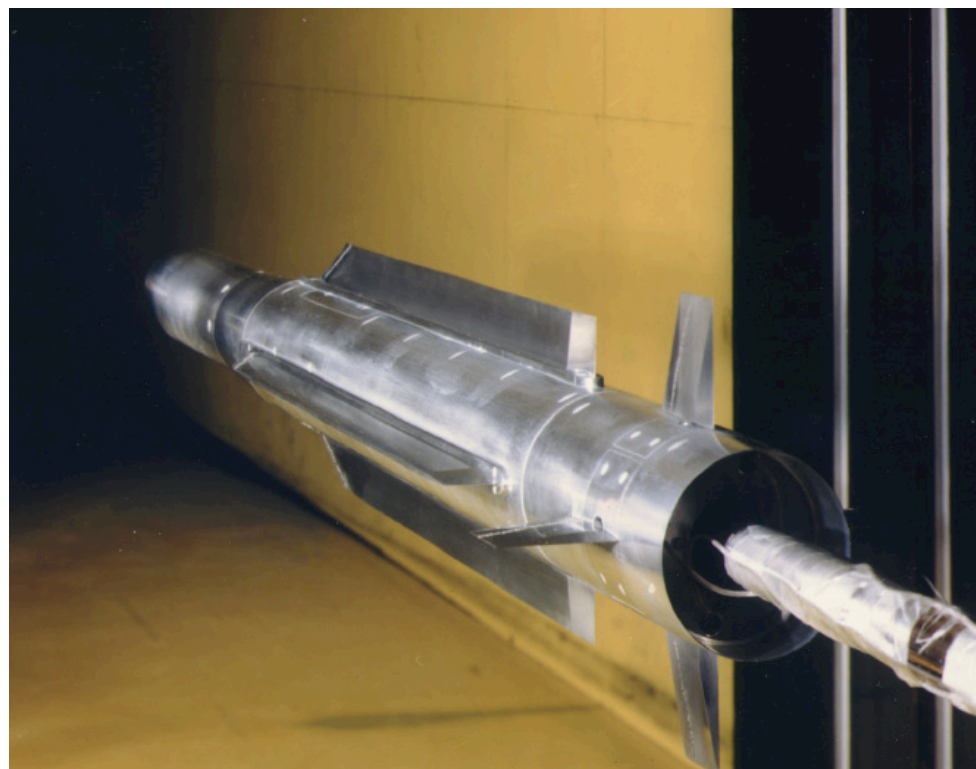


Figure 14. Rear view of configuration 1 in test section 1 of UPWT.

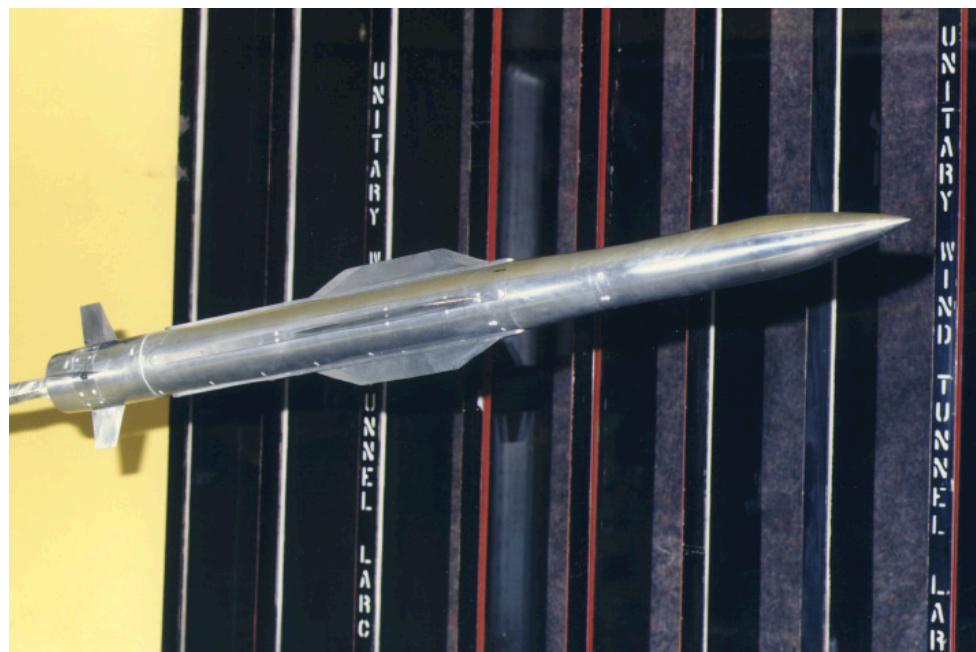


Figure 15. Side view of configuration 2 in test section 2 of UPWT.



Figure 16. Configuration 7 in UPWT test section 2 showing model mounting setup.



Figure 17. Tail fin check loads being applied to configuration 7 in test section 2 of UPWT.

STRAKE-TAIL MISSILE		TEST	1529	RUN	1	CONFIGURATION	1	MACH	2.36	PHI	90.0	
ALPHA	DEL1	DEL2	DEL3	DEL4	CNF	CAF	CPM	CRM	CYM	CSF	CNF1	CHM1
-2.15	0.0	0.0	0.0	0.0	-0.3150	0.3035	-0.0816	-0.0078	0.0351	-0.0404	-0.0227	0.0030
-1.13	0.0	0.0	0.0	0.0	-0.1533	0.2974	-0.1058	-0.0083	0.0419	-0.0414	-0.0005	0.0020
-0.17	0.0	0.0	0.0	0.0	-0.0202	0.2957	-0.0147	-0.0086	0.0465	-0.0383	0.0256	0.0013
0.84	0.0	0.0	0.0	0.0	0.1289	0.2977	0.0235	-0.0072	0.0413	-0.0367	0.0478	0.0004
1.84	0.0	0.0	0.0	0.0	0.2804	0.3015	0.0275	-0.0065	0.0369	-0.0385	0.0670	-0.0002
3.86	0.0	0.0	0.0	0.0	0.7295	0.3059	-0.3090	-0.0071	0.0354	-0.0350	0.1091	-0.0014
5.85	0.0	0.0	0.0	0.0	1.2525	0.3200	-0.8056	-0.0062	0.0445	-0.0358	0.1466	-0.0006
7.82	0.0	0.0	0.0	0.0	1.8963	0.3259	-1.6564	-0.0064	0.0540	-0.0366	0.1908	-0.0020
9.90	0.0	0.0	0.0	0.0	2.6415	0.3179	-2.6094	-0.0080	0.0585	-0.0342	0.2410	-0.0012
13.83	0.0	0.0	0.0	0.0	4.3000	0.3295	-4.5096	-0.0047	0.0509	-0.0354	0.3495	-0.0005
16.82	0.0	0.0	0.0	0.0	5.6877	0.3305	-6.1575	-0.0038	0.0313	-0.0184	0.4457	0.0000
19.84	0.0	0.0	0.0	0.0	7.1672	0.3446	-8.2222	-0.0051	0.0411	-0.0103	0.5342	0.0004
STRAKE-TAIL MISSILE		TEST	1529	RUN	2	CONFIGURATION	1	MACH	2.36	PHI	68.0	
ALPHA	DEL1	DEL2	DEL3	DEL4	CNF	CAF	CPM	CRM	CYM	CSF	CNF1	CHM1
-1.16	0.0	0.0	0.0	0.0	-0.1504	0.2976	-0.1329	-0.0031	0.0255	-0.0320	0.0030	0.0022
-0.18	0.0	0.0	0.0	0.0	-0.0038	0.2940	-0.0312	-0.0040	0.0258	-0.0293	0.0283	0.0015
0.88	0.0	0.0	0.0	0.0	0.1336	0.2946	0.0215	-0.0044	0.0420	-0.0321	0.0512	0.0008
1.84	0.0	0.0	0.0	0.0	0.2937	0.3007	0.0086	-0.0031	0.0638	-0.0432	0.0658	0.0001
3.85	0.0	0.0	0.0	0.0	0.7039	0.3070	-0.2379	0.0005	0.1716	-0.0835	0.0957	-0.0010
5.86	0.0	0.0	0.0	0.0	1.2005	0.3144	-0.6091	0.0020	0.4247	-0.1696	0.1204	-0.0023
7.87	0.0	0.0	0.0	0.0	1.7863	0.3160	-1.2192	0.0026	0.7790	-0.2783	0.1421	-0.0035
9.80	0.0	0.0	0.0	0.0	2.4048	0.3162	-1.8040	-0.0007	1.2643	-0.4163	0.1602	-0.0036
13.79	0.0	0.0	0.0	0.0	3.9014	0.3266	-3.0777	-0.0059	2.4844	-0.8316	0.2386	-0.0024
16.84	0.0	0.0	0.0	0.0	5.1593	0.3396	-4.2808	-0.1169	3.4563	-1.0841	0.3349	-0.0025
19.76	0.0	0.0	0.0	0.0	6.6182	0.3546	-6.6839	-0.2032	3.4603	-1.0771	0.4778	-0.0019

(a) Left side of page.

Figure 18. First page of ASCII column-tabulated data file.

RNFT 2.0	FINSET	1	CBM1	CNF2	CHM2	CBM2	CNF3	CHM3	CBM3	CNF4	CHM4	CBM4
-0.0457	0.0415	0.0001	-0.0116	0.0192	-0.0010	0.0226	0.0392	0.0011	-0.0102			
-0.0309	0.0409	0.0001	-0.0129	-0.0012	-0.0003	0.0098	0.0398	0.0012	-0.0096			
-0.0157	0.0419	0.0002	-0.0137	-0.0248	0.0004	-0.0043	0.0395	0.0014	-0.0093			
-0.0010	0.0420	0.0001	-0.0152	-0.0457	0.0013	-0.0214	0.0392	0.0015	-0.0087			
0.0116	0.0414	0.0002	-0.0161	-0.0668	0.0022	-0.0349	0.0385	0.0016	-0.0080			
0.0355	0.0427	0.0002	-0.0168	-0.1047	0.0030	-0.0581	0.0388	0.0018	-0.0089			
0.0552	0.0430	0.0002	-0.0183	-0.1427	0.0018	-0.0742	0.0402	0.0019	-0.0101			
0.0788	0.0432	0.0001	-0.0198	-0.1710	0.0027	-0.0957	0.0406	0.0018	-0.0103			
0.1001	0.0446	0.0002	-0.0210	9.9999	9.9999	9.9999	0.0412	0.0018	-0.0112			
0.1459	0.0435	0.0007	-0.0250	9.9999	9.9999	9.9999	0.0303	0.0010	-0.0129			
0.1866	0.0465	0.0006	-0.0282	9.9999	9.9999	9.9999	0.0228	0.0008	-0.0112			
0.2258	0.0559	0.0003	-0.0283	9.9999	9.9999	9.9999	0.0176	0.0007	-0.0078			

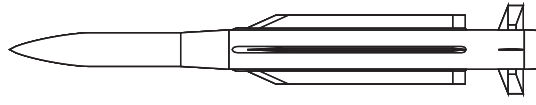
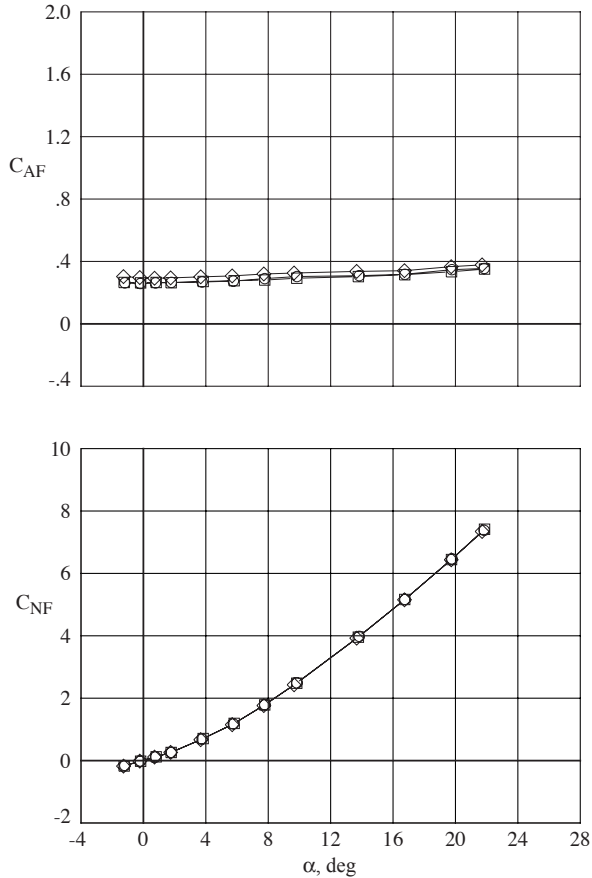
RNFT 2.0	FINSET	1	CBM1	CNF2	CHM2	CBM2	CNF3	CHM3	CBM3	CNF4	CHM4	CBM4
-0.0308	0.0296	0.0003	-0.0193	-0.0112	-0.0005	0.0063	0.0521	0.0011	-0.0038			
-0.0156	0.0398	0.0000	-0.0138	-0.0325	0.0002	-0.0081	0.0411	0.0012	-0.0095			
-0.0004	0.0487	-0.0003	-0.0079	-0.0537	0.0010	-0.0243	0.0310	0.0014	-0.0144			
0.0100	0.0613	-0.0006	-0.0022	-0.0744	0.0019	-0.0385	0.0264	0.0016	-0.0182			
0.0283	0.0827	-0.0010	0.0096	-0.1172	0.0022	-0.0641	0.0196	0.0020	-0.0256			
0.0443	0.1062	-0.0012	0.0193	-0.1594	0.0021	-0.0842	0.0142	0.0021	-0.0317			
0.0591	0.1304	-0.0009	0.0290	-0.1405	0.0000	-0.1109	0.0042	0.0029	-0.0387			
0.0632	0.1626	-0.0004	0.0414	9.9999	9.9999	9.9999	-0.1011	0.0052	-0.0513			
0.0939	0.2356	-0.0005	0.0650	9.9999	9.9999	9.9999	0.0053	0.0061	-0.0522			
0.1261	0.3077	-0.0004	0.0931	9.9999	9.9999	9.9999	0.0929	0.0062	-0.0010			
0.1902	0.3824	0.0007	0.1253	9.9999	9.9999	9.9999	0.1331	0.0051	0.0341			

(b) Right side of page.

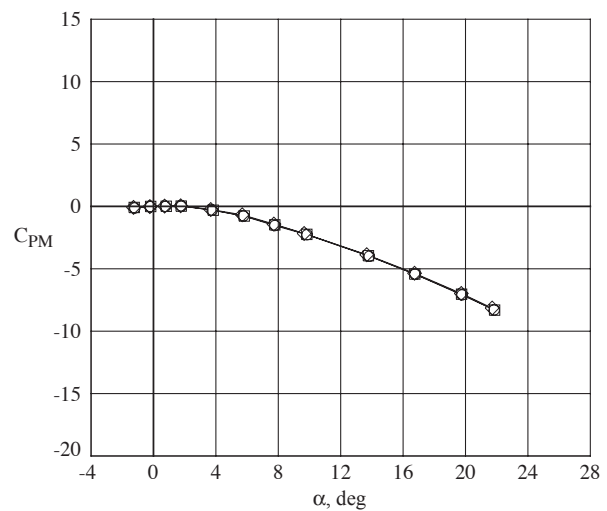
Figure 18. Concluded.

TEST	RUN	POINT	CONFIG	MACH
RNFT	H0	Q	PINF	TTO
ALPHA	PHI	DEL1	DEL2	DEL3
DEL4	CNF1	CHM1	CBM1	CNF2
CHM2	CBM2	CNF3	CHM3	CBM3
CNF4	CHM4	CBM4	CNFBA	CAFBA
CPMBA	CRMBA	CYMB	CSFBA	FINSET
0.1529000E+04	0.1000000E+01	0.2000000E+02	0.1000000E+01	0.2360000E+01
0.2002020E+01	0.1487660E+04	0.4222960E+03	0.1083170E+03	0.1250000E+03
-0.2151810E+01	0.9000050E+02	-0.3000000E-03	-0.3000000E-03	-0.3000000E-03
-0.3000000E-03	-0.2269000E-01	0.2950000E-02	-0.4570646E-01	0.4151000E-01
0.9000000E-04	-0.1163366E-01	0.1924000E-01	-0.1050000E-02	0.2255416E-01
0.3924000E-01	0.1120000E-02	-0.1019584E-01	-0.3150200E+00	0.3034600E+00
-0.8162000E-01	-0.7810000E-02	0.3508000E-01	-0.4041000E-01	0.1000000E+01
0.1529000E+04	0.1000000E+01	0.2100000E+02	0.1000000E+01	0.2360000E+01
0.2001770E+01	0.1487520E+04	0.4222550E+03	0.1083060E+03	0.1250000E+03
-0.1125330E+01	0.9000050E+02	-0.3000000E-03	-0.3000000E-03	-0.3000000E-03
-0.3000000E-03	-0.4900000E-03	0.2020000E-02	-0.3087166E-01	0.4089000E-01
0.1400000E-03	-0.1287474E-01	-0.1170000E-02	-0.2800000E-03	0.9765221E-02
0.3980000E-01	0.1220000E-02	-0.9596800E-02	-0.1533200E+00	0.2974300E+00
-0.1058300E+00	-0.8330000E-02	0.4193000E-01	-0.4136000E-01	0.1000000E+01
0.1529000E+04	0.1000000E+01	0.2200000E+02	0.1000000E+01	0.2360000E+01
0.2000750E+01	0.1487090E+04	0.4221330E+03	0.1082750E+03	0.1250000E+03
-0.1690600E+00	0.9000050E+02	-0.3000000E-03	-0.3000000E-03	-0.3000000E-03
-0.3000000E-03	0.2560000E-01	0.1280000E-02	-0.1573960E-01	0.4185000E-01
0.1700000E-03	-0.1372210E-01	-0.2482000E-01	0.4400000E-03	-0.4343879E-02
0.3948000E-01	0.1360000E-02	-0.9297679E-02	-0.2022000E-01	0.2957100E+00
-0.1467000E-01	-0.8620000E-02	0.4654000E-01	-0.3827000E-01	0.1000000E+01
0.1529000E+04	0.1000000E+01	0.2300000E+02	0.1000000E+01	0.2360000E+01
0.2002500E+01	0.1488530E+04	0.4225410E+03	0.1083800E+03	0.1250000E+03
0.8437200E+00	0.9000050E+02	-0.3000000E-03	-0.3000000E-03	-0.3000000E-03
-0.3000000E-03	0.4778000E-01	0.4200000E-03	-0.9754784E-03	0.4203000E-01
0.1400000E-03	-0.1515598E-01	-0.4569000E-01	0.1290000E-02	-0.2136846E-01
0.3916000E-01	0.1460000E-02	-0.8708558E-02	0.1289200E+00	0.2977500E+00
0.2354000E-01	-0.7210000E-02	0.4126000E-01	-0.3667000E-01	0.1000000E+01
0.1529000E+04	0.1000000E+01	0.2400000E+02	0.1000000E+01	0.2360000E+01
0.2000200E+01	0.1487520E+04	0.4222550E+03	0.1083060E+03	0.1250000E+03
0.1843610E+01	0.9000050E+02	-0.3000000E-03	-0.3000000E-03	-0.3000000E-03
-0.3000000E-03	0.6700000E-01	-0.2100000E-03	0.1156800E-01	0.4139000E-01
0.2300000E-03	-0.1609774E-01	-0.6679000E-01	0.2150000E-02	-0.3487586E-01
0.3853000E-01	0.1570000E-02	-0.7974979E-02	0.2803800E+00	0.3014600E+00
0.2750000E-01	-0.6520000E-02	0.3688000E-01	-0.3851000E-01	0.1000000E+01
0.1529000E+04	0.1000000E+01	0.2500000E+02	0.1000000E+01	0.2360000E+01
0.2000500E+01	0.1488530E+04	0.4225410E+03	0.1083800E+03	0.1250000E+03
0.3856540E+01	0.9000050E+02	-0.3000000E-03	-0.3000000E-03	-0.3000000E-03
-0.3000000E-03	0.1090900E+00	-0.1420000E-02	0.3545406E-01	0.4270000E-01
0.2200000E-03	-0.1678820E-01	-0.1046600E+00	0.2980000E-02	-0.5809845E-01
0.3876000E-01	0.1750000E-02	-0.8902160E-02	0.7294900E+00	0.3058800E+00
-0.3090300E+00	-0.7110000E-02	0.3543000E-01	-0.3502000E-01	0.1000000E+01

Figure 19. First page of free-format ASCII SIF data file.

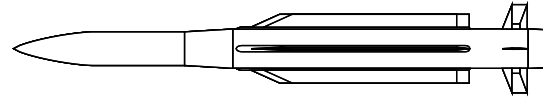
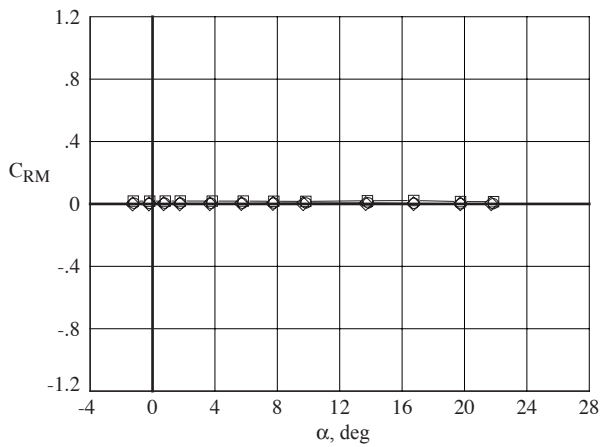
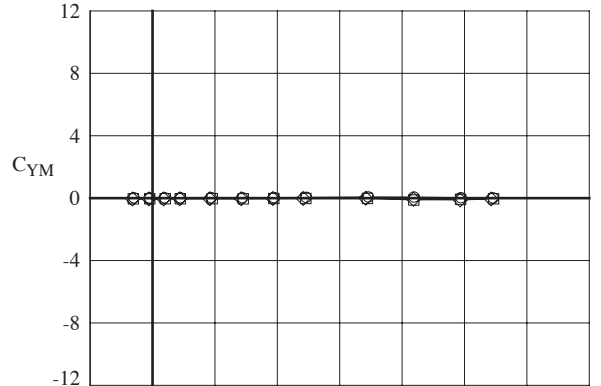


Run	Config	Mach	ϕ	δ_1	δ_2	δ_3	δ_4	$\delta_p/\delta_Y/\delta_R$
○ 95	SN-LS-T	2.86	0.0	0.0	0.0	0.0	0.0	0/0/0
□ 89	SN-LS-T	2.86	-90.0	0.0	0.0	0.0	0.0	0/0/0
◇ 74	SN-LS-T	2.86	90.0	0.0	0.0	0.0	0.0	0/0/0

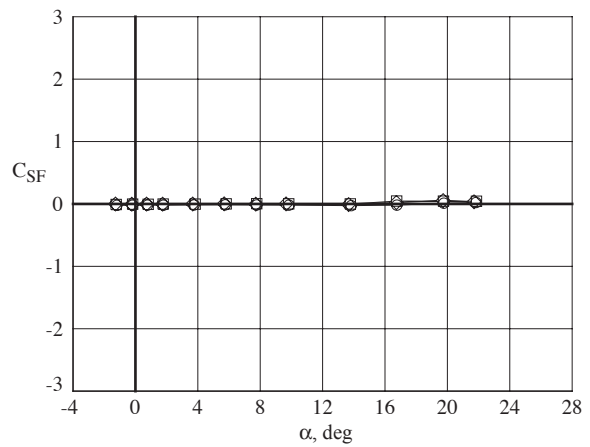


(a) Configuration longitudinal loads.

Figure 20. Data repeatability assessment.

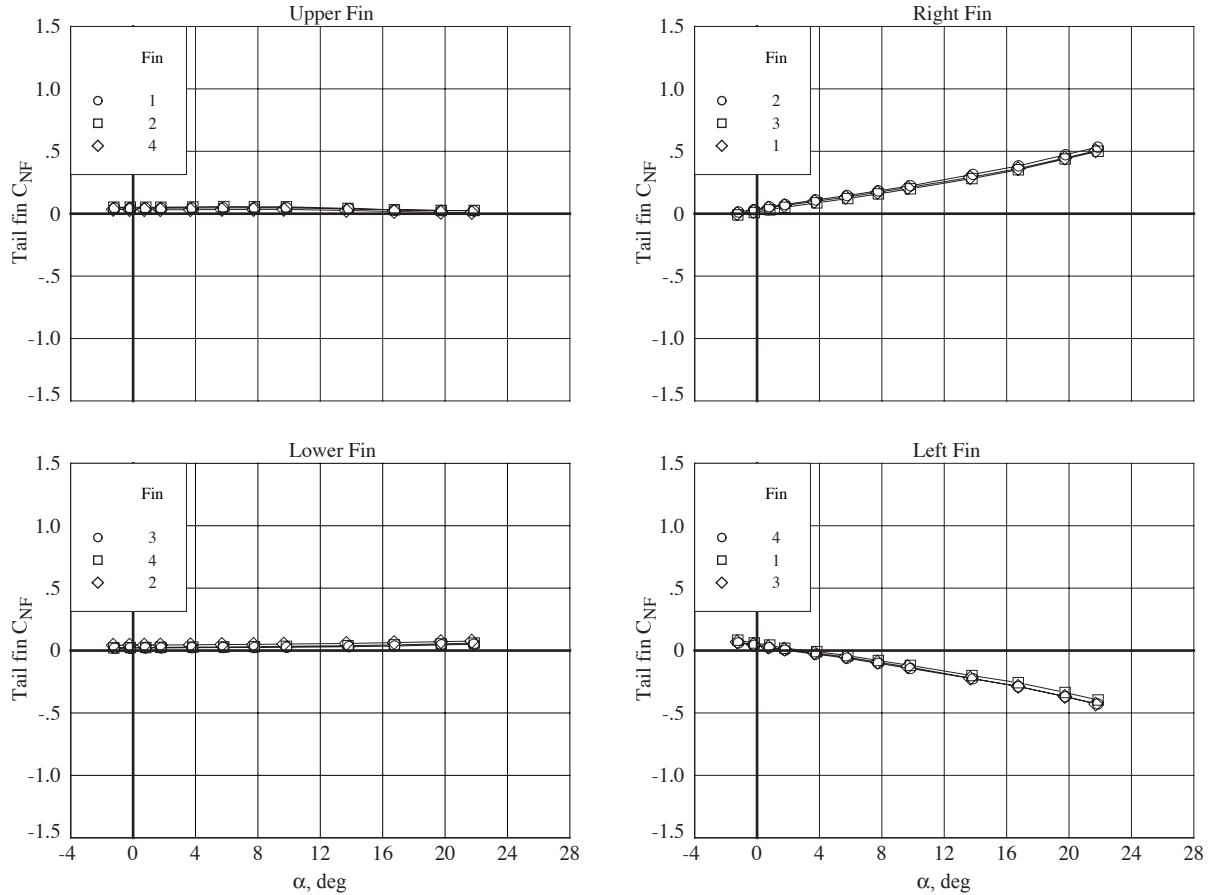


Run	Config	Mach	ϕ	δ_1	δ_2	δ_3	δ_4	$\delta_p/\delta_Y/\delta_R$
○ 95	SN-LS-T	2.86	0.0	0.0	0.0	0.0	0.0	0/0/0
□ 89	SN-LS-T	2.86	-90.0	0.0	0.0	0.0	0.0	0/0/0
◇ 74	SN-LS-T	2.86	90.0	0.0	0.0	0.0	0.0	0/0/0



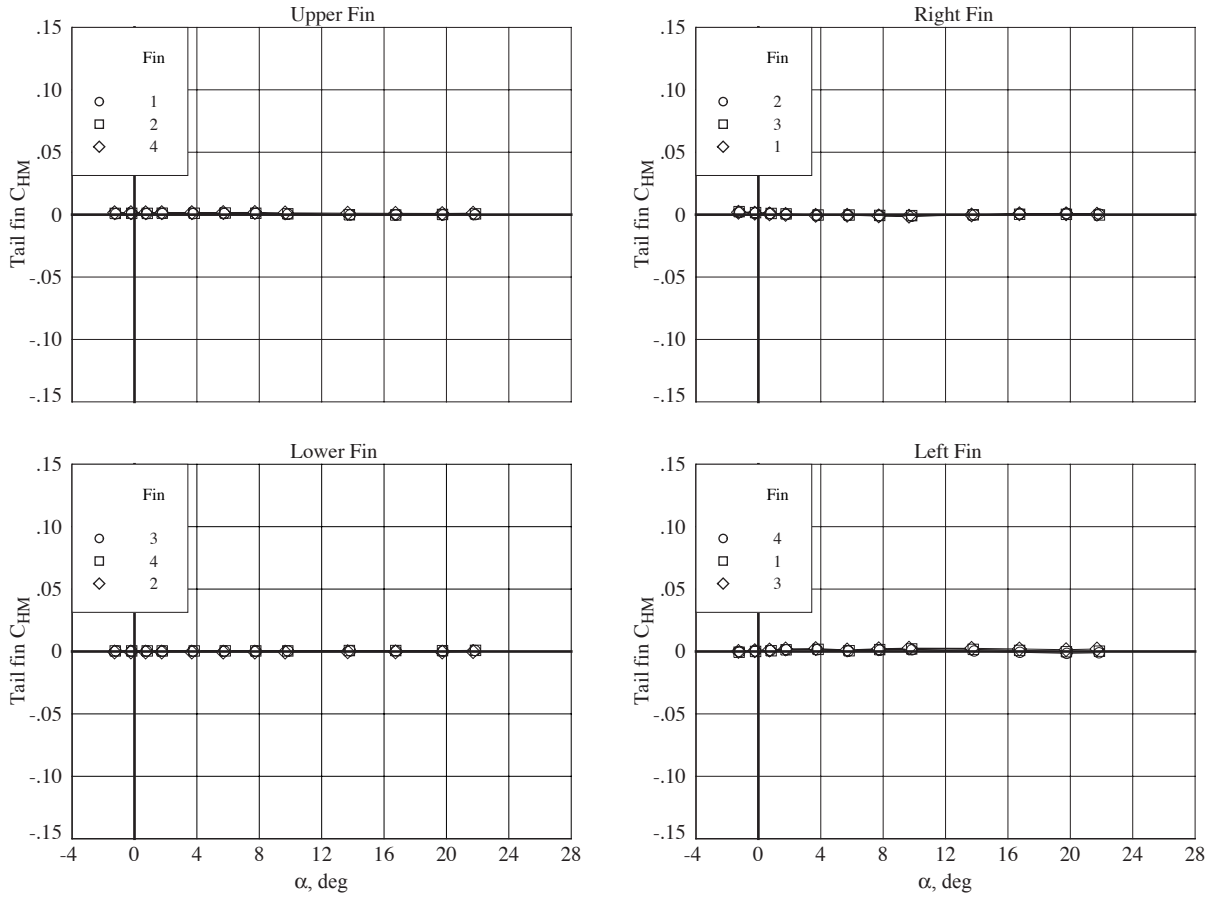
(b) Configuration lateral-directional loads.

Figure 20. Continued.



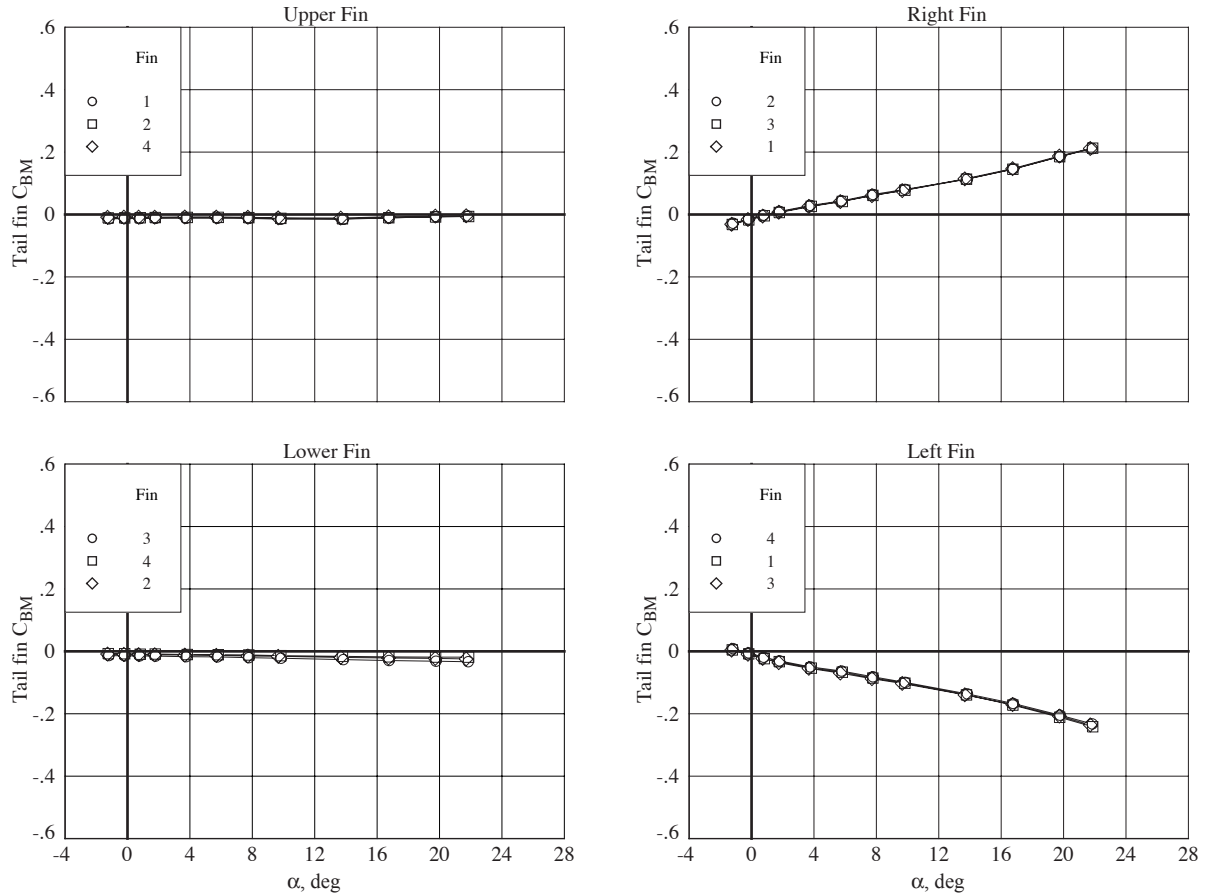
(c) Tail fin normal force.

Figure 20. Continued.



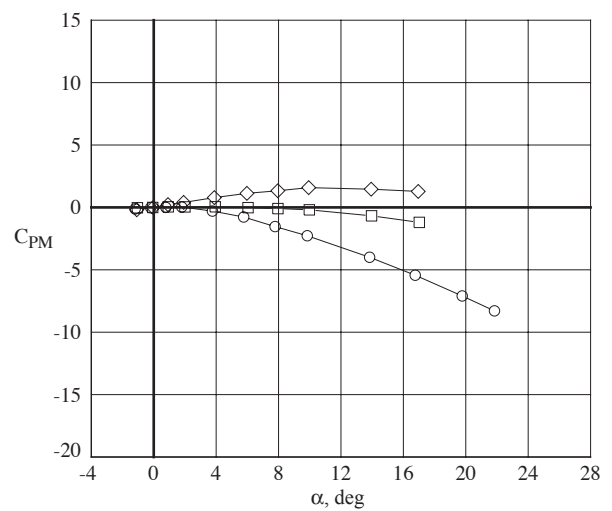
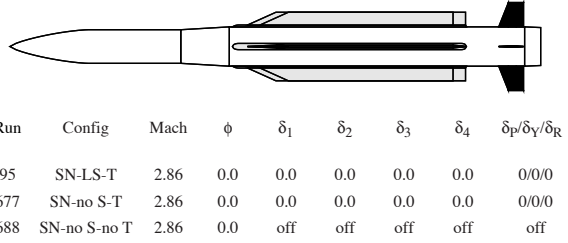
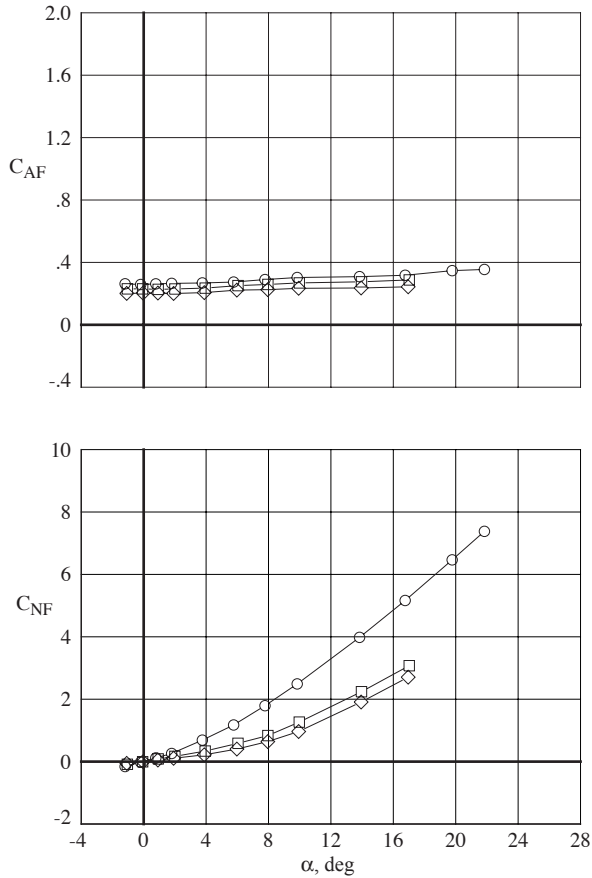
(d) Tail fin hinge moment.

Figure 20. Continued.



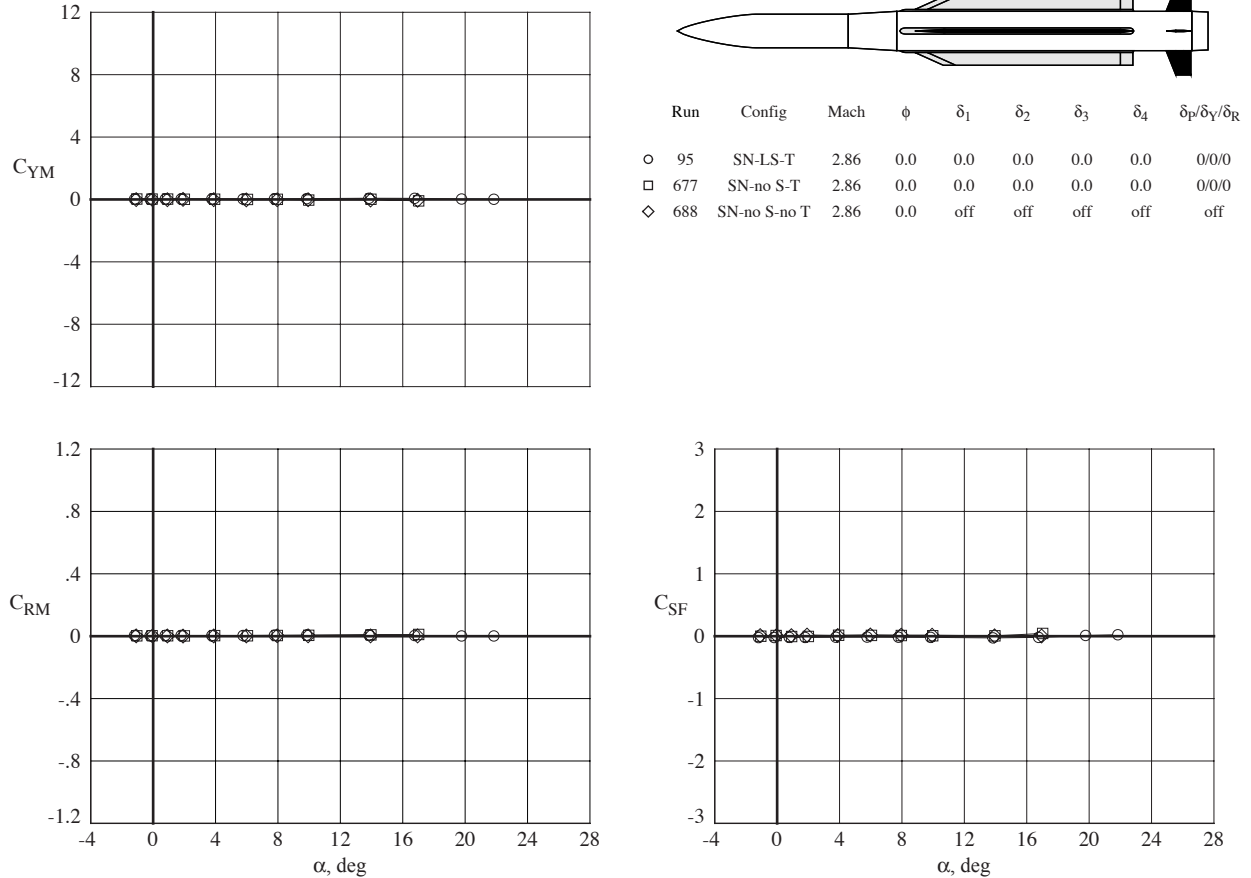
(e) Tail fin bending moment.

Figure 20. Concluded.



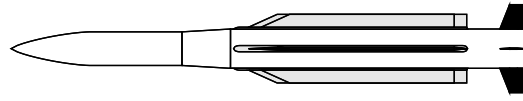
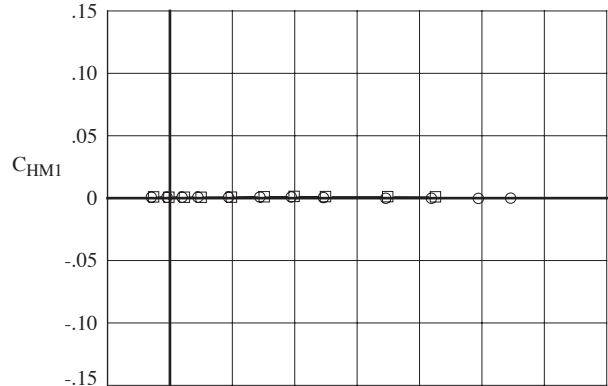
(a) Configuration longitudinal loads.

Figure 21. Configuration buildup.

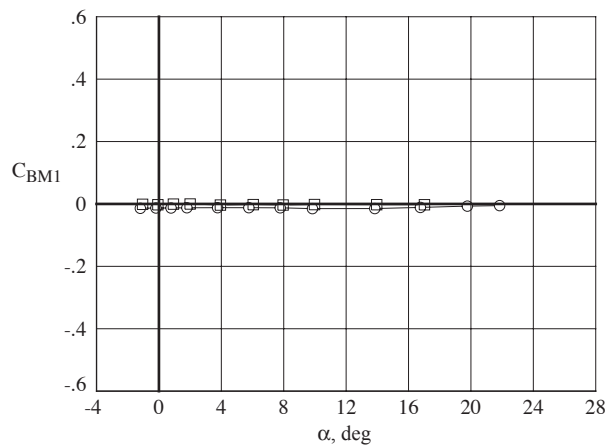
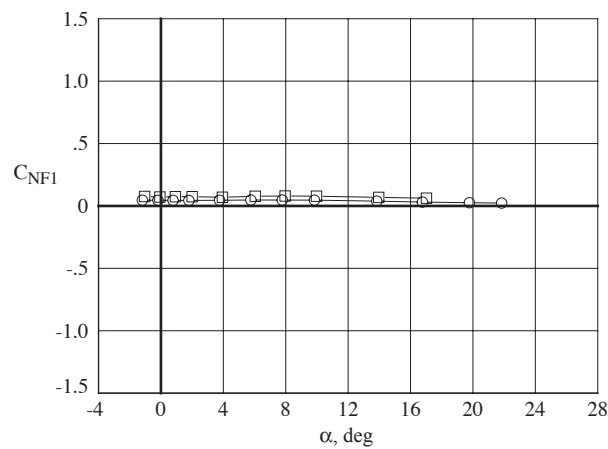


(b) Configuration lateral-directional loads.

Figure 21. Continued.

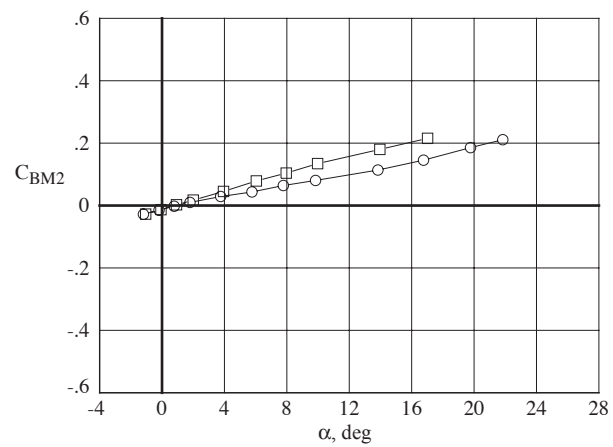
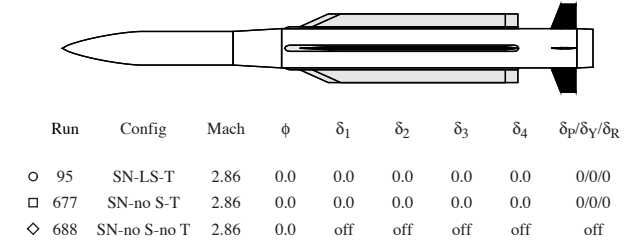
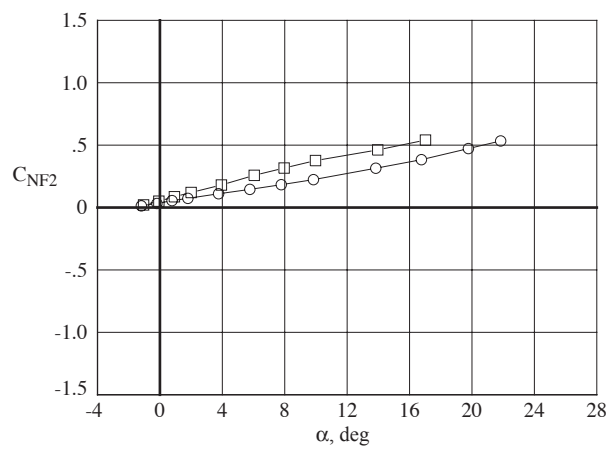
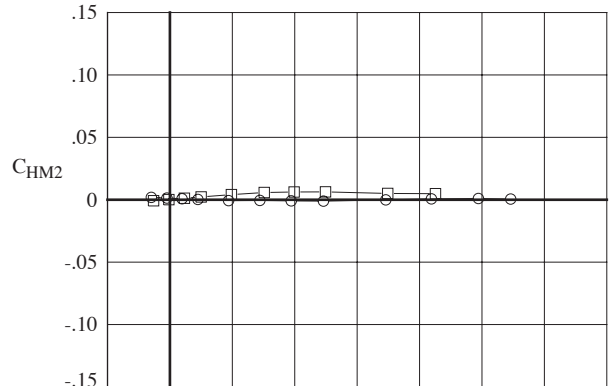


Run	Config	Mach	ϕ	δ_1	δ_2	δ_3	δ_4	$\delta_p/\delta_Y/\delta_R$
95	SN-LS-T	2.86	0.0	0.0	0.0	0.0	0.0	0/0/0
677	SN-no S-T	2.86	0.0	0.0	0.0	0.0	0.0	0/0/0
688	SN-no S-no T	2.86	0.0	off	off	off	off	off



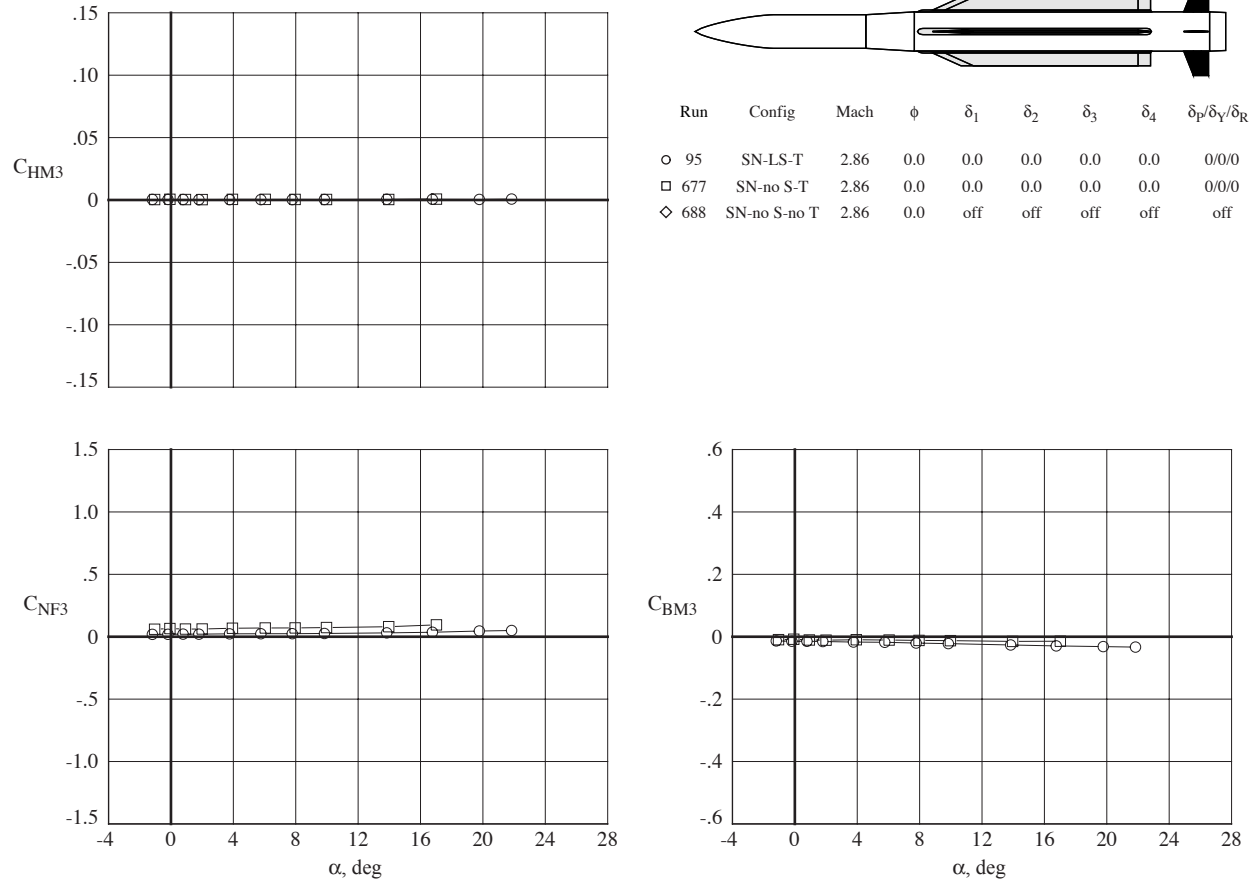
(c) Tail fin 1 loads.

Figure 21. Continued.



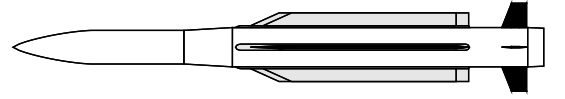
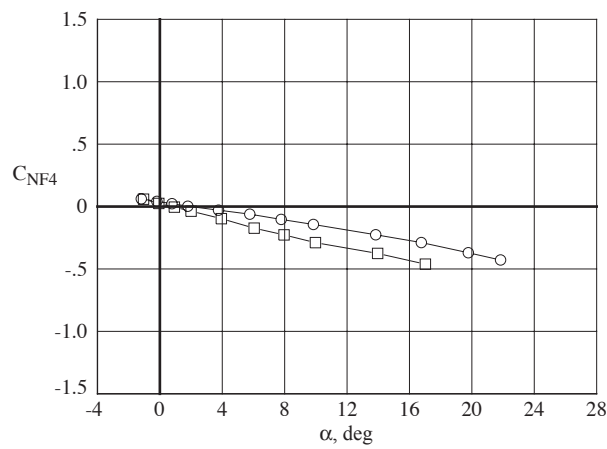
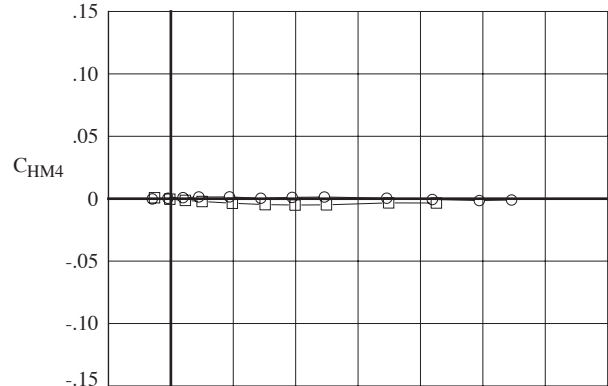
(d) Tail fin 2 loads.

Figure 21. Continued.

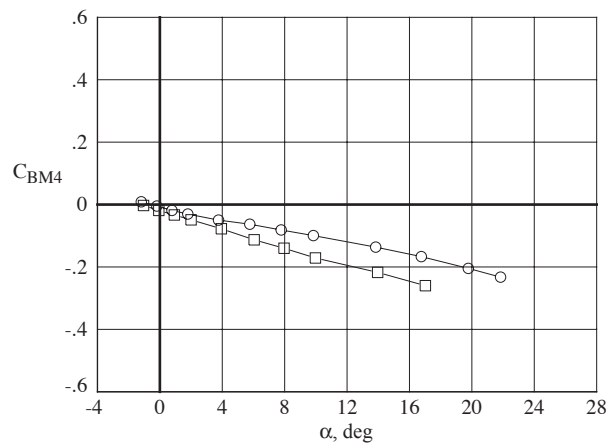


(e) Tail fin 3 loads.

Figure 21. Continued.

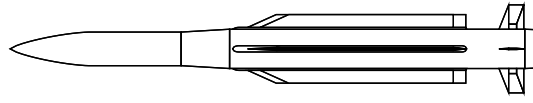
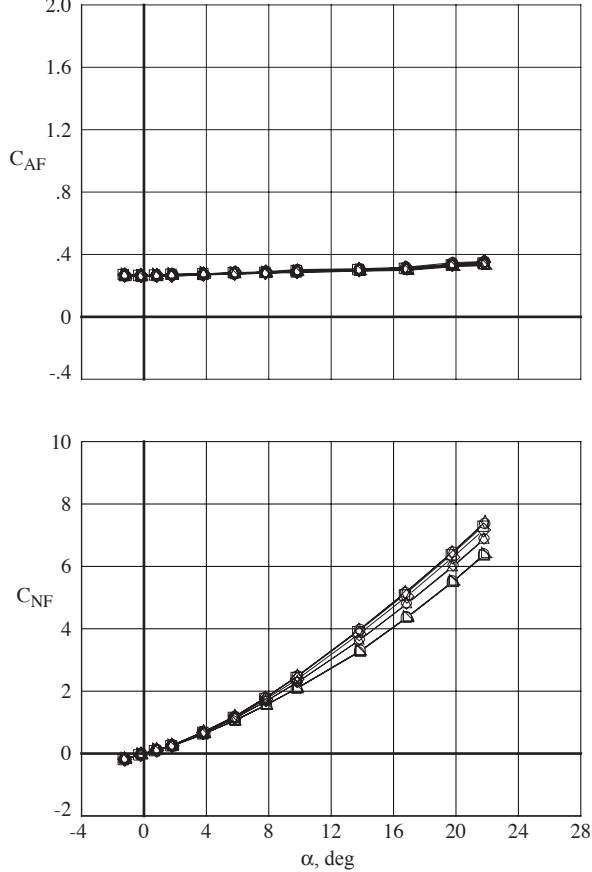


Run	Config	Mach	ϕ	δ_1	δ_2	δ_3	δ_4	$\delta_p/\delta_Y/\delta_R$
○ 95	SN-LS-T	2.86	0.0	0.0	0.0	0.0	0.0	0/0/0
□ 677	SN-no S-T	2.86	0.0	0.0	0.0	0.0	0.0	0/0/0
◇ 688	SN-no S-no T	2.86	0.0	off	off	off	off	off

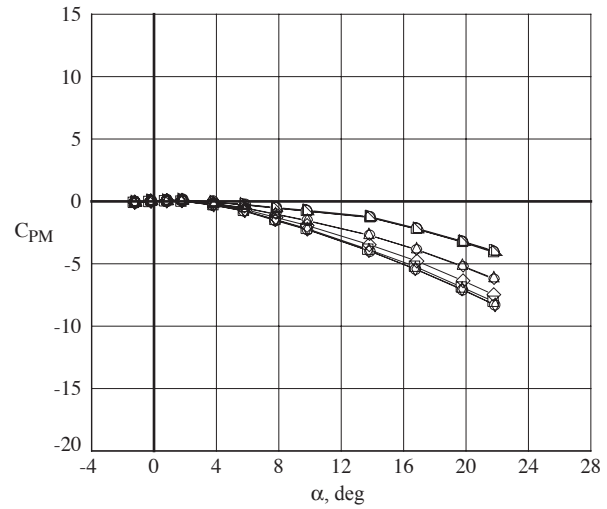


(f) Tail fin 4 loads.

Figure 21. Concluded.

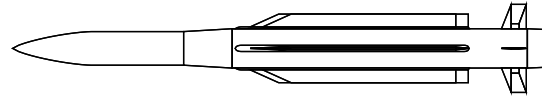
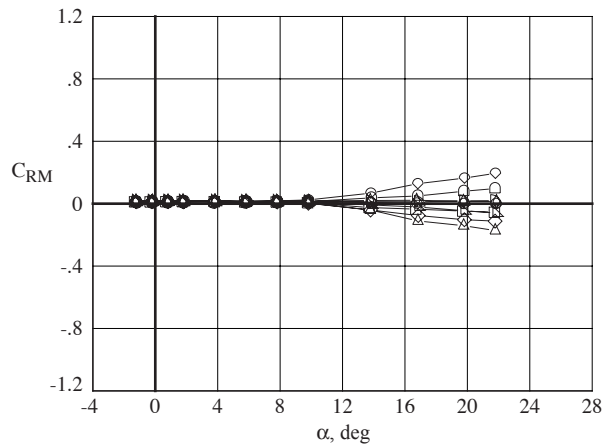
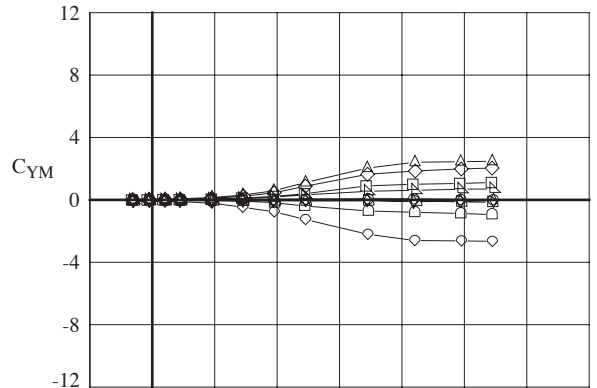


Run	Config	Mach	ϕ	δ_1	δ_2	δ_3	δ_4	$\delta_p/\delta_Y/\delta_R$
○ 95	SN-LS-T	2.86	0.0	0.0	0.0	0.0	0.0	0/0/0
□ 82	SN-LS-T	2.86	-5.0	0.0	0.0	0.0	0.0	0/0/0
◇ 83	SN-LS-T	2.86	-12.0	0.0	0.0	0.0	0.0	0/0/0
△ 84	SN-LS-T	2.86	-22.0	0.0	0.0	0.0	0.0	0/0/0
▽ 85	SN-LS-T	2.86	-40.0	0.0	0.0	0.0	0.0	0/0/0
▷ 86	SN-LS-T	2.86	-45.0	0.0	0.0	0.0	0.0	0/0/0
◁ 87	SN-LS-T	2.86	-50.0	0.0	0.0	0.0	0.0	0/0/0
◊ 88	SN-LS-T	2.86	-68.0	0.0	0.0	0.0	0.0	0/0/0
♦ 89	SN-LS-T	2.86	-90.0	0.0	0.0	0.0	0.0	0/0/0

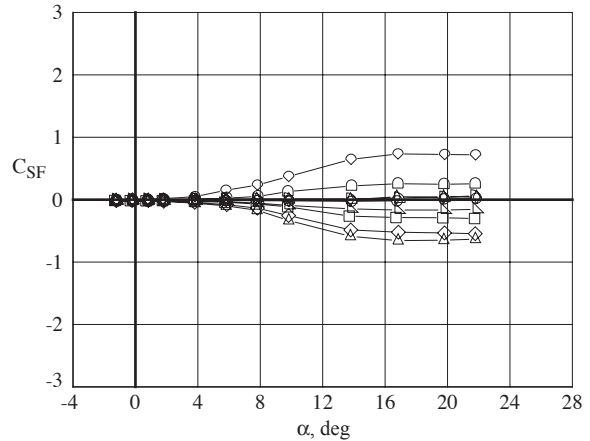


(a) Configuration longitudinal loads.

Figure 22. Effects of roll angle.

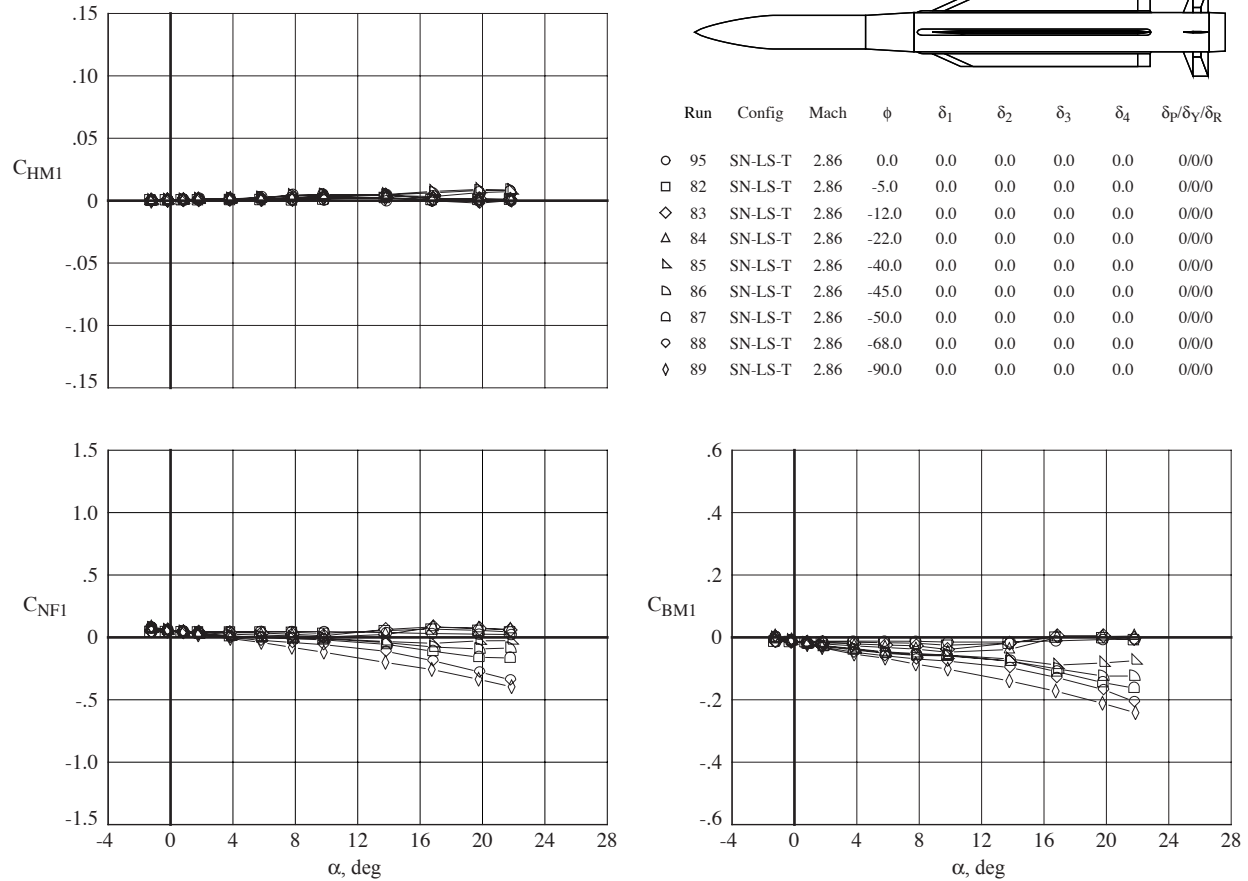


Run	Config	Mach	ϕ	δ_1	δ_2	δ_3	δ_4	$\delta_P/\delta_Y/\delta_R$
○ 95	SN-LS-T	2.86	0.0	0.0	0.0	0.0	0.0	0/0/0
□ 82	SN-LS-T	2.86	-5.0	0.0	0.0	0.0	0.0	0/0/0
◇ 83	SN-LS-T	2.86	-12.0	0.0	0.0	0.0	0.0	0/0/0
△ 84	SN-LS-T	2.86	-22.0	0.0	0.0	0.0	0.0	0/0/0
▽ 85	SN-LS-T	2.86	-40.0	0.0	0.0	0.0	0.0	0/0/0
▷ 86	SN-LS-T	2.86	-45.0	0.0	0.0	0.0	0.0	0/0/0
◁ 87	SN-LS-T	2.86	-50.0	0.0	0.0	0.0	0.0	0/0/0
○ 88	SN-LS-T	2.86	-68.0	0.0	0.0	0.0	0.0	0/0/0
◇ 89	SN-LS-T	2.86	-90.0	0.0	0.0	0.0	0.0	0/0/0



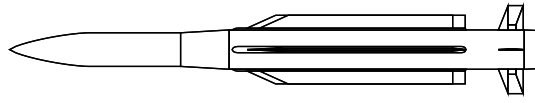
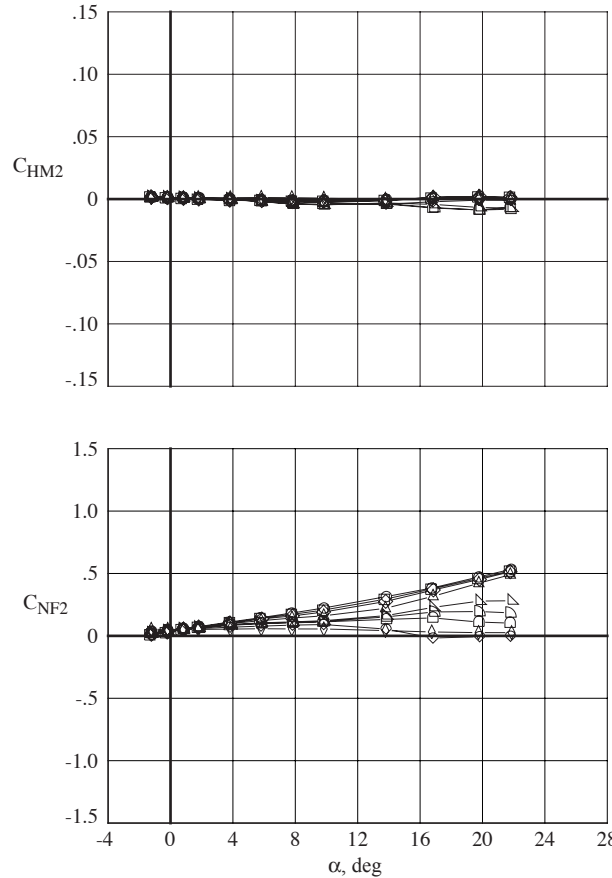
(b) Configuration lateral-directional loads.

Figure 22. Continued.

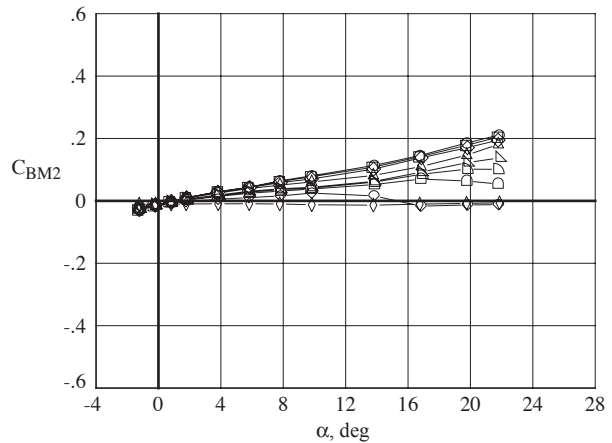
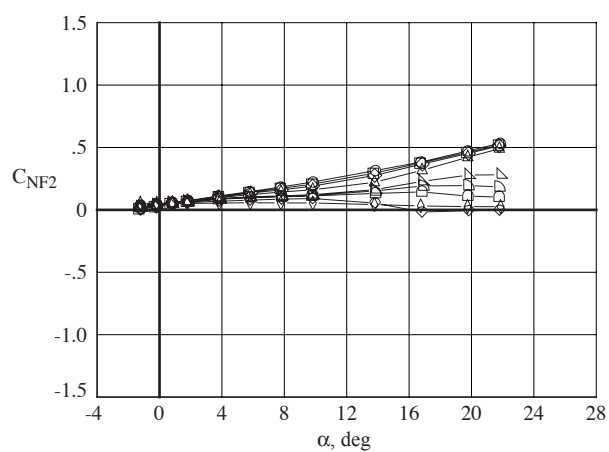


(c) Tail fin 1 loads.

Figure 22. Continued.

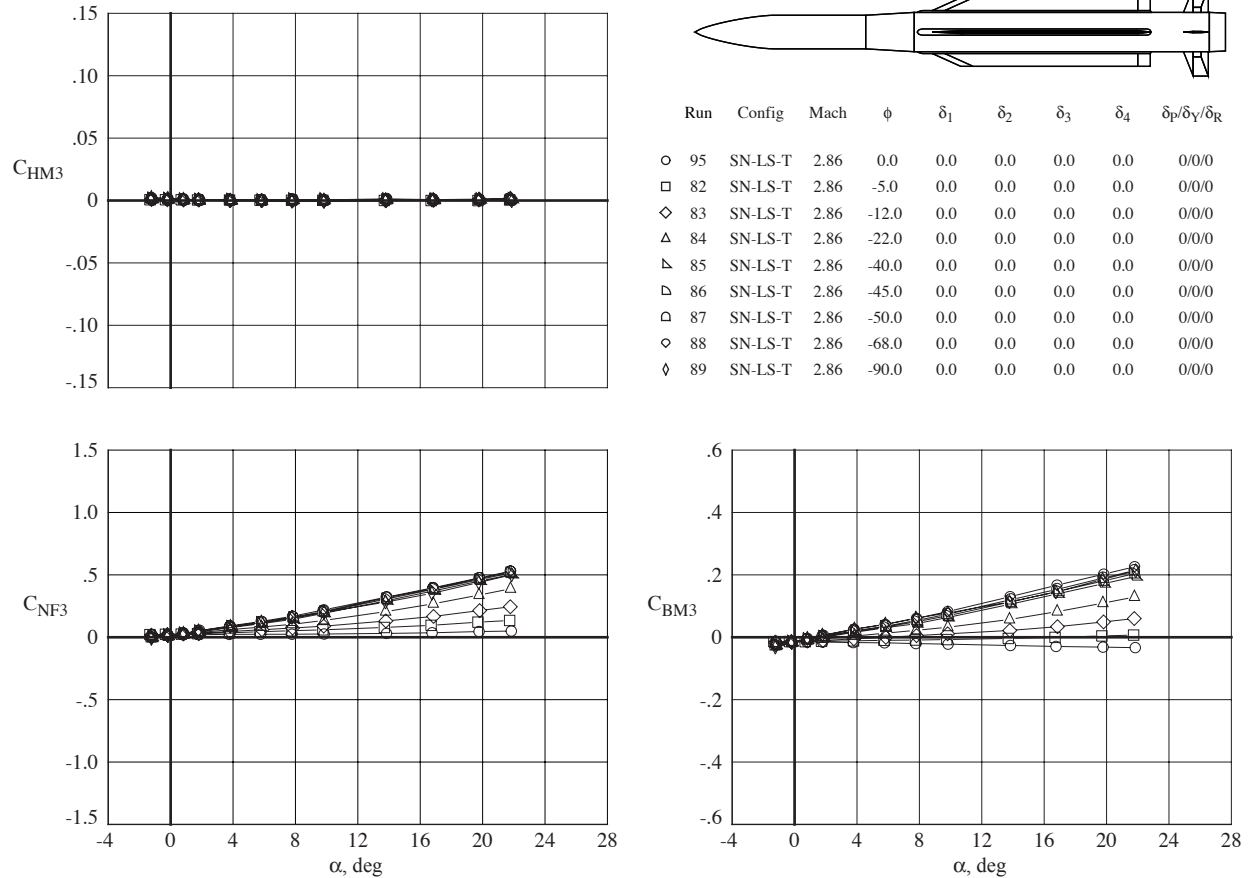


Run	Config	Mach	ϕ	δ_1	δ_2	δ_3	δ_4	$\delta_p/\delta_Y/\delta_R$
○ 95	SN-LS-T	2.86	0.0	0.0	0.0	0.0	0.0	0/0/0
□ 82	SN-LS-T	2.86	-5.0	0.0	0.0	0.0	0.0	0/0/0
◇ 83	SN-LS-T	2.86	-12.0	0.0	0.0	0.0	0.0	0/0/0
△ 84	SN-LS-T	2.86	-22.0	0.0	0.0	0.0	0.0	0/0/0
▽ 85	SN-LS-T	2.86	-40.0	0.0	0.0	0.0	0.0	0/0/0
▷ 86	SN-LS-T	2.86	-45.0	0.0	0.0	0.0	0.0	0/0/0
◁ 87	SN-LS-T	2.86	-50.0	0.0	0.0	0.0	0.0	0/0/0
◇ 88	SN-LS-T	2.86	-68.0	0.0	0.0	0.0	0.0	0/0/0
▽ 89	SN-LS-T	2.86	-90.0	0.0	0.0	0.0	0.0	0/0/0



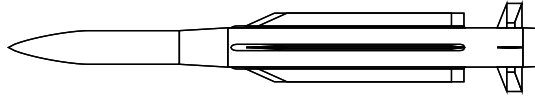
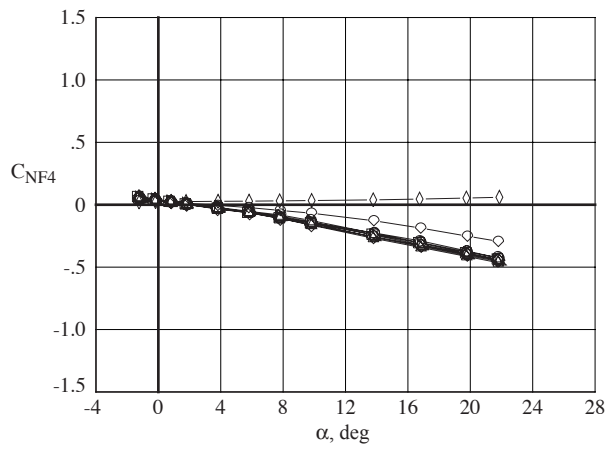
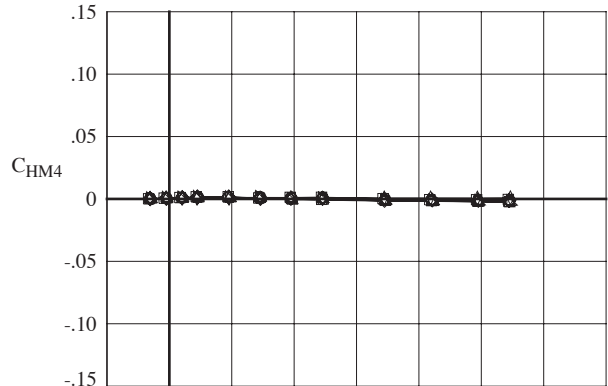
(d) Tail fin 2 loads.

Figure 22. Continued.

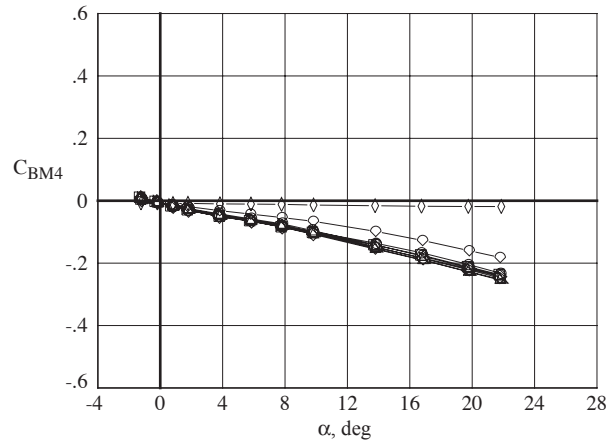


(e) Tail fin 3 loads.

Figure 22. Continued.

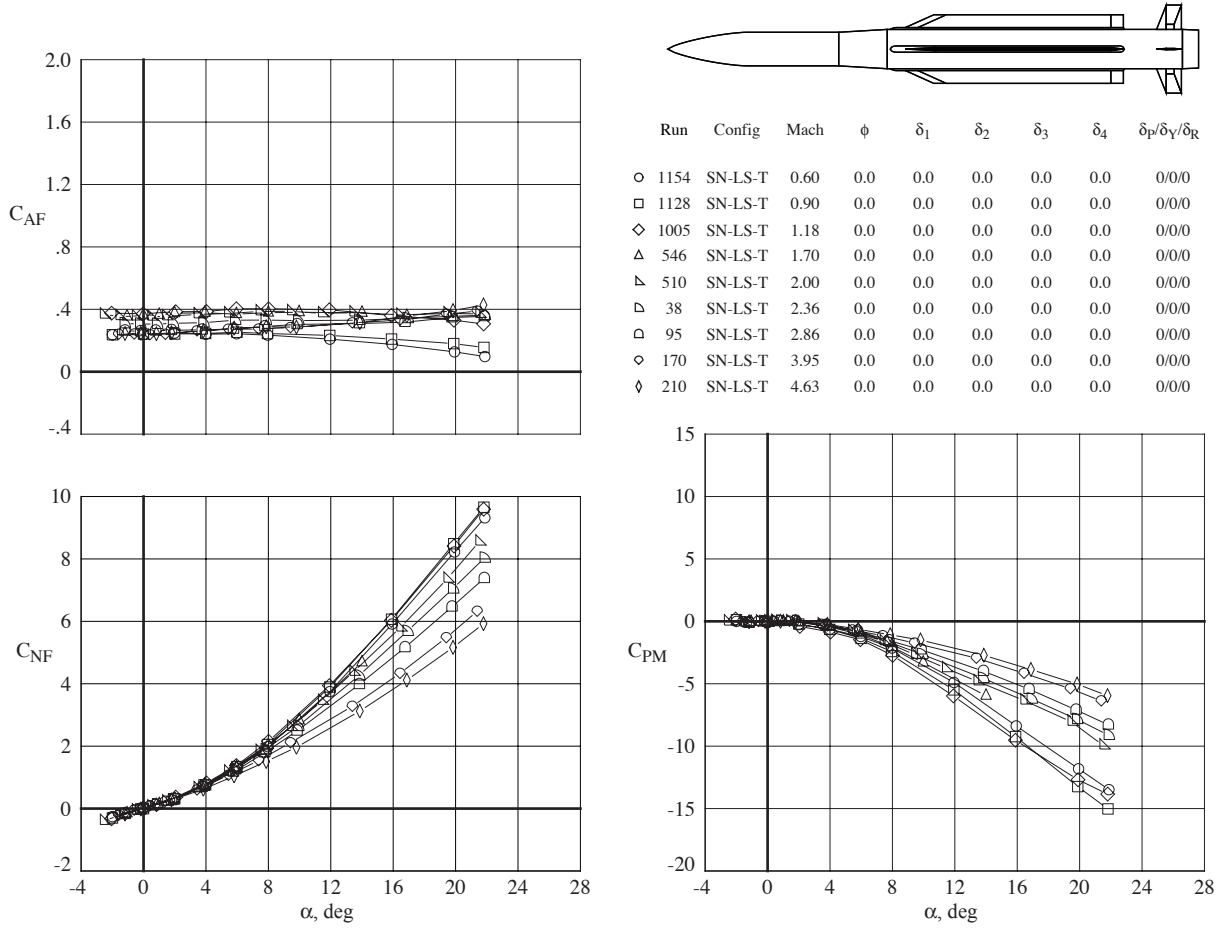


Run	Config	Mach	ϕ	δ ₁	δ ₂	δ ₃	δ ₄	δ _P /δ _Y /δ _R
○ 95	SN-LS-T	2.86	0.0	0.0	0.0	0.0	0.0	0/0/0
□ 82	SN-LS-T	2.86	-5.0	0.0	0.0	0.0	0.0	0/0/0
◇ 83	SN-LS-T	2.86	-12.0	0.0	0.0	0.0	0.0	0/0/0
△ 84	SN-LS-T	2.86	-22.0	0.0	0.0	0.0	0.0	0/0/0
▽ 85	SN-LS-T	2.86	-40.0	0.0	0.0	0.0	0.0	0/0/0
□ 86	SN-LS-T	2.86	-45.0	0.0	0.0	0.0	0.0	0/0/0
□ 87	SN-LS-T	2.86	-50.0	0.0	0.0	0.0	0.0	0/0/0
◇ 88	SN-LS-T	2.86	-68.0	0.0	0.0	0.0	0.0	0/0/0
◇ 89	SN-LS-T	2.86	-90.0	0.0	0.0	0.0	0.0	0/0/0



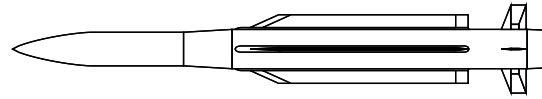
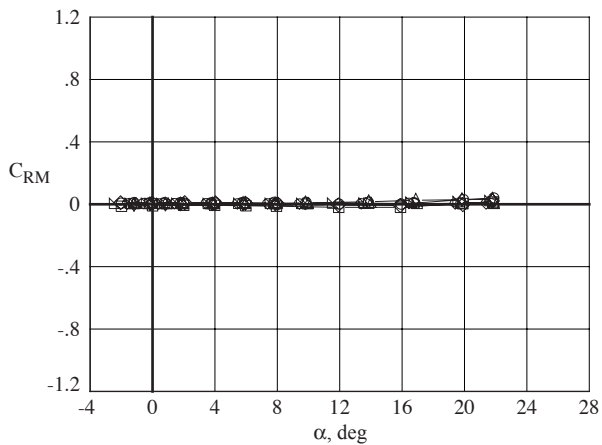
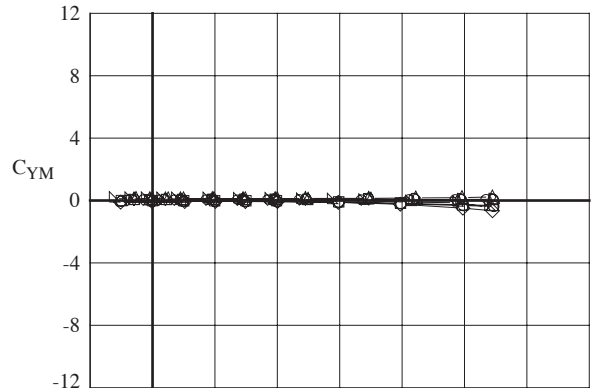
(f) Tail fin 4 loads.

Figure 22. Concluded.

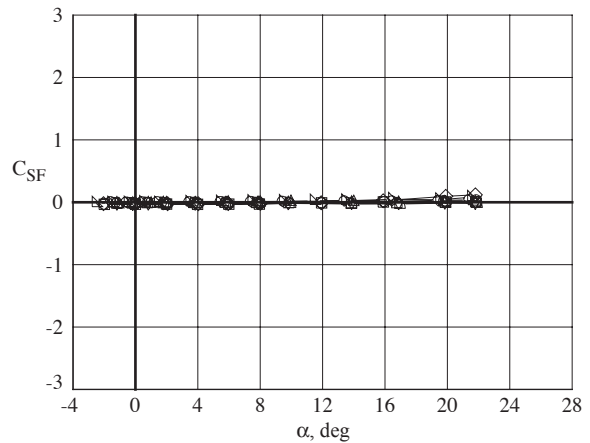


(a) Configuration longitudinal loads.

Figure 23. Effects of Mach number.

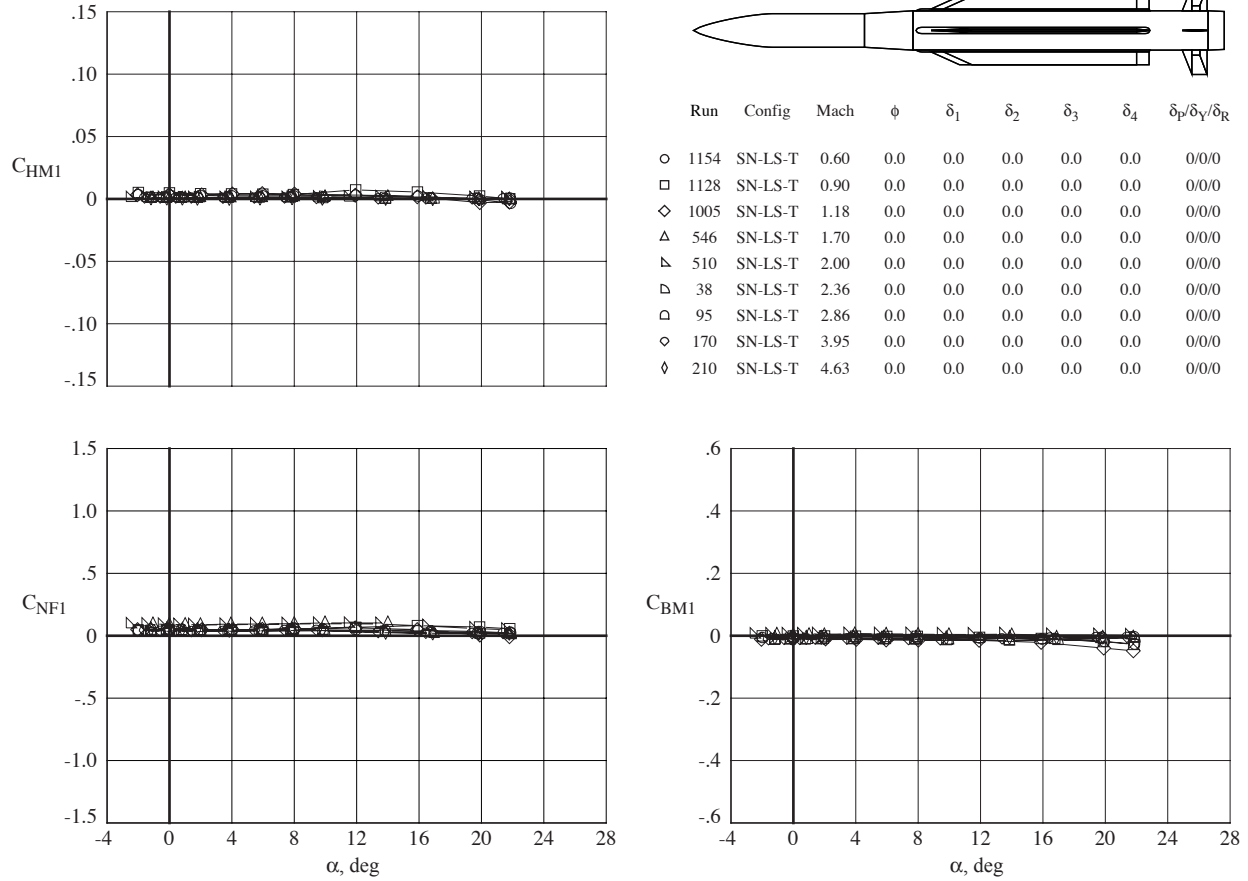


Run	Config	Mach	ϕ	δ_1	δ_2	δ_3	δ_4	$\delta_P/\delta_Y/\delta_R$
○ 1154	SN-LS-T	0.60	0.0	0.0	0.0	0.0	0.0	0/0/0
□ 1128	SN-LS-T	0.90	0.0	0.0	0.0	0.0	0.0	0/0/0
◇ 1005	SN-LS-T	1.18	0.0	0.0	0.0	0.0	0.0	0/0/0
△ 546	SN-LS-T	1.70	0.0	0.0	0.0	0.0	0.0	0/0/0
▽ 510	SN-LS-T	2.00	0.0	0.0	0.0	0.0	0.0	0/0/0
▷ 38	SN-LS-T	2.36	0.0	0.0	0.0	0.0	0.0	0/0/0
□ 95	SN-LS-T	2.86	0.0	0.0	0.0	0.0	0.0	0/0/0
◇ 170	SN-LS-T	3.95	0.0	0.0	0.0	0.0	0.0	0/0/0
◊ 210	SN-LS-T	4.63	0.0	0.0	0.0	0.0	0.0	0/0/0



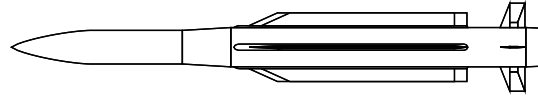
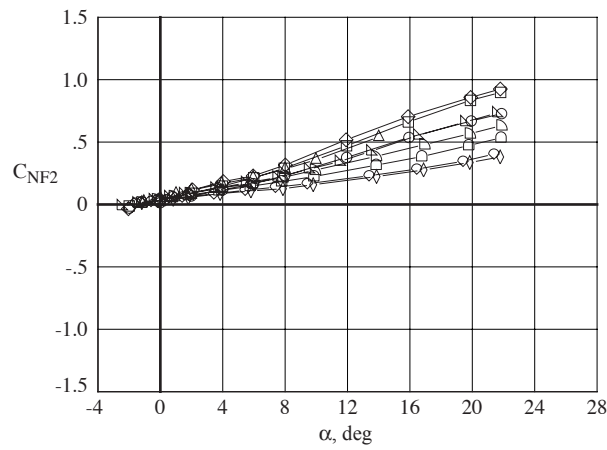
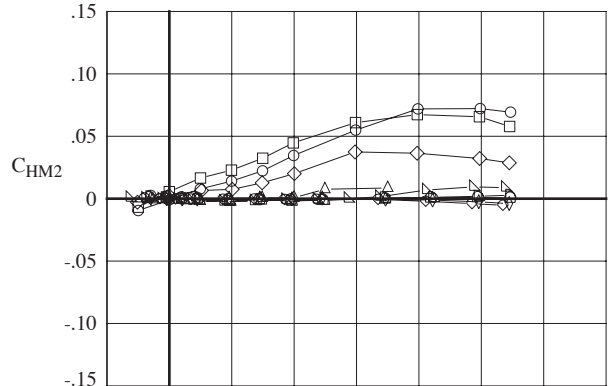
(b) Configuration lateral-directional loads.

Figure 23. Continued.

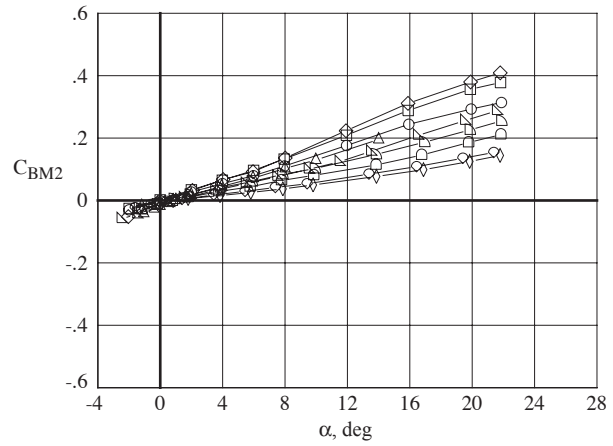


(c) Tail fin 1 loads.

Figure 23. Continued.

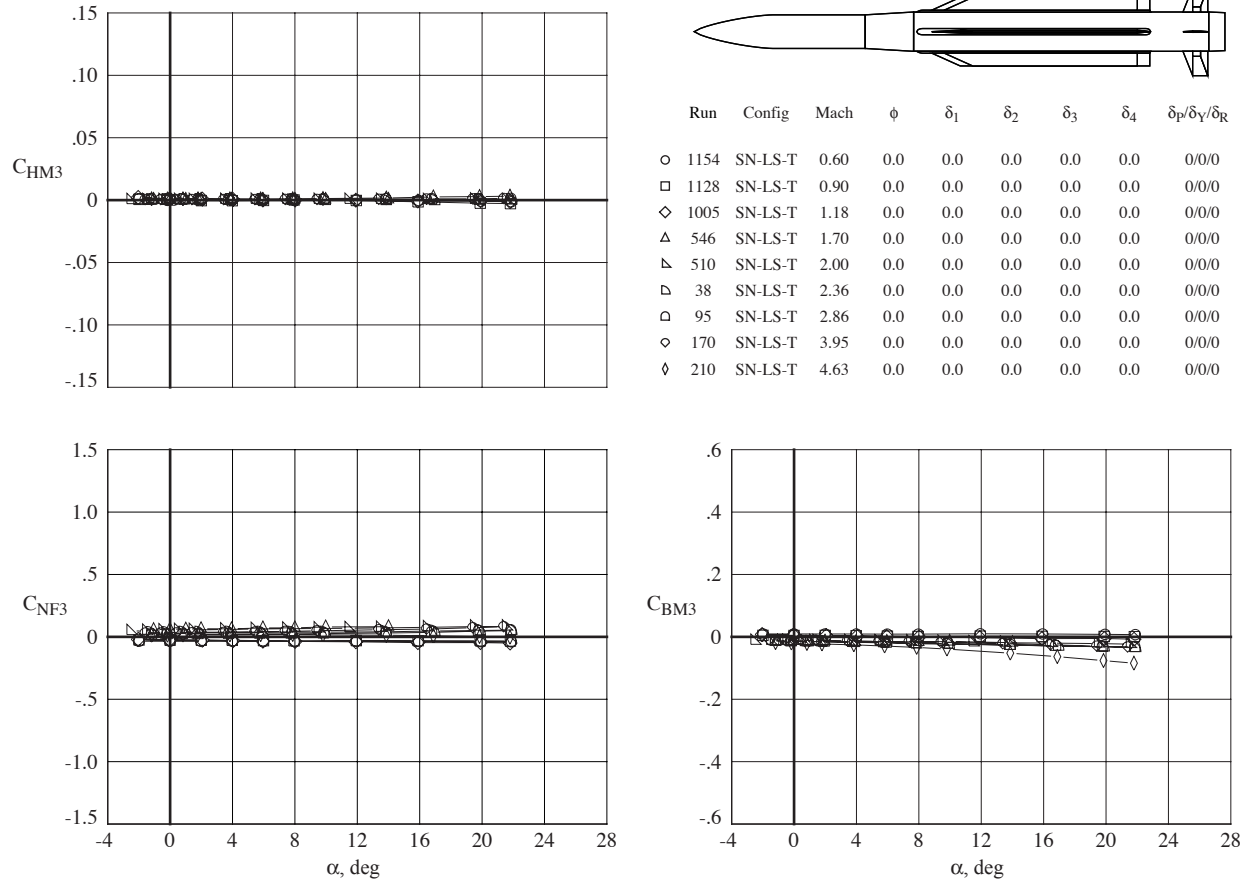


Run	Config	Mach	ϕ	δ_1	δ_2	δ_3	δ_4	$\delta_P/\delta_Y/\delta_R$
1154	SN-LS-T	0.60	0.0	0.0	0.0	0.0	0.0	0/0/0
1128	SN-LS-T	0.90	0.0	0.0	0.0	0.0	0.0	0/0/0
1005	SN-LS-T	1.18	0.0	0.0	0.0	0.0	0.0	0/0/0
546	SN-LS-T	1.70	0.0	0.0	0.0	0.0	0.0	0/0/0
510	SN-LS-T	2.00	0.0	0.0	0.0	0.0	0.0	0/0/0
38	SN-LS-T	2.36	0.0	0.0	0.0	0.0	0.0	0/0/0
95	SN-LS-T	2.86	0.0	0.0	0.0	0.0	0.0	0/0/0
170	SN-LS-T	3.95	0.0	0.0	0.0	0.0	0.0	0/0/0
210	SN-LS-T	4.63	0.0	0.0	0.0	0.0	0.0	0/0/0



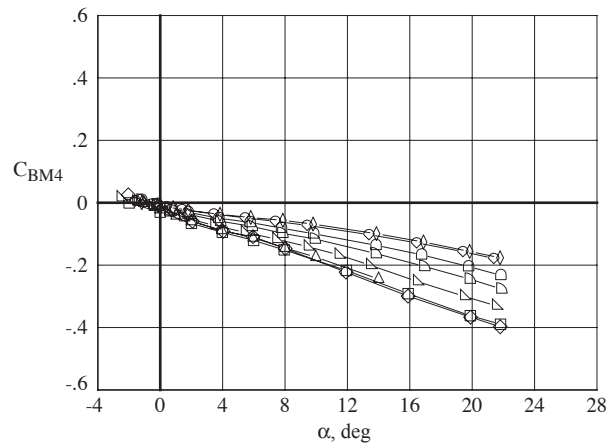
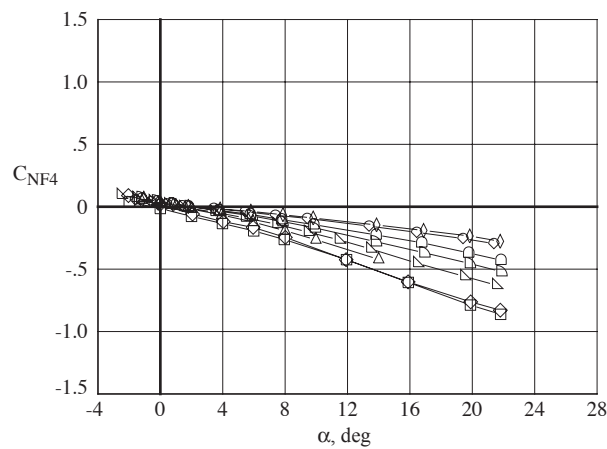
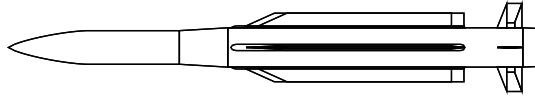
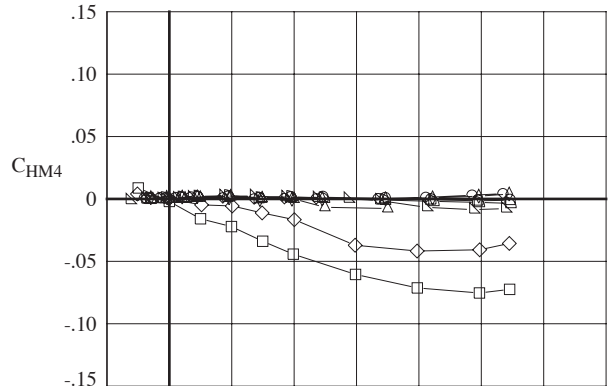
(d) Tail fin 2 loads.

Figure 23. Continued.



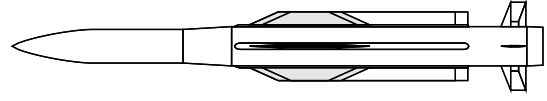
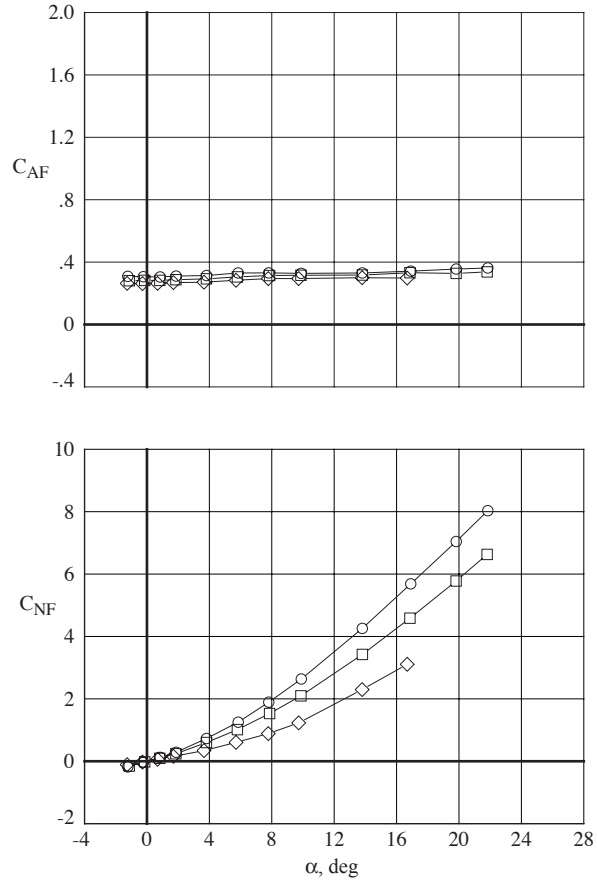
(e) Tail fin 3 loads.

Figure 23. Continued.

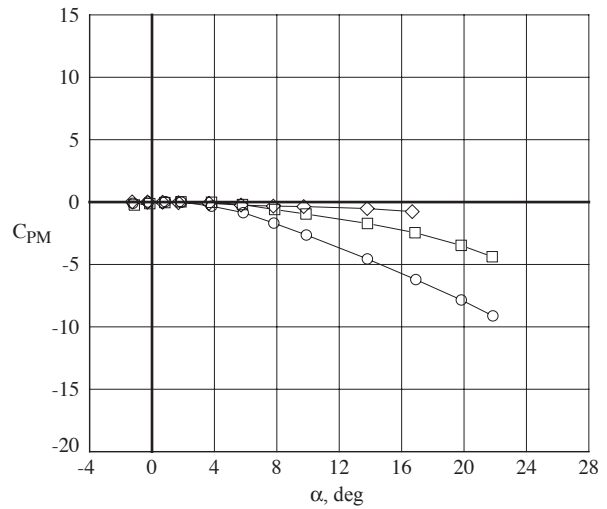


(f) Tail fin 4 loads.

Figure 23. Concluded.

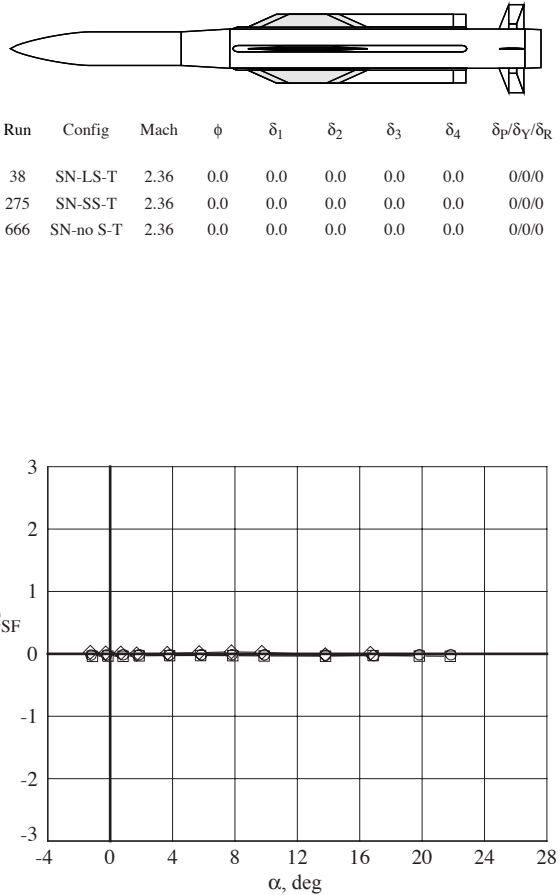
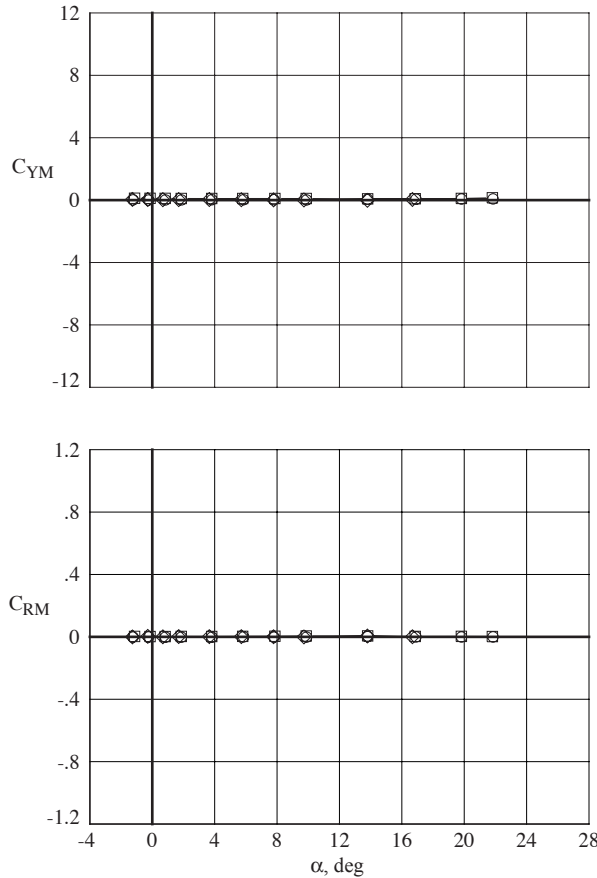


Run	Config	Mach	ϕ	δ_1	δ_2	δ_3	δ_4	$\delta_p/\delta_Y/\delta_R$
38	SN-LS-T	2.36	0.0	0.0	0.0	0.0	0.0	0/0/0
275	SN-SS-T	2.36	0.0	0.0	0.0	0.0	0.0	0/0/0
666	SN-no S-T	2.36	0.0	0.0	0.0	0.0	0.0	0/0/0



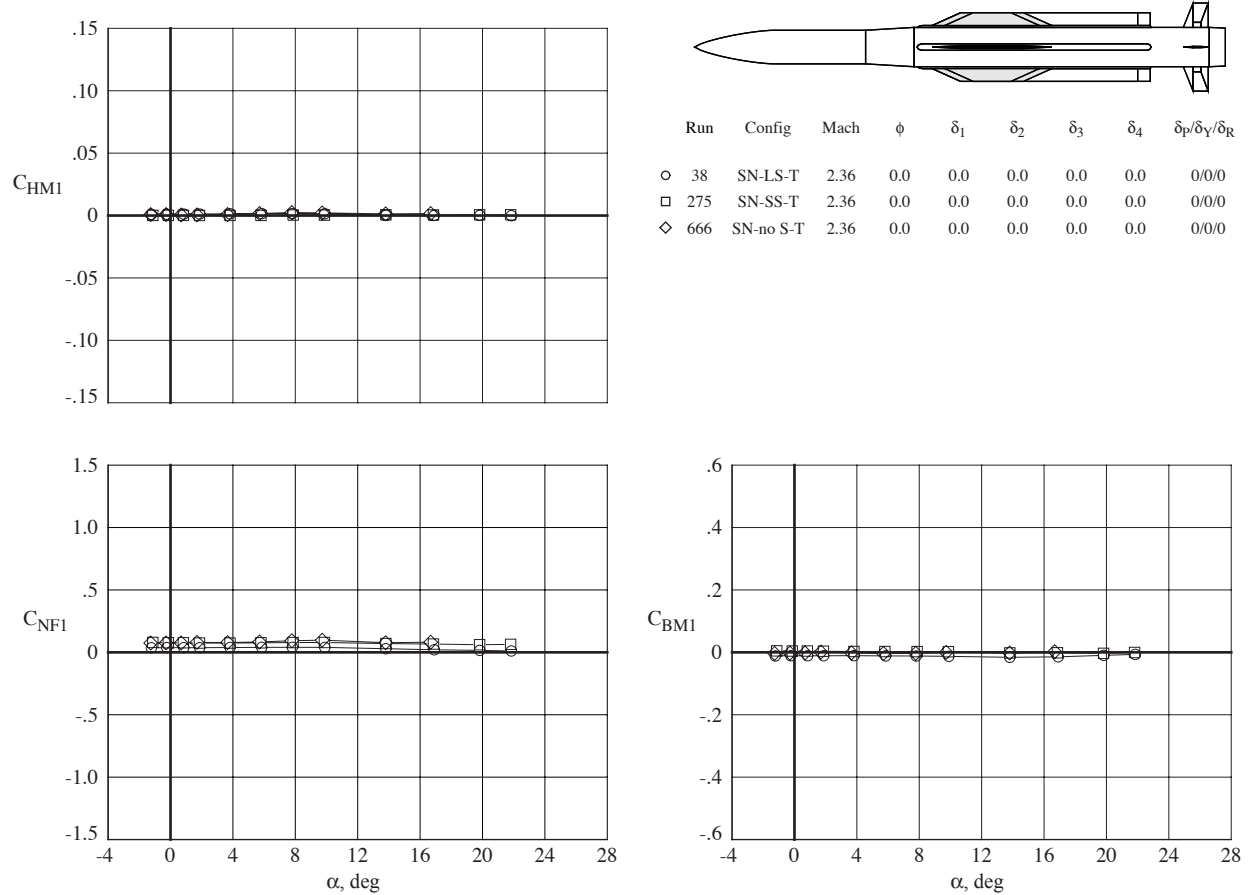
(a) Configuration longitudinal loads.

Figure 24. Effects of strake length.



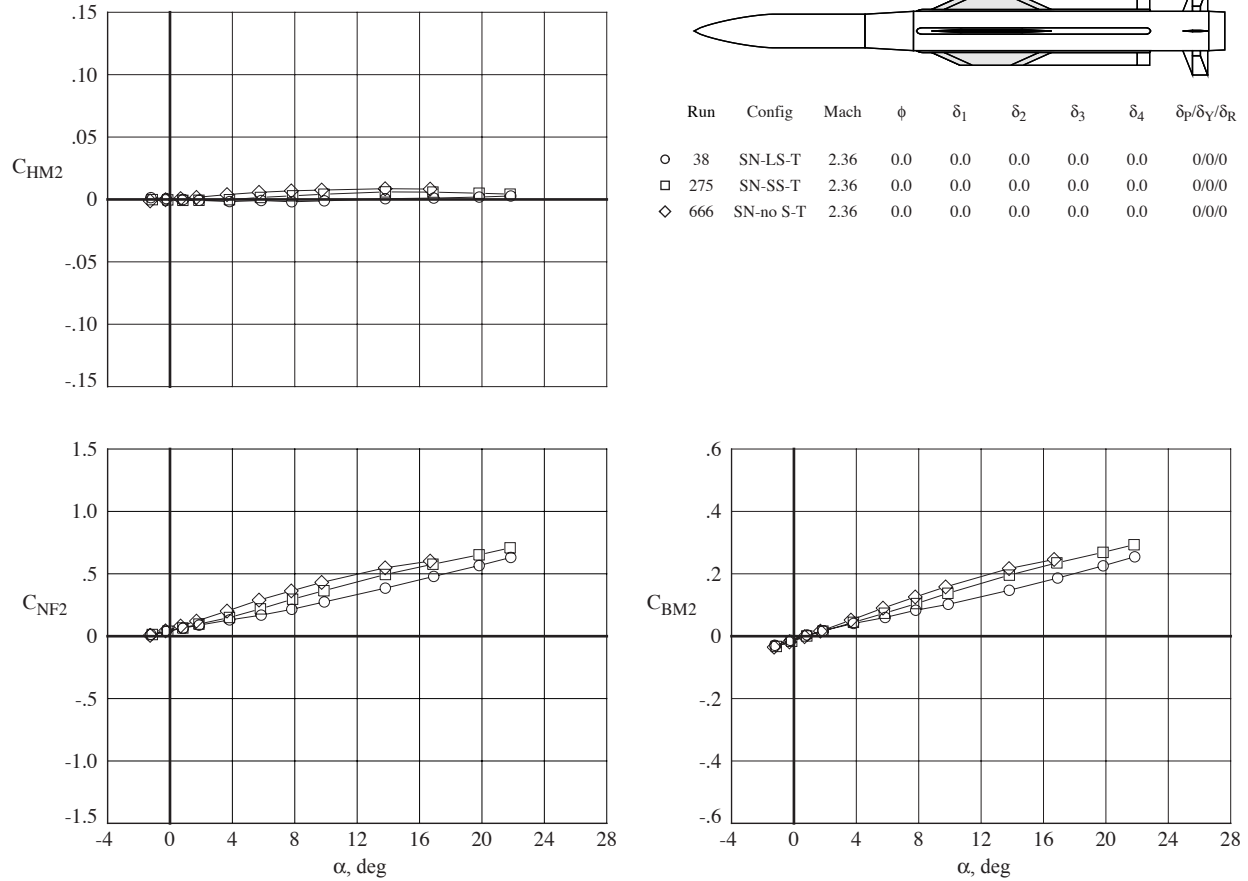
(b) Configuration lateral-directional loads.

Figure 24. Continued.



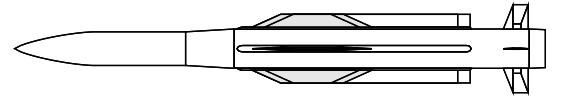
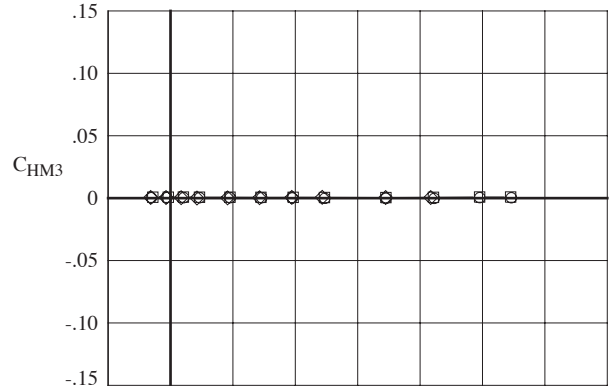
(c) Tail fin 1 loads.

Figure 24. Continued.

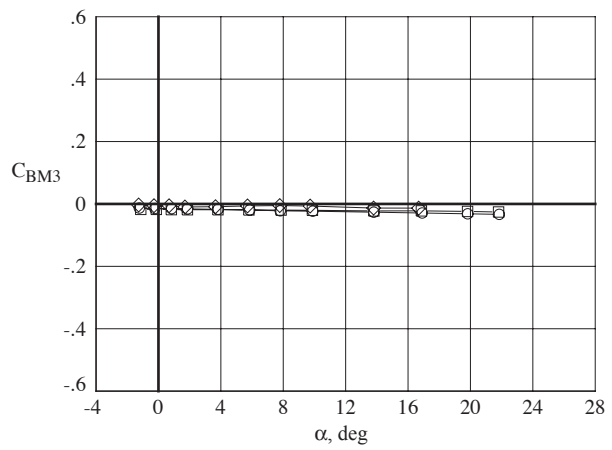
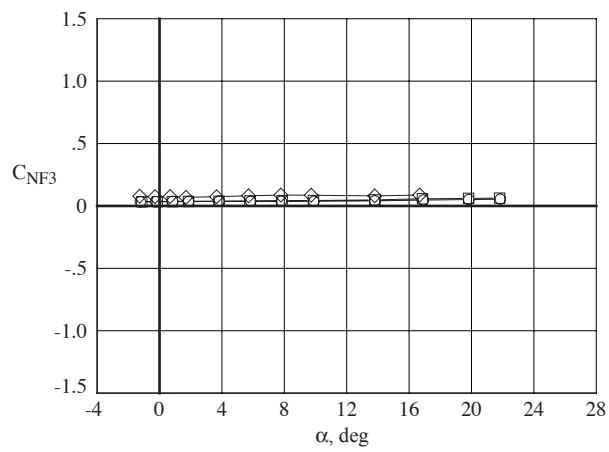


(d) Tail fin 2 loads.

Figure 24. Continued.

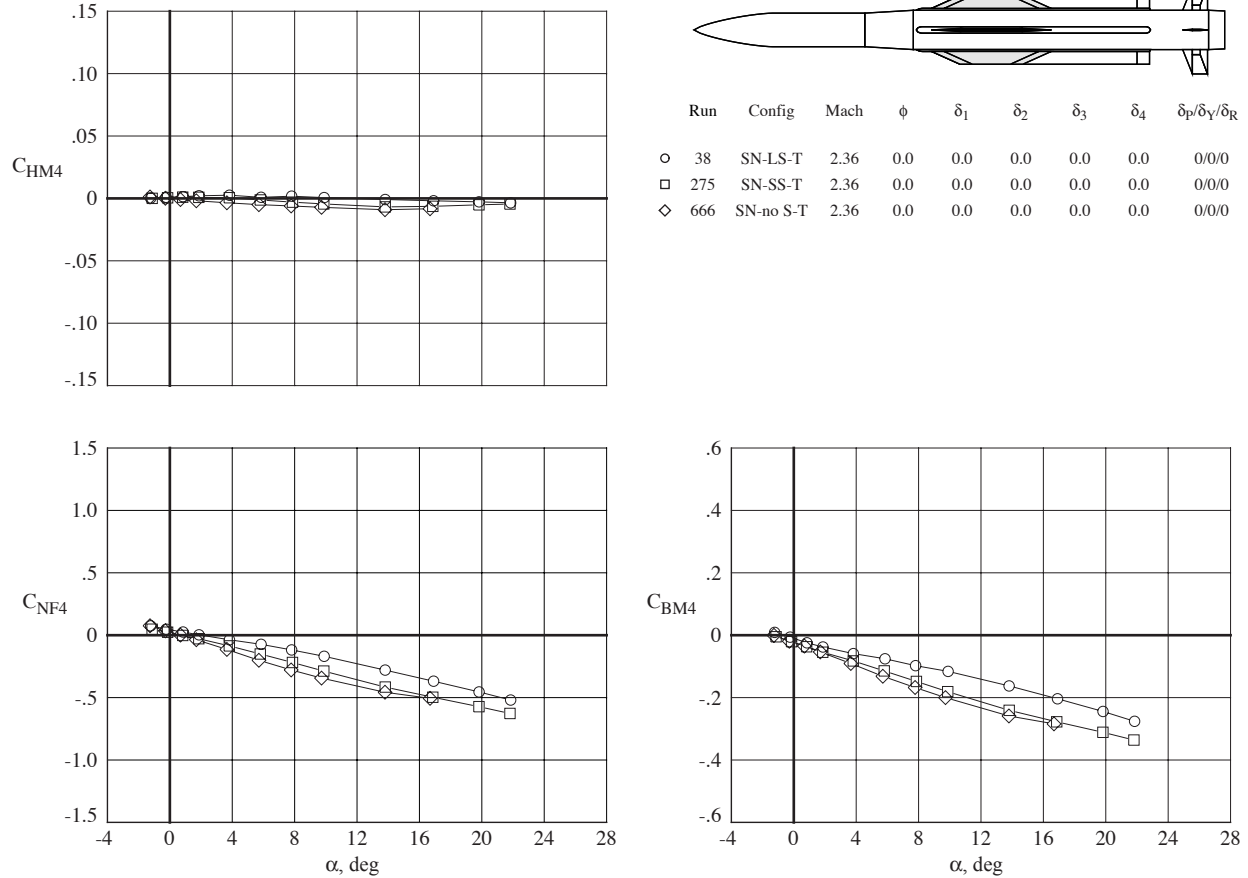


Run	Config	Mach	ϕ	δ ₁	δ ₂	δ ₃	δ ₄	δ _P /δ _Y /δ _R
38	SN-LS-T	2.36	0.0	0.0	0.0	0.0	0.0	0/0/0
275	SN-SS-T	2.36	0.0	0.0	0.0	0.0	0.0	0/0/0
666	SN-no S-T	2.36	0.0	0.0	0.0	0.0	0.0	0/0/0



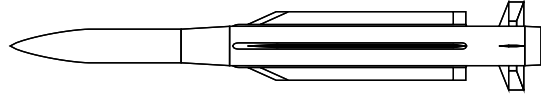
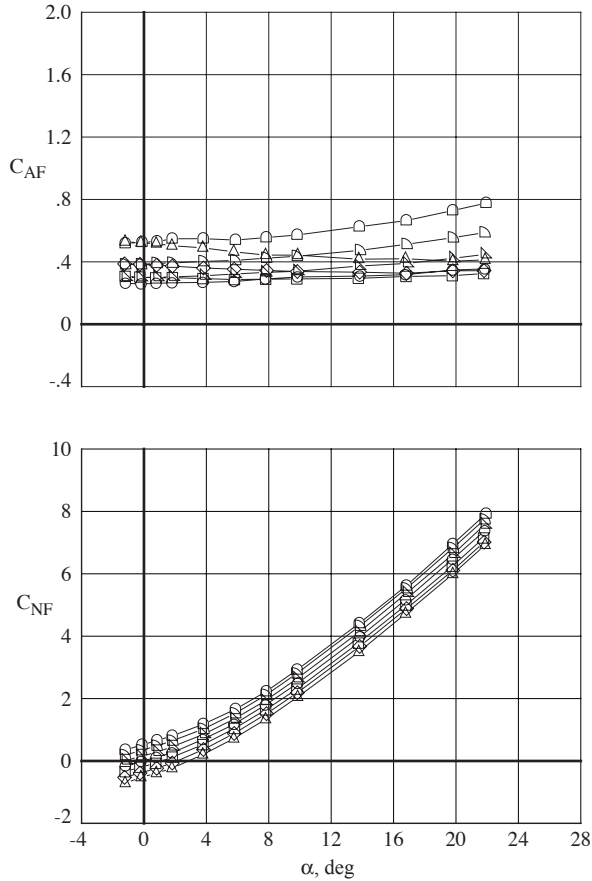
(e) Tail fin 3 loads.

Figure 24. Continued.

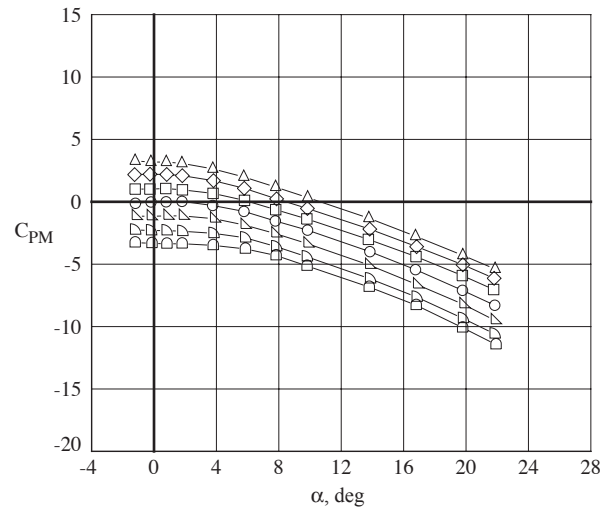


(f) Tail fin 4 loads.

Figure 24. Concluded.

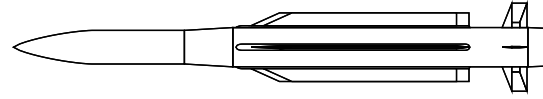
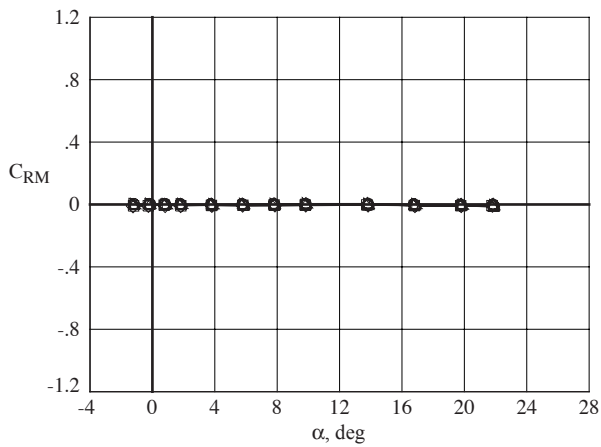
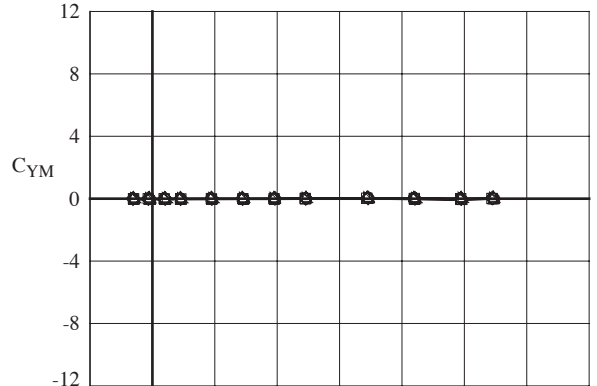


Run	Config	Mach	ϕ	δ_1	δ_2	δ_3	δ_4	$\delta_p/\delta_Y/\delta_R$
○ 95	SN-LS-T	2.86	0.0	0.0	0.0	0.0	0.0	0/0/0
□ 96	SN-LS-T	2.86	0.0	0.0	10.0	0.0	-10.0	10/0/0
◇ 97	SN-LS-T	2.86	0.0	0.0	20.0	0.0	-20.0	20/0/0
△ 98	SN-LS-T	2.86	0.0	0.0	30.0	0.0	-30.0	30/0/0
▽ 99	SN-LS-T	2.86	0.0	0.0	-10.0	0.0	10.0	-10/0/0
▽ 100	SN-LS-T	2.86	0.0	0.0	-20.0	0.0	20.0	-20/0/0
▽ 101	SN-LS-T	2.86	0.0	0.0	-30.0	0.0	30.0	-30/0/0

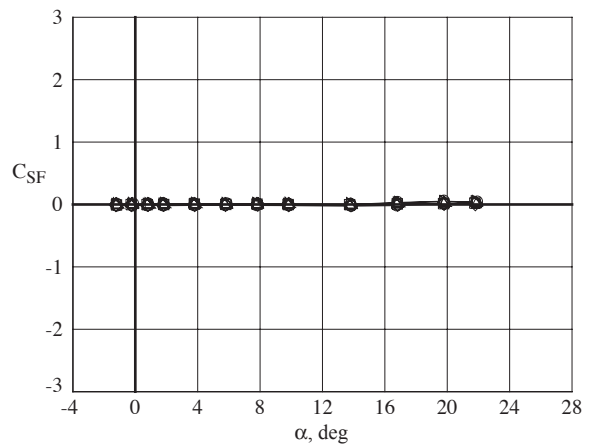


(a) Configuration longitudinal loads.

Figure 25. Effects of 2-fin pitch control deflections.

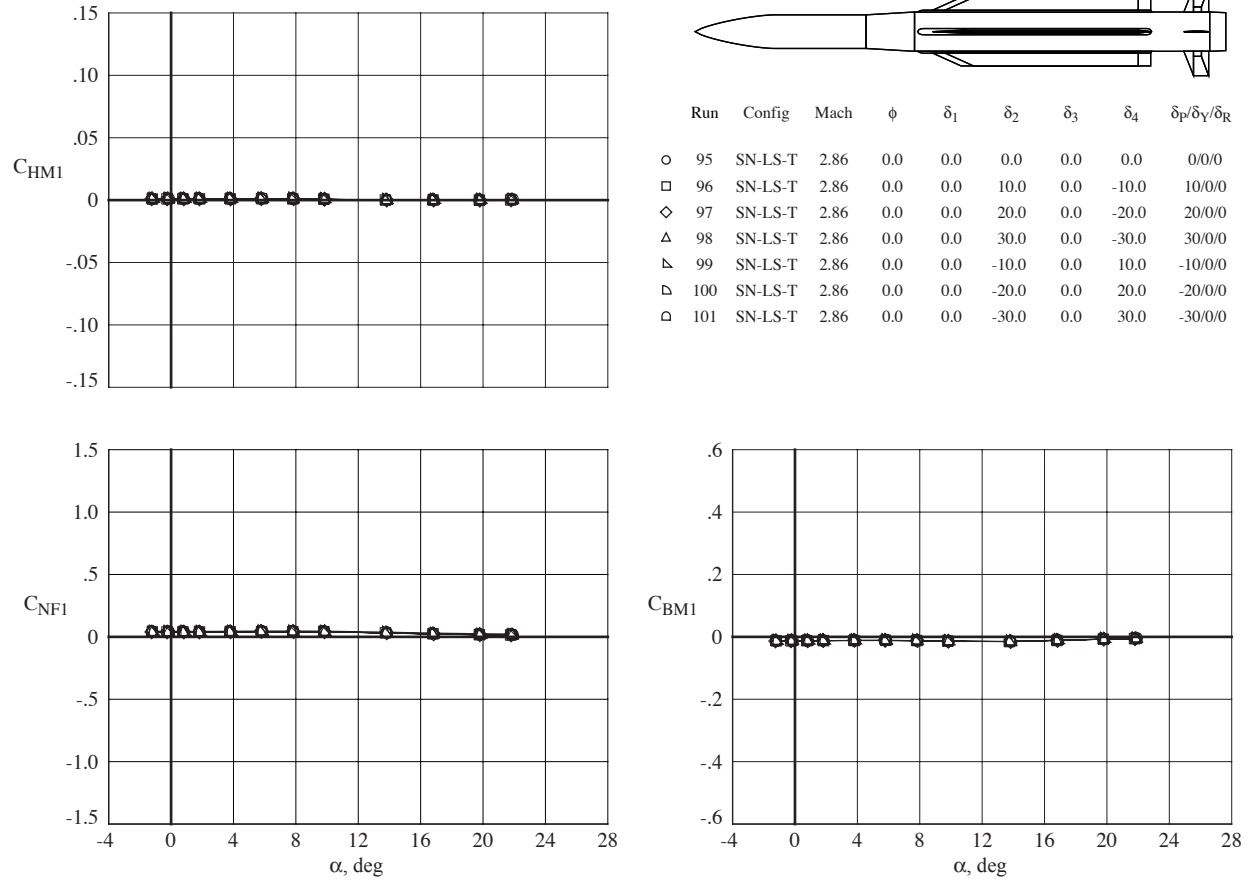


Run	Config	Mach	ϕ	δ_1	δ_2	δ_3	δ_4	$\delta_p/\delta_Y/\delta_R$
○ 95	SN-LS-T	2.86	0.0	0.0	0.0	0.0	0.0	0/0/0
□ 96	SN-LS-T	2.86	0.0	0.0	10.0	0.0	-10.0	10/0/0
◇ 97	SN-LS-T	2.86	0.0	0.0	20.0	0.0	-20.0	20/0/0
△ 98	SN-LS-T	2.86	0.0	0.0	30.0	0.0	-30.0	30/0/0
▽ 99	SN-LS-T	2.86	0.0	0.0	-10.0	0.0	10.0	-10/0/0
▷ 100	SN-LS-T	2.86	0.0	0.0	-20.0	0.0	20.0	-20/0/0
◁ 101	SN-LS-T	2.86	0.0	0.0	-30.0	0.0	30.0	-30/0/0



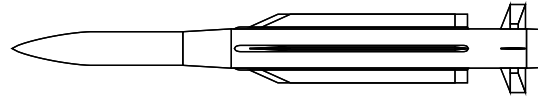
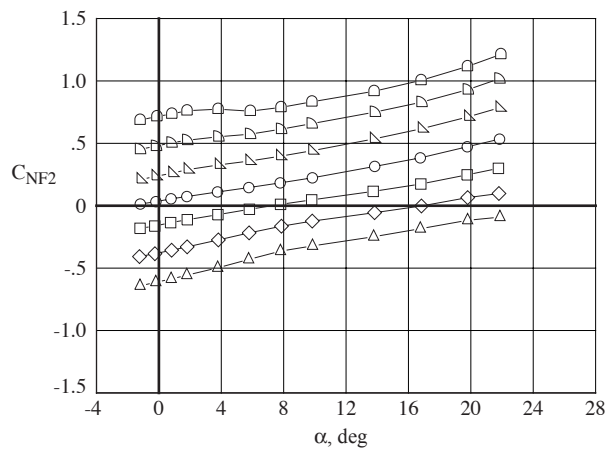
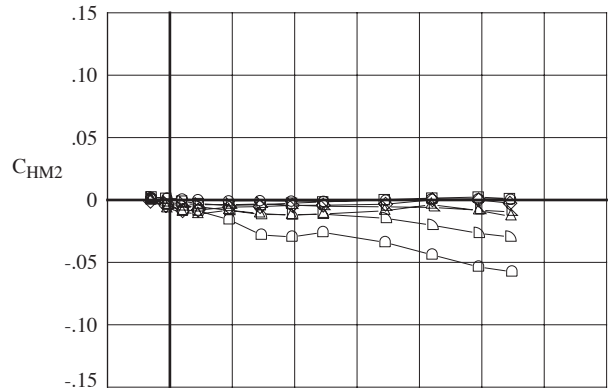
(b) Configuration lateral-directional loads.

Figure 25. Continued.

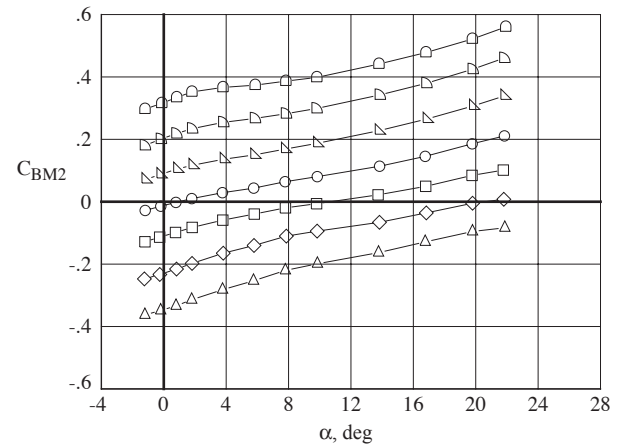


(c) Tail fin 1 loads.

Figure 25. Continued.

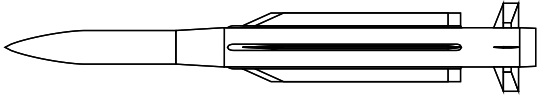
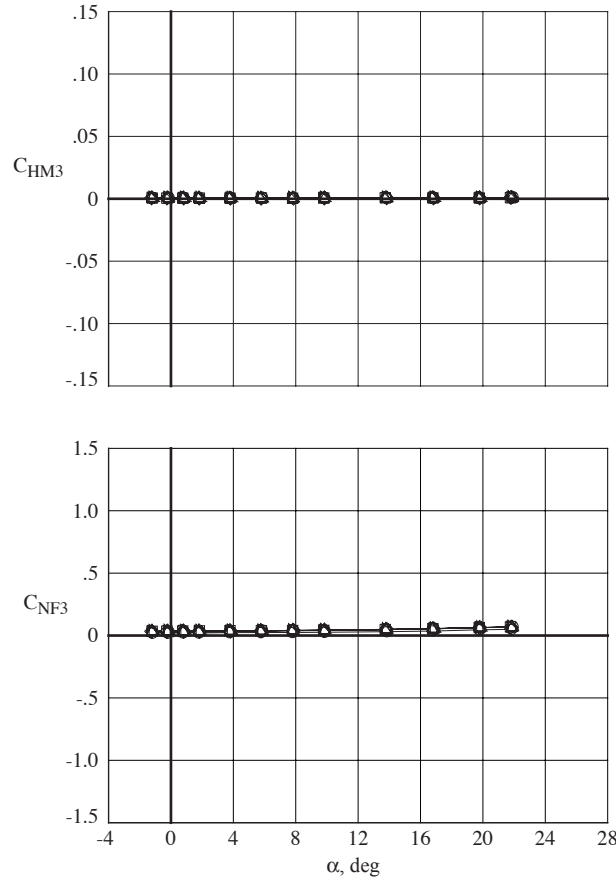


Run	Config	Mach	ϕ	δ_1	δ_2	δ_3	δ_4	$\delta_p/\delta_Y/\delta_R$
o 95	SN-LS-T	2.86	0.0	0.0	0.0	0.0	0.0	0/0/0
□ 96	SN-LS-T	2.86	0.0	0.0	10.0	0.0	-10.0	10/0/0
◇ 97	SN-LS-T	2.86	0.0	0.0	20.0	0.0	-20.0	20/0/0
△ 98	SN-LS-T	2.86	0.0	0.0	30.0	0.0	-30.0	30/0/0
▽ 99	SN-LS-T	2.86	0.0	0.0	-10.0	0.0	10.0	-10/0/0
□ 100	SN-LS-T	2.86	0.0	0.0	-20.0	0.0	20.0	-20/0/0
□ 101	SN-LS-T	2.86	0.0	0.0	-30.0	0.0	30.0	-30/0/0

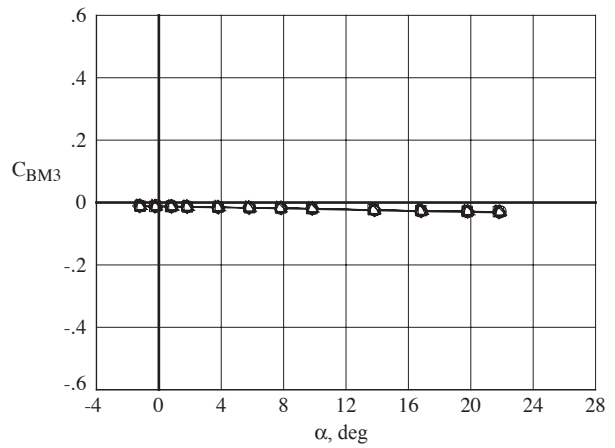


(d) Tail fin 2 loads.

Figure 25. Continued.

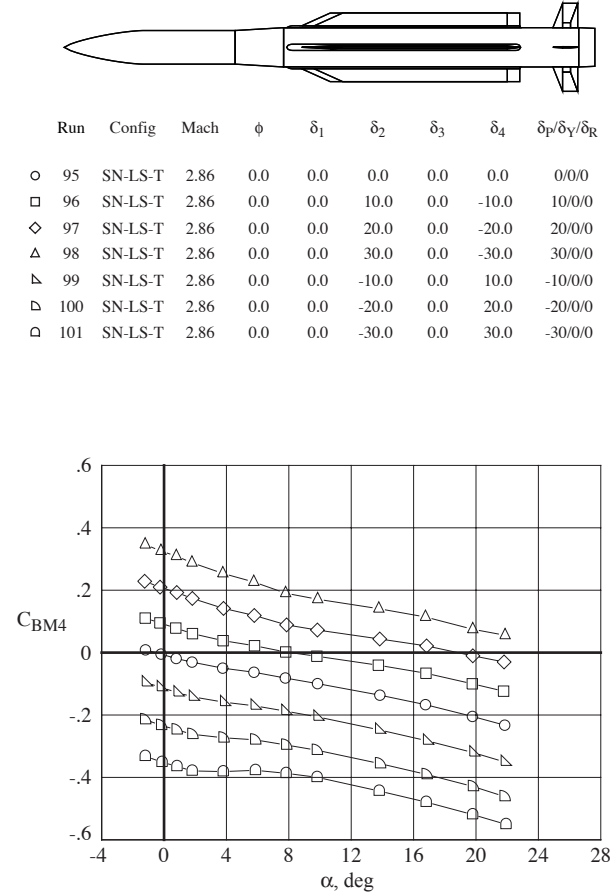
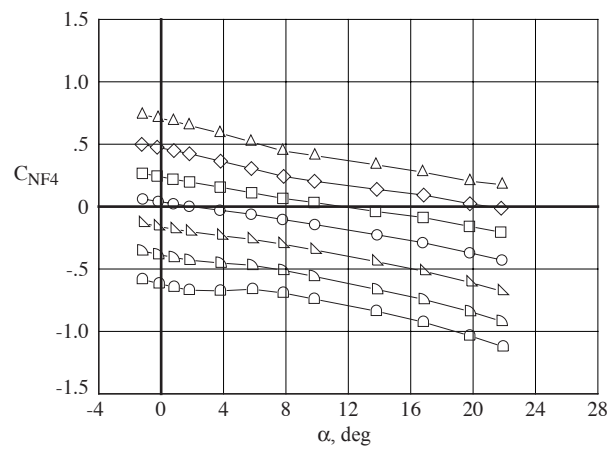
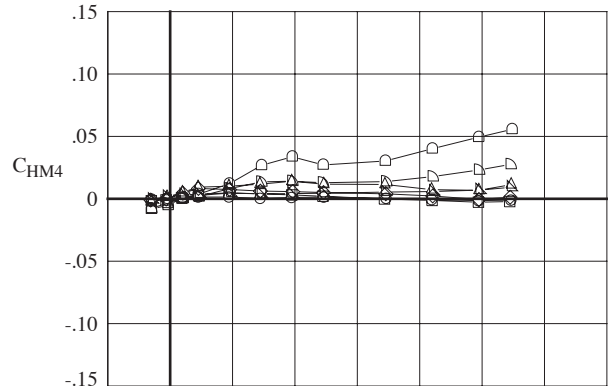


Run	Config	Mach	ϕ	δ_1	δ_2	δ_3	δ_4	$\delta_p/\delta_Y/\delta_R$
○ 95	SN-LS-T	2.86	0.0	0.0	0.0	0.0	0.0	0/0/0
□ 96	SN-LS-T	2.86	0.0	0.0	10.0	0.0	-10.0	10/0/0
◇ 97	SN-LS-T	2.86	0.0	0.0	20.0	0.0	-20.0	20/0/0
△ 98	SN-LS-T	2.86	0.0	0.0	30.0	0.0	-30.0	30/0/0
▽ 99	SN-LS-T	2.86	0.0	0.0	-10.0	0.0	10.0	-10/0/0
△ 100	SN-LS-T	2.86	0.0	0.0	-20.0	0.0	20.0	-20/0/0
□ 101	SN-LS-T	2.86	0.0	0.0	-30.0	0.0	30.0	-30/0/0



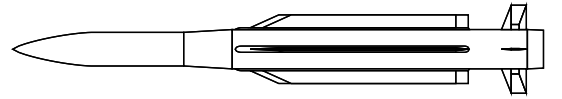
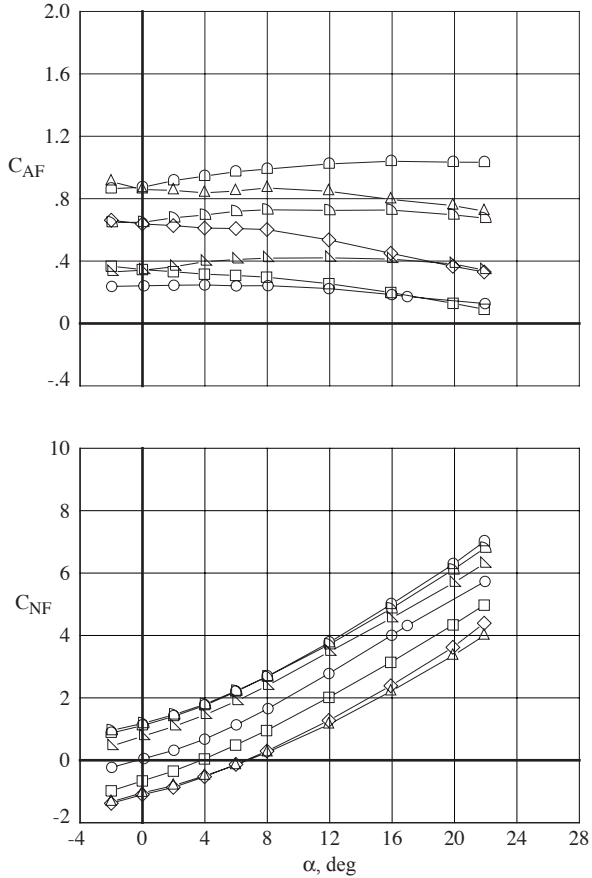
(e) Tail fin 3 loads.

Figure 25. Continued.

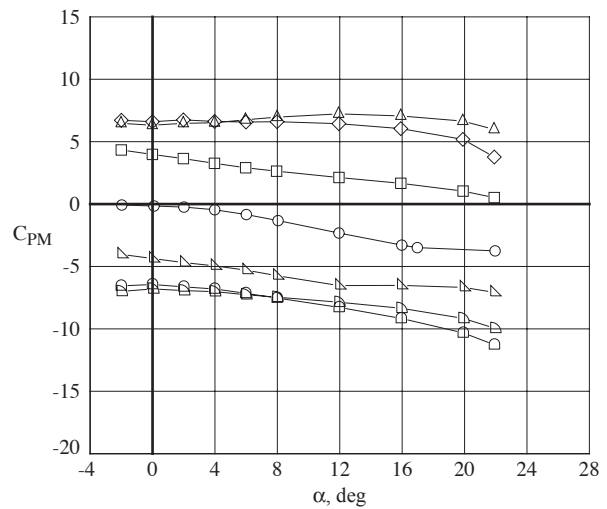


(f) Tail fin 4 loads.

Figure 25. Concluded.

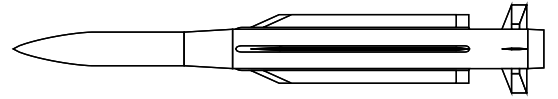
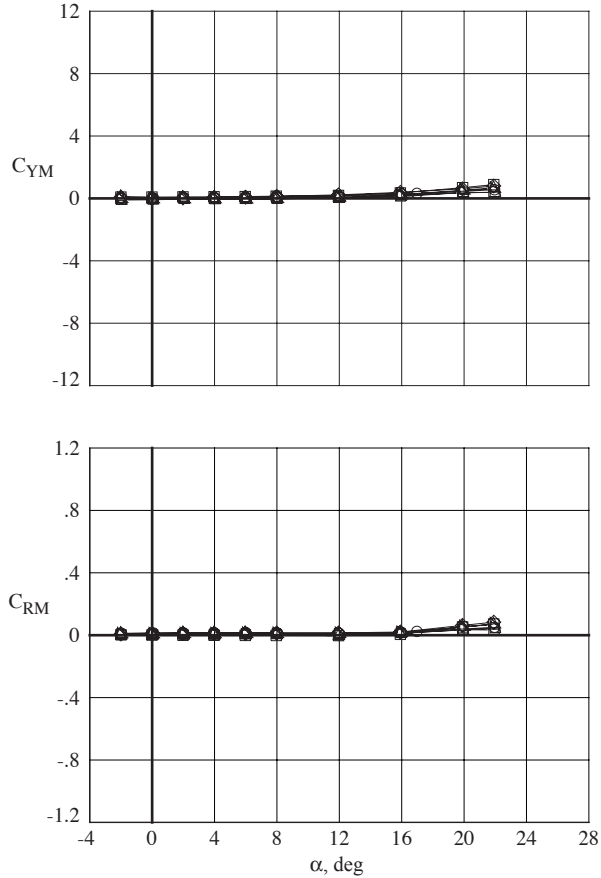


Run	Config	Mach	ϕ	δ_1	δ_2	δ_3	δ_4	$\delta_p/\delta_Y/\delta_R$
○ 1165	SN-LS-T	0.60	-45.0	0.0	0.0	0.0	0.0	0/0/0
□ 1170	SN-LS-T	0.60	-45.0	-10.0	10.0	10.0	-10.0	10/0/0
◇ 1171	SN-LS-T	0.60	-45.0	-20.0	20.0	20.0	-20.0	20/0/0
△ 1172	SN-LS-T	0.60	-45.0	-30.0	30.0	30.0	-30.0	30/0/0
▲ 1167	SN-LS-T	0.60	-45.0	10.0	-10.0	-10.0	10.0	-10/0/0
◆ 1168	SN-LS-T	0.60	-45.0	20.0	-20.0	-20.0	20.0	-20/0/0
◆ 1169	SN-LS-T	0.60	-45.0	30.0	-30.0	-30.0	30.0	-30/0/0

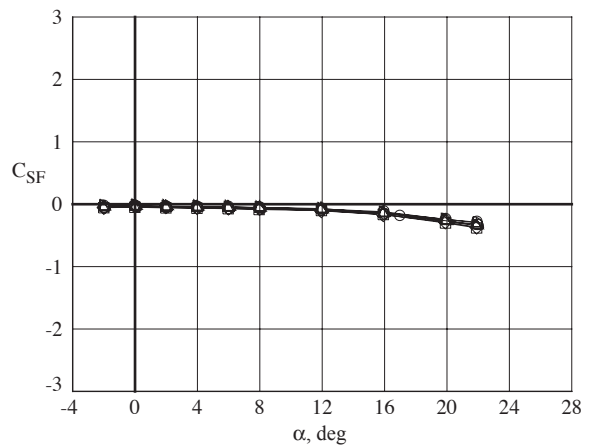


(a) Configuration longitudinal loads.

Figure 26. Effects of 4-fin pitch control deflections.

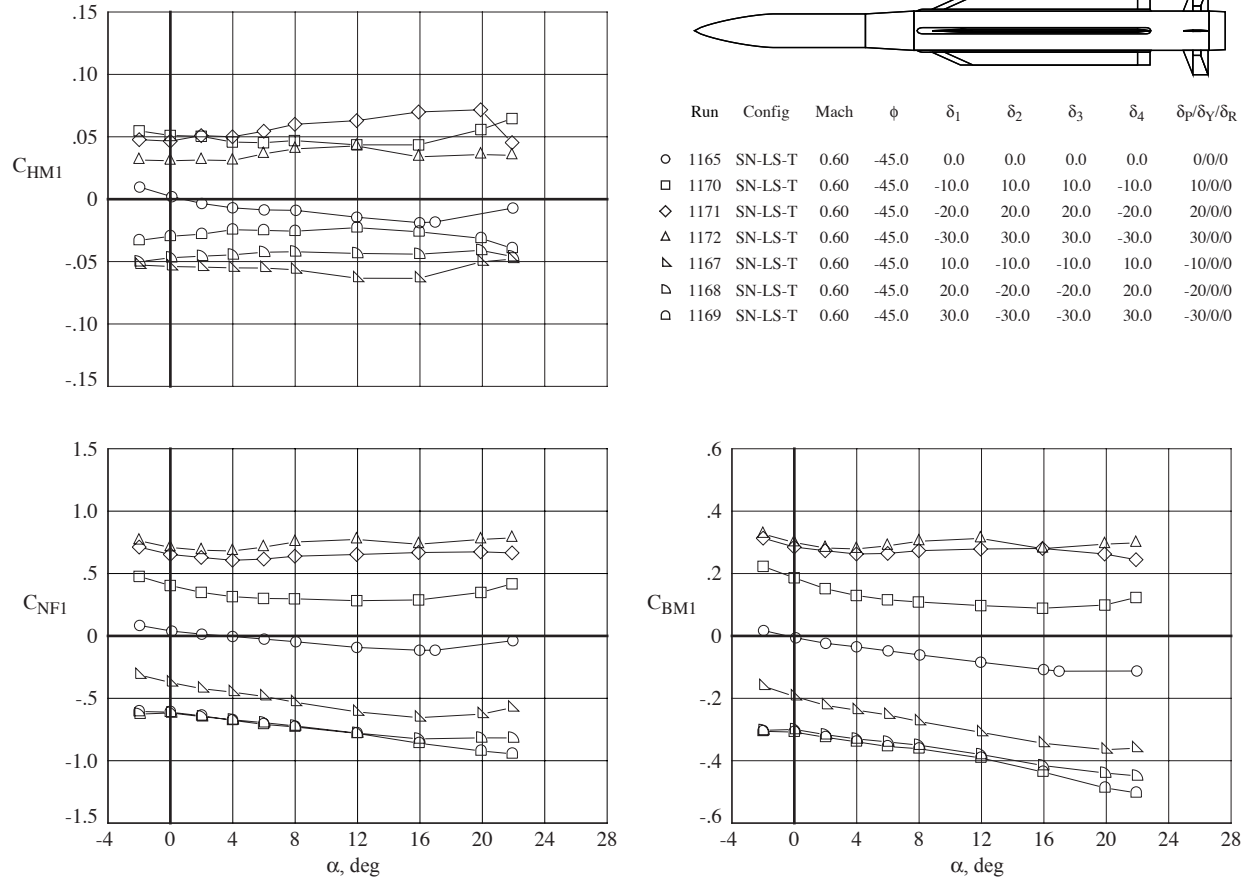


Run	Config	Mach	ϕ	δ_1	δ_2	δ_3	δ_4	$\delta_p/\delta_Y/\delta_R$
1165	SN-LS-T	0.60	-45.0	0.0	0.0	0.0	0.0	0/0/0
1170	SN-LS-T	0.60	-45.0	-10.0	10.0	10.0	-10.0	10/0/0
1171	SN-LS-T	0.60	-45.0	-20.0	20.0	20.0	-20.0	20/0/0
1172	SN-LS-T	0.60	-45.0	-30.0	30.0	30.0	-30.0	30/0/0
1167	SN-LS-T	0.60	-45.0	10.0	-10.0	-10.0	10.0	-10/0/0
1168	SN-LS-T	0.60	-45.0	20.0	-20.0	-20.0	20.0	-20/0/0
1169	SN-LS-T	0.60	-45.0	30.0	-30.0	-30.0	30.0	-30/0/0



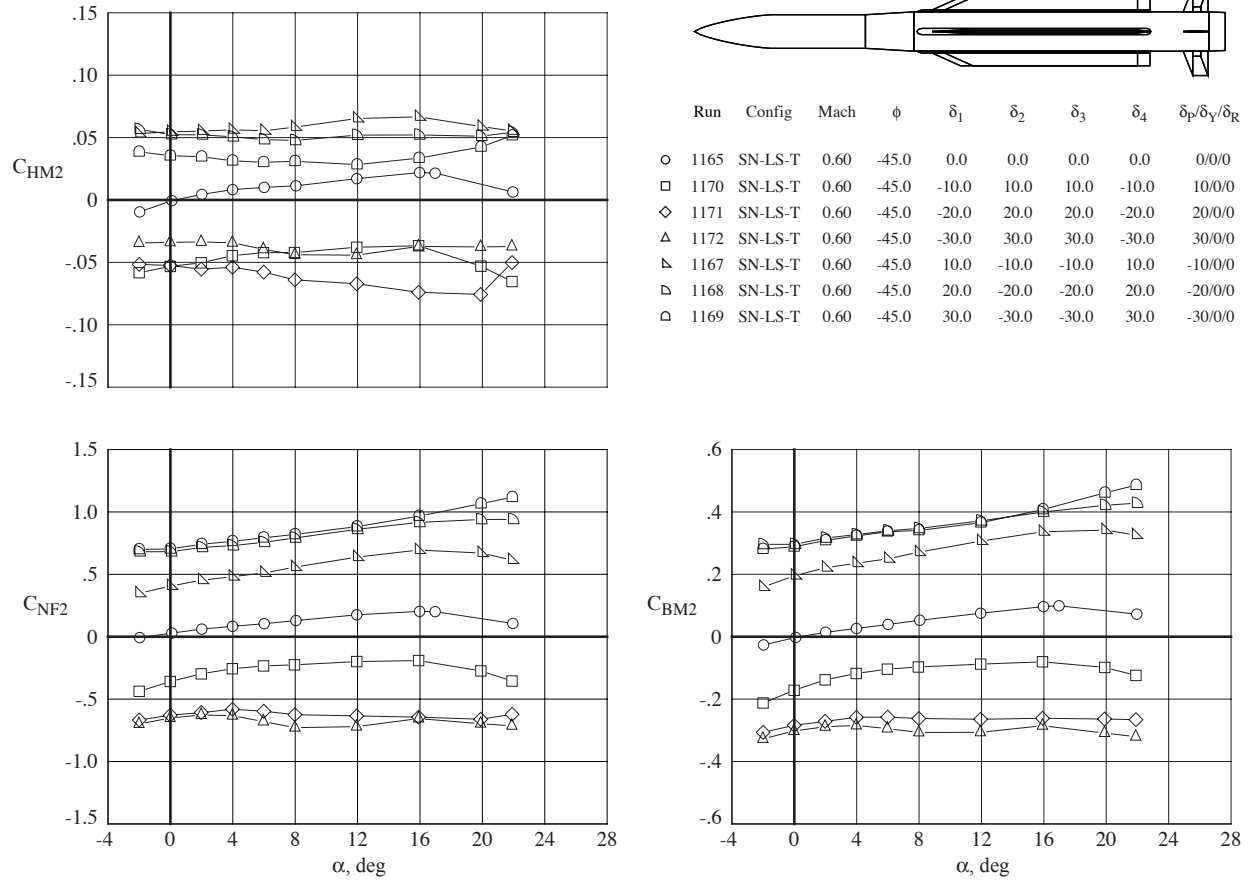
(b) Configuration lateral-directional loads.

Figure 26. Continued.



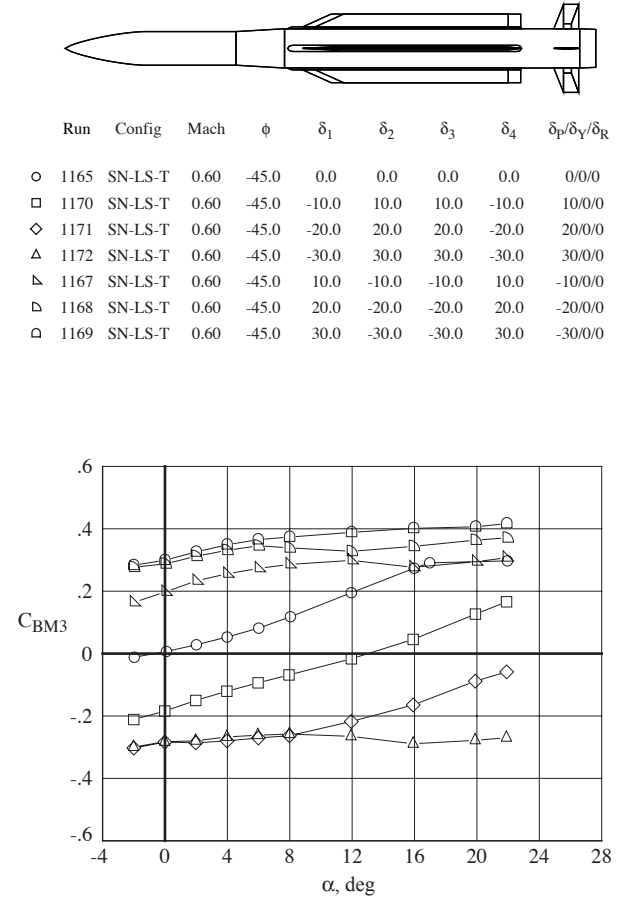
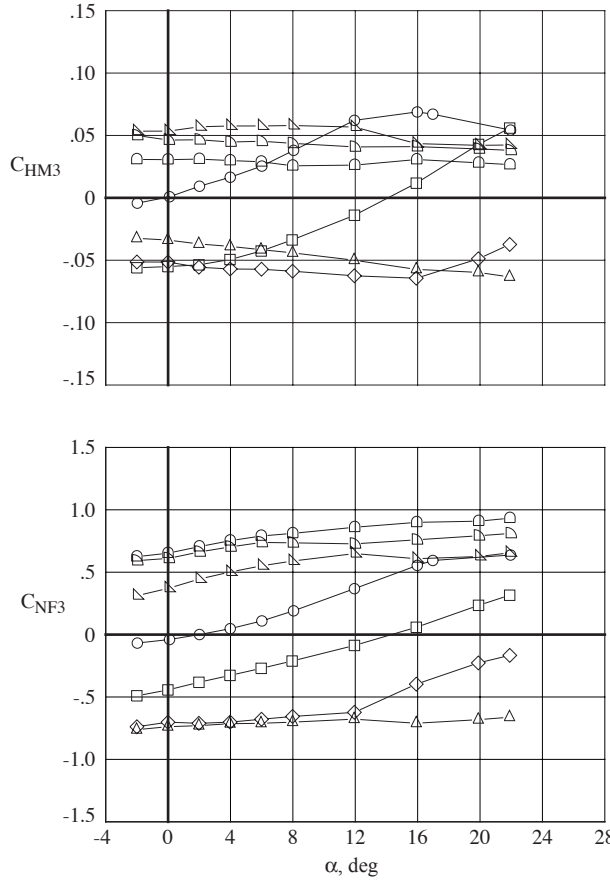
(c) Tail fin 1 loads.

Figure 26. Continued.



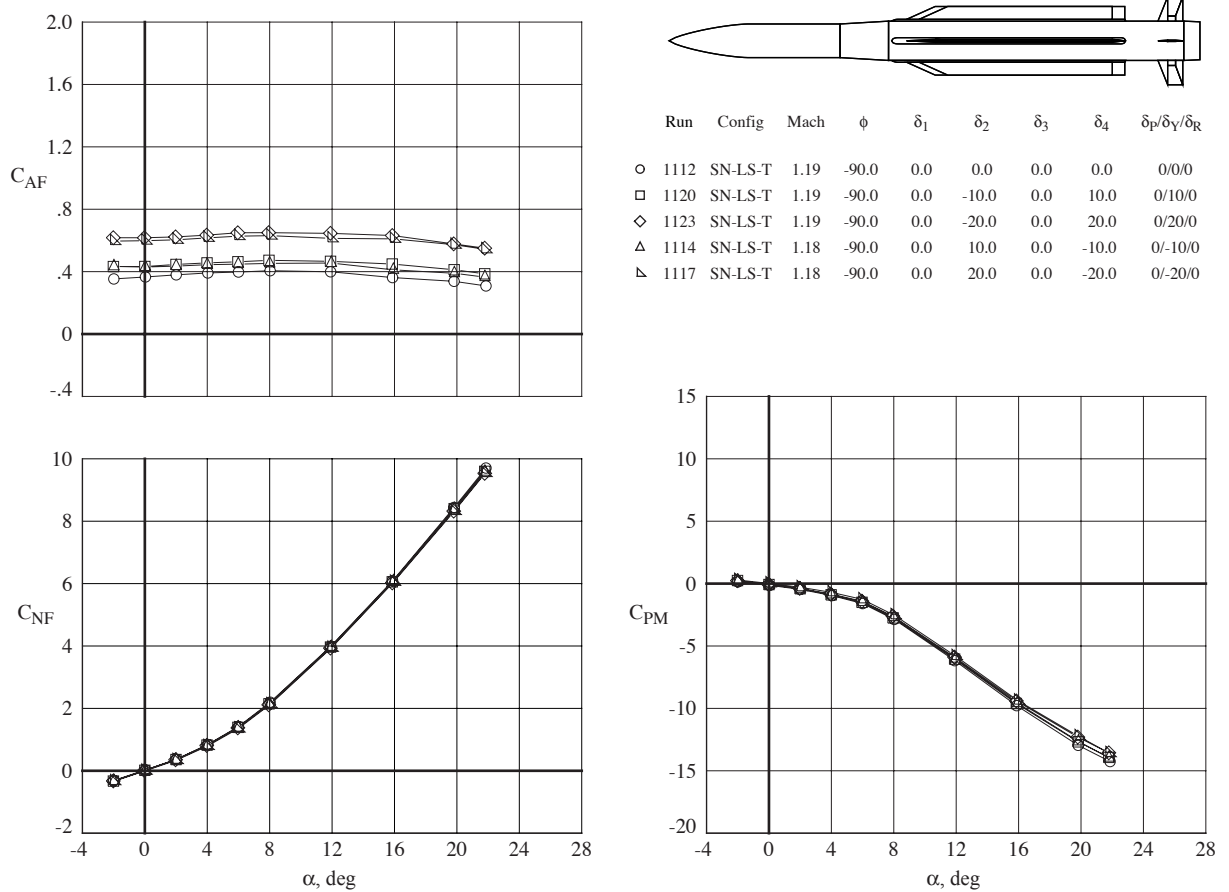
(d) Tail fin 2 loads.

Figure 26. Continued.



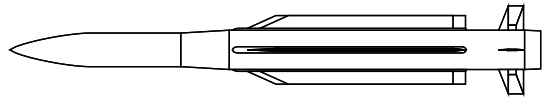
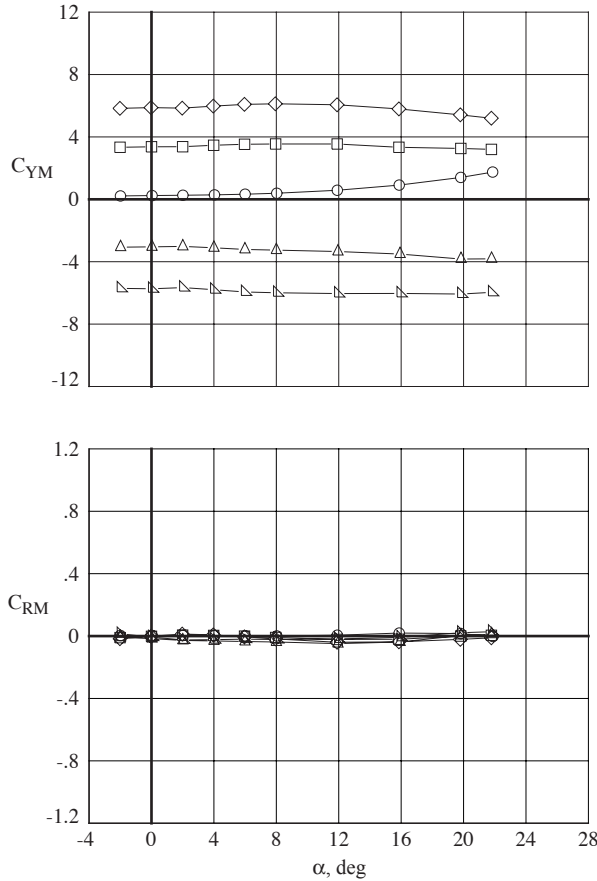
(e) Tail fin 3 loads.

Figure 26. Concluded.

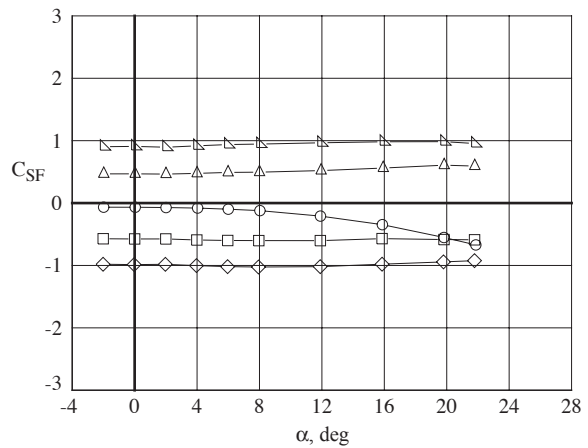


(a) Configuration longitudinal loads.

Figure 27. Effects of yaw control deflections.

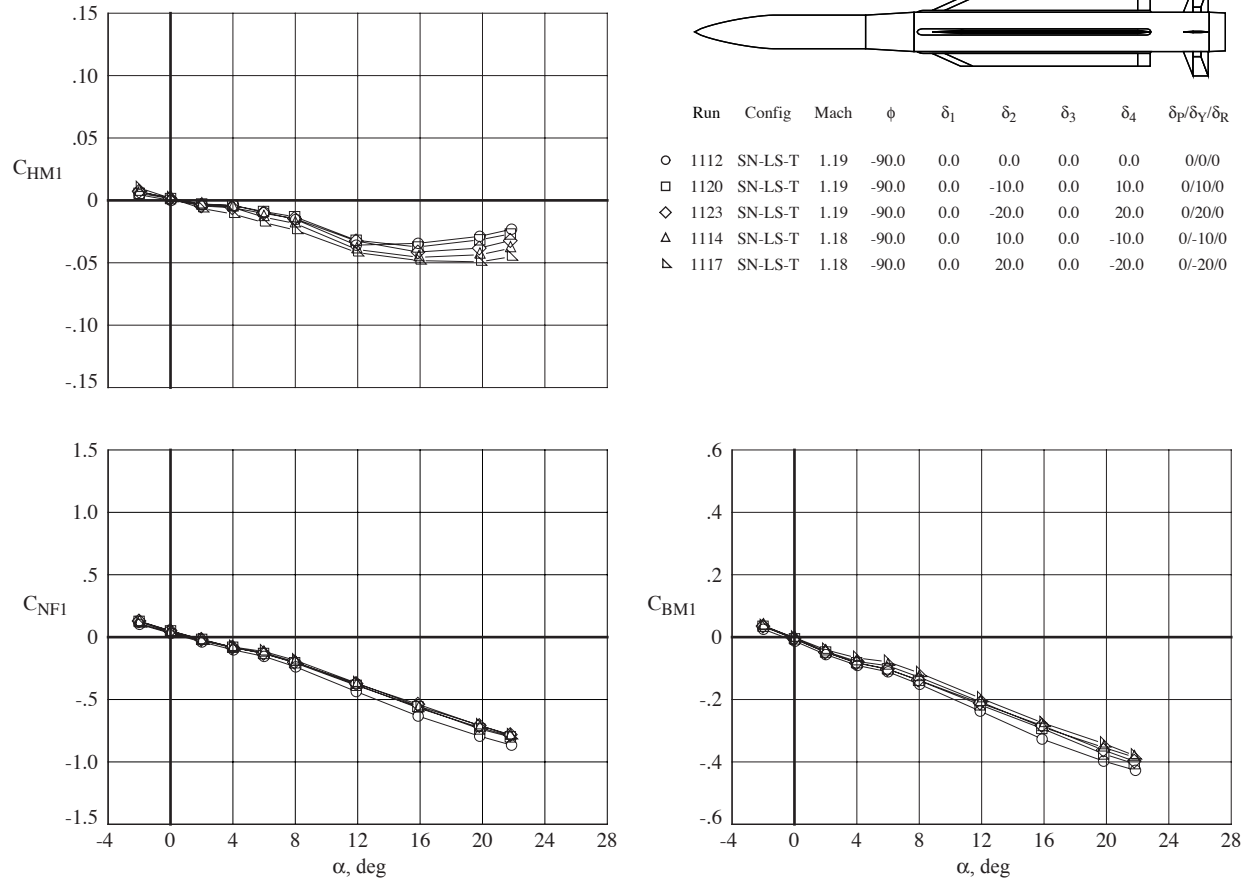


Run	Config	Mach	ϕ	δ_1	δ_2	δ_3	δ_4	$\delta p/\delta Y/\delta R$
1112	SN-LS-T	1.19	-90.0	0.0	0.0	0.0	0.0	0/0/0
1120	SN-LS-T	1.19	-90.0	0.0	-10.0	0.0	10.0	0/10/0
1123	SN-LS-T	1.19	-90.0	0.0	-20.0	0.0	20.0	0/20/0
1114	SN-LS-T	1.18	-90.0	0.0	10.0	0.0	-10.0	0/-10/0
1117	SN-LS-T	1.18	-90.0	0.0	20.0	0.0	-20.0	0/-20/0



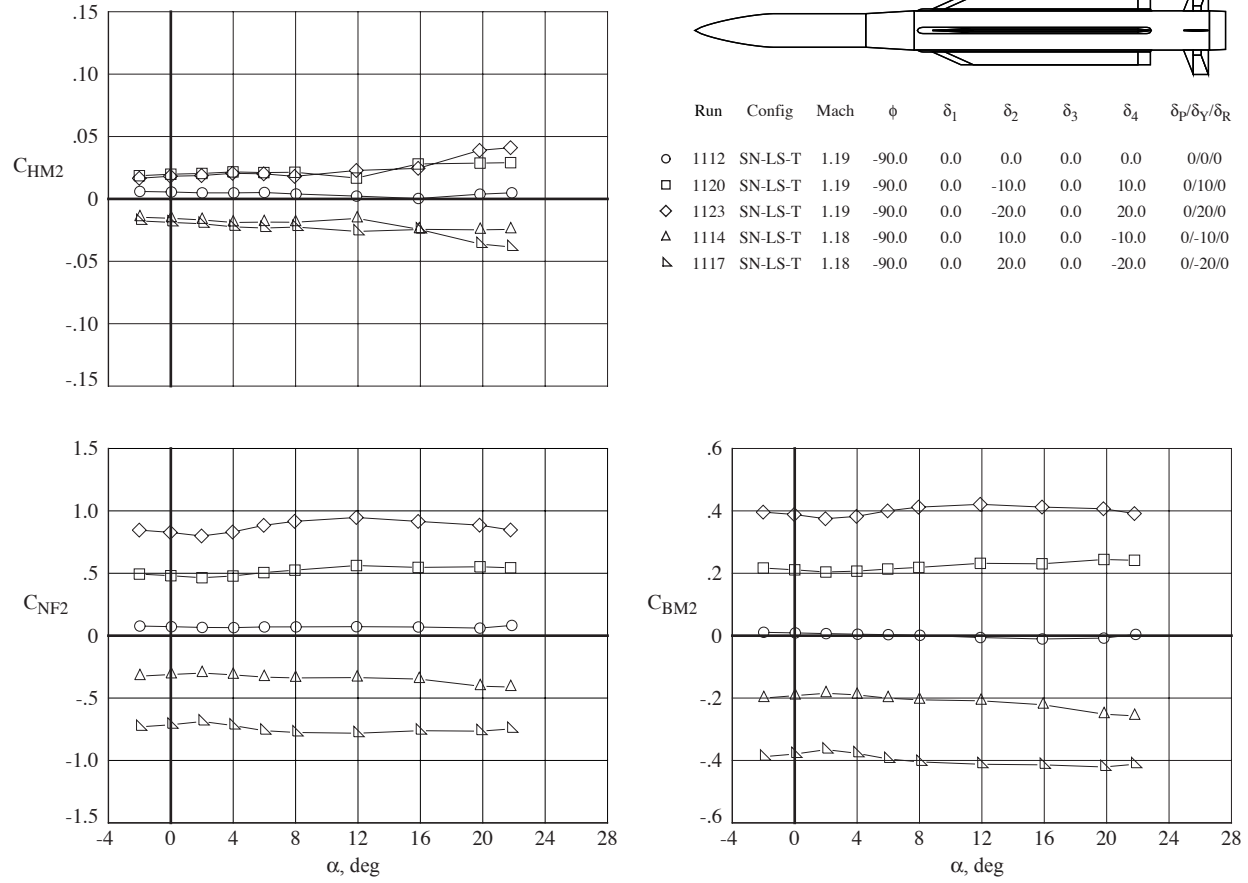
(b) Configuration lateral-directional loads.

Figure 27. Continued.



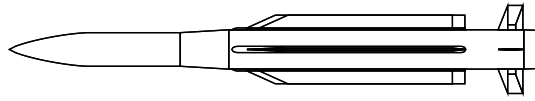
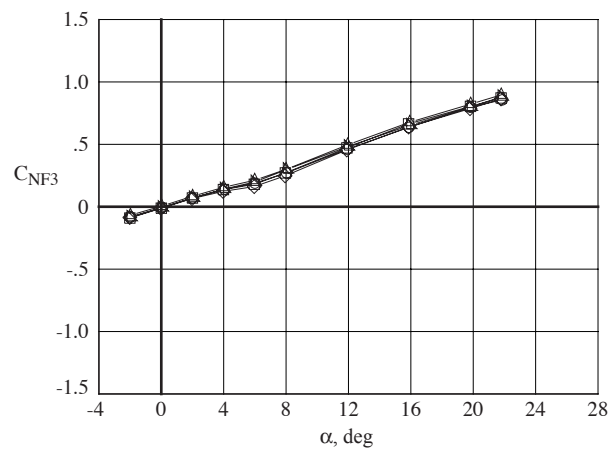
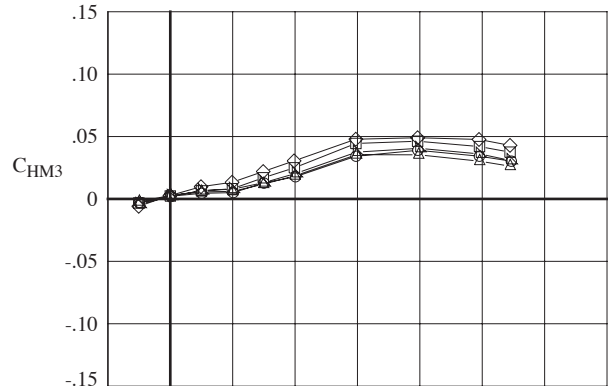
(c) Tail fin 1 loads.

Figure 27. Continued.

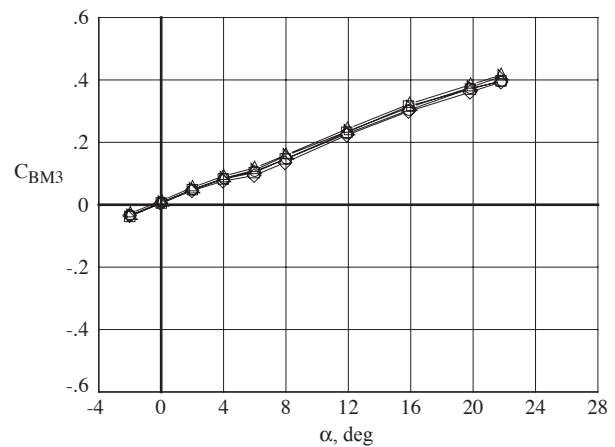


(d) Tail fin 2 loads.

Figure 27. Continued.

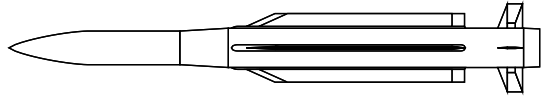
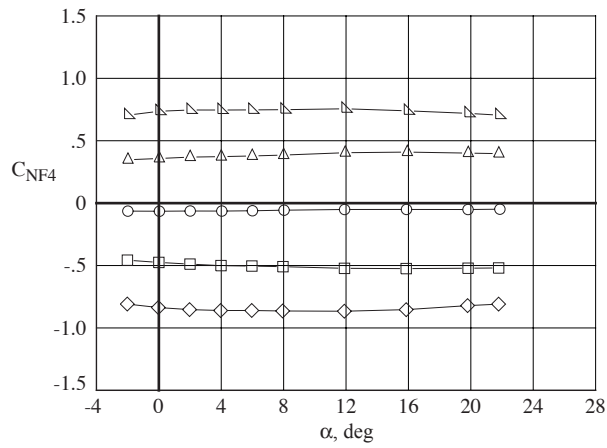
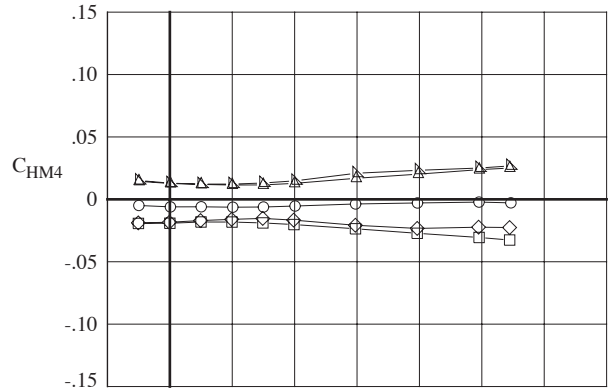


Run	Config	Mach	ϕ	δ_1	δ_2	δ_3	δ_4	$\delta_p/\delta_Y/\delta_R$
○ 1112	SN-LS-T	1.19	-90.0	0.0	0.0	0.0	0.0	0/0/0
□ 1120	SN-LS-T	1.19	-90.0	0.0	-10.0	0.0	10.0	0/10/0
◇ 1123	SN-LS-T	1.19	-90.0	0.0	-20.0	0.0	20.0	0/20/0
△ 1114	SN-LS-T	1.18	-90.0	0.0	10.0	0.0	-10.0	0/-10/0
▽ 1117	SN-LS-T	1.18	-90.0	0.0	20.0	0.0	-20.0	0/-20/0

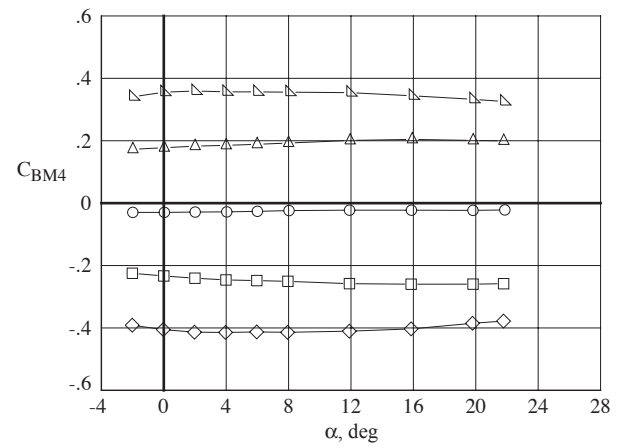


(e) Tail fin 3 loads.

Figure 27. Continued.

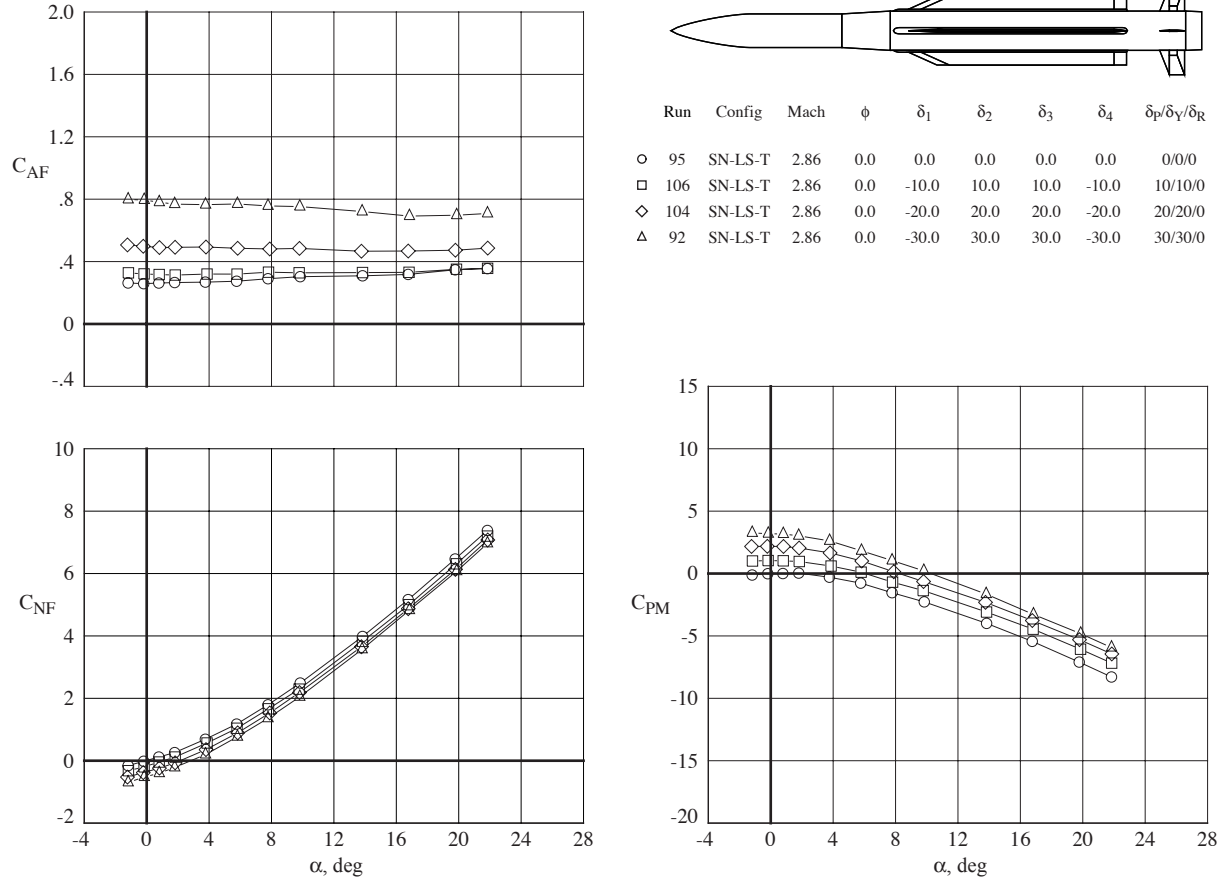


Run	Config	Mach	ϕ	δ ₁	δ ₂	δ ₃	δ ₄	δ _P /δ _Y /δ _R
○ 1112	SN-LS-T	1.19	-90.0	0.0	0.0	0.0	0.0	0/0/0
□ 1120	SN-LS-T	1.19	-90.0	0.0	-10.0	0.0	10.0	0/10/0
◇ 1123	SN-LS-T	1.19	-90.0	0.0	-20.0	0.0	20.0	0/20/0
△ 1114	SN-LS-T	1.18	-90.0	0.0	10.0	0.0	-10.0	0/-10/0
▽ 1117	SN-LS-T	1.18	-90.0	0.0	20.0	0.0	-20.0	0/-20/0



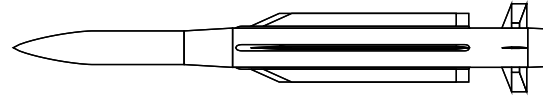
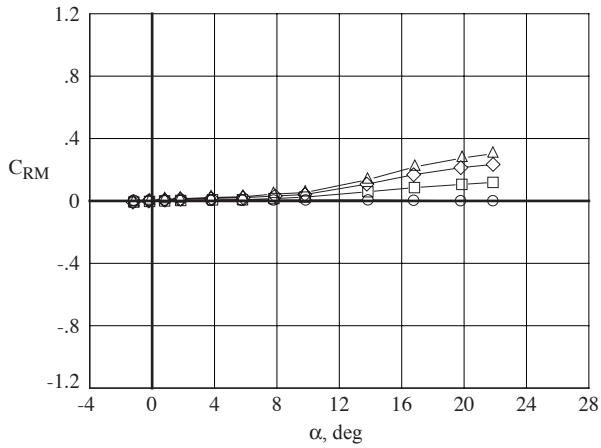
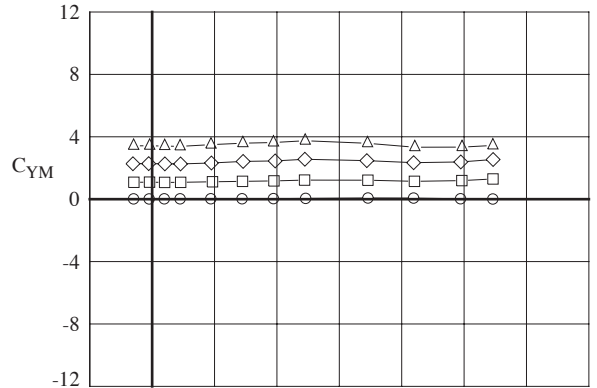
(f) Tail fin 4 loads.

Figure 27. Concluded.

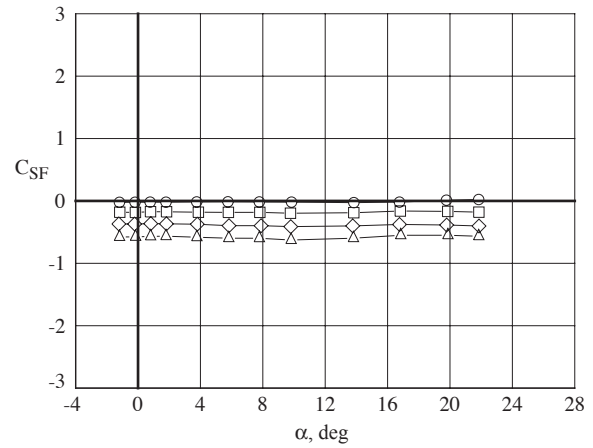


(a) Configuration longitudinal loads.

Figure 28. Effects of pitch-yaw control deflections.

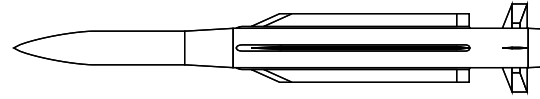
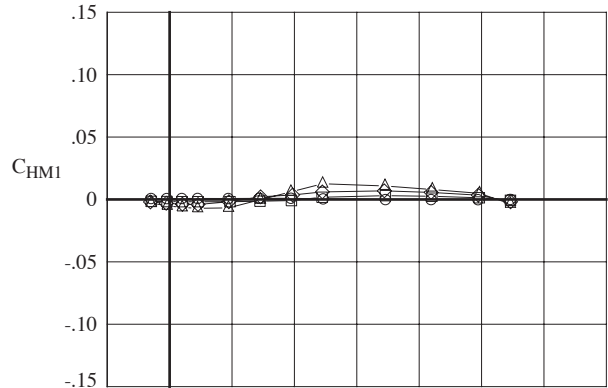


Run	Config	Mach	ϕ	δ_1	δ_2	δ_3	δ_4	$\delta_p/\delta_Y/\delta_R$
95	SN-LS-T	2.86	0.0	0.0	0.0	0.0	0.0	0/0/0
106	SN-LS-T	2.86	0.0	-10.0	10.0	10.0	-10.0	10/10/0
104	SN-LS-T	2.86	0.0	-20.0	20.0	20.0	-20.0	20/20/0
92	SN-LS-T	2.86	0.0	-30.0	30.0	30.0	-30.0	30/30/0

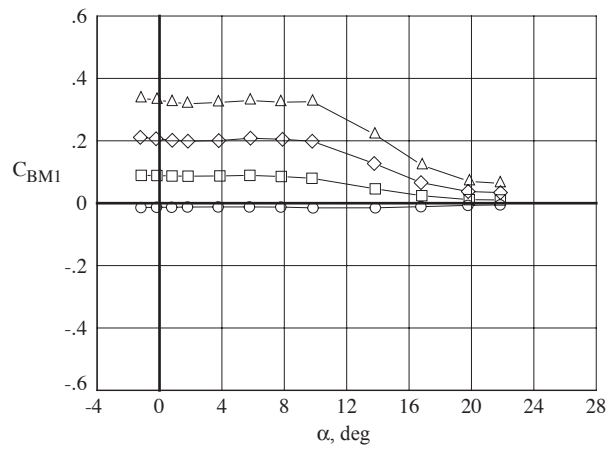
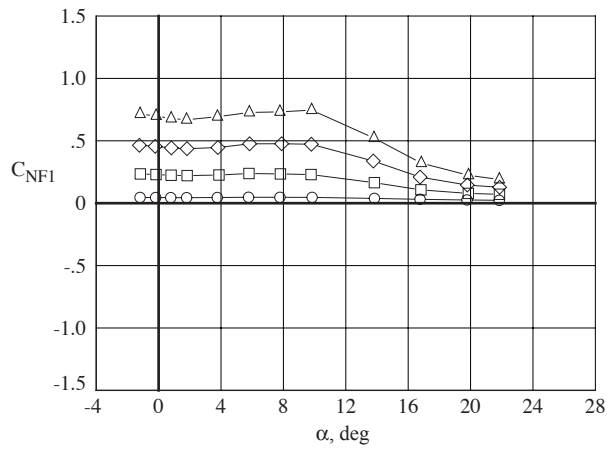


(b) Configuration lateral-directional loads.

Figure 28. Continued.

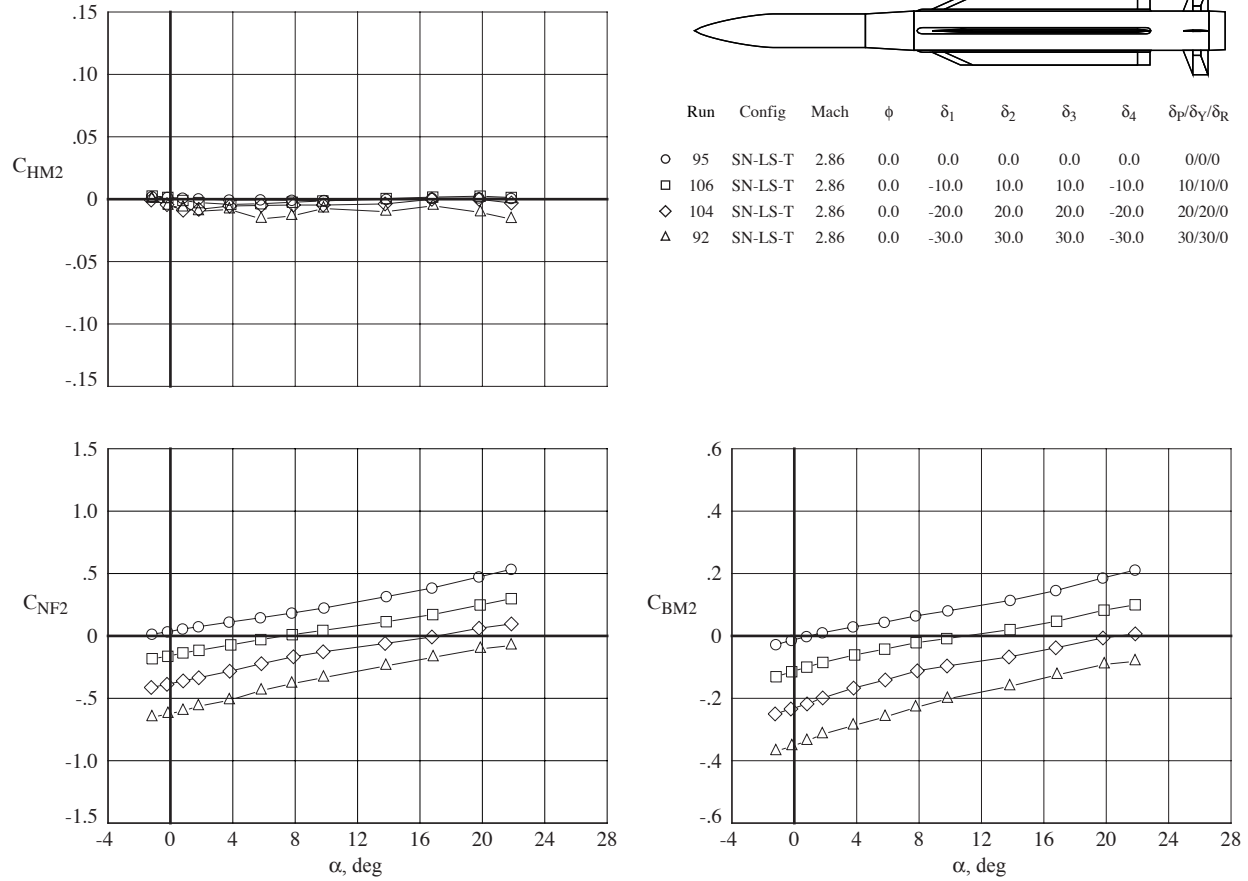


Run	Config	Mach	ϕ	δ_1	δ_2	δ_3	δ_4	$\delta_P/\delta_Y/\delta_R$
○ 95	SN-LS-T	2.86	0.0	0.0	0.0	0.0	0.0	0/0/0
□ 106	SN-LS-T	2.86	0.0	-10.0	10.0	10.0	-10.0	10/10/0
◇ 104	SN-LS-T	2.86	0.0	-20.0	20.0	20.0	-20.0	20/20/0
△ 92	SN-LS-T	2.86	0.0	-30.0	30.0	30.0	-30.0	30/30/0



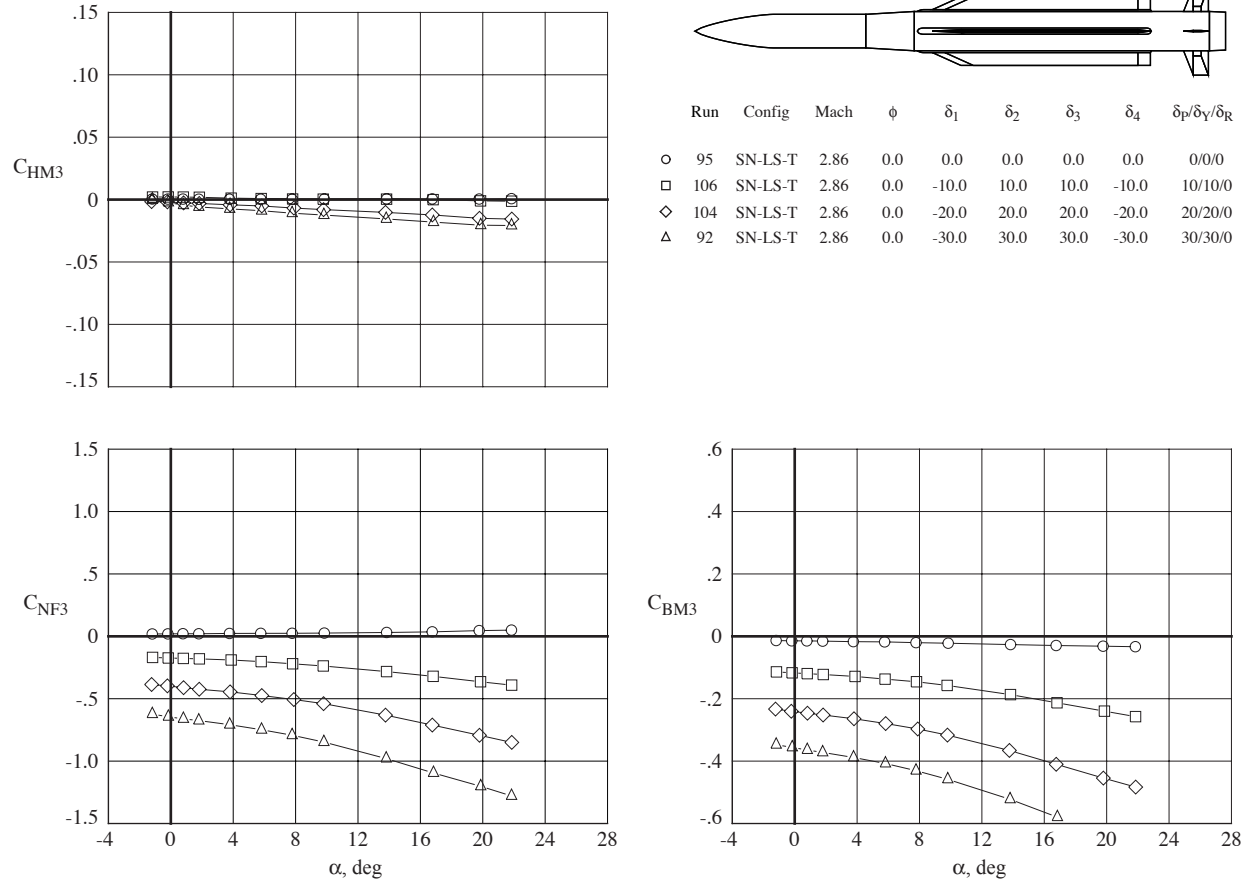
(c) Tail fin 1 loads.

Figure 28. Continued.



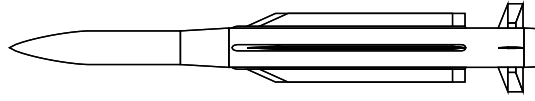
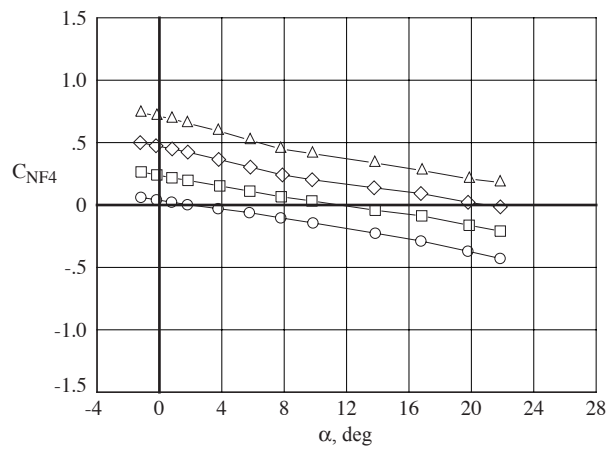
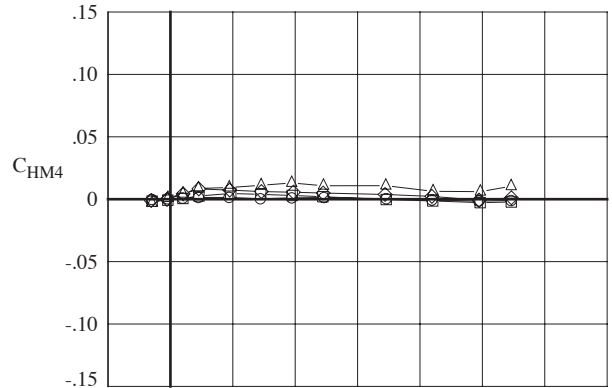
(d) Tail fin 2 loads.

Figure 28. Continued.

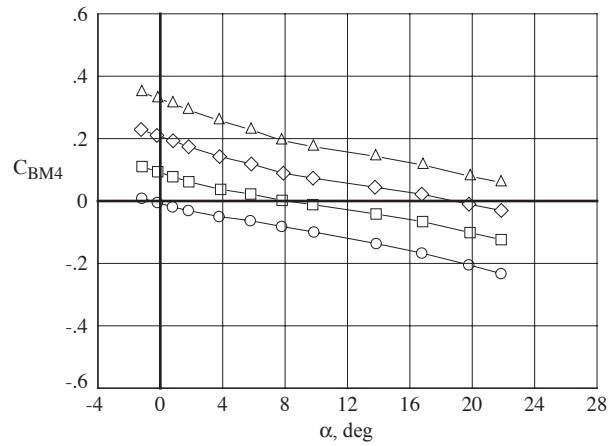


(e) Tail fin 3 loads.

Figure 28. Continued.

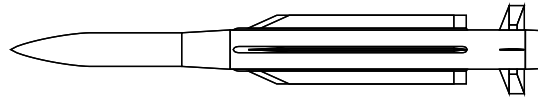
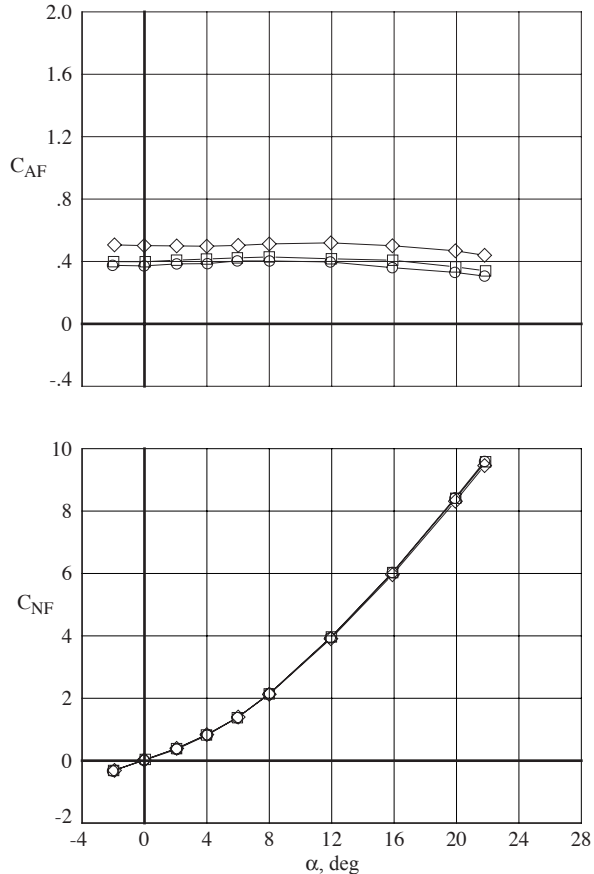


Run	Config	Mach	ϕ	δ_1	δ_2	δ_3	δ_4	$\delta_p/\delta_Y/\delta_R$
○ 95	SN-LS-T	2.86	0.0	0.0	0.0	0.0	0.0	0/0/0
□ 106	SN-LS-T	2.86	0.0	-10.0	10.0	10.0	-10.0	10/10/0
◇ 104	SN-LS-T	2.86	0.0	-20.0	20.0	20.0	-20.0	20/20/0
△ 92	SN-LS-T	2.86	0.0	-30.0	30.0	30.0	-30.0	30/30/0

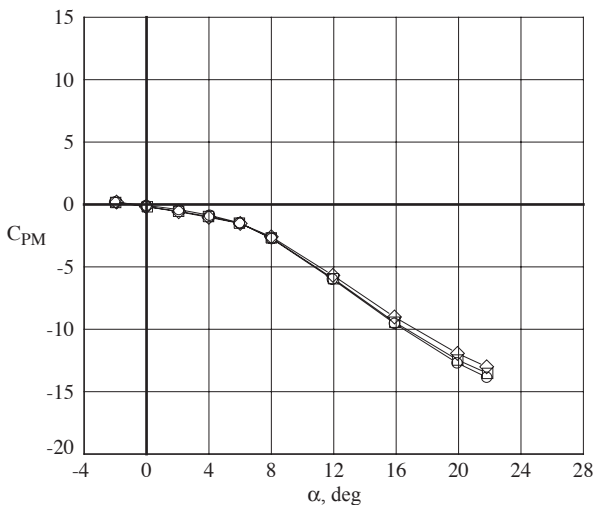


(f) Tail fin 4 loads.

Figure 28. Concluded.

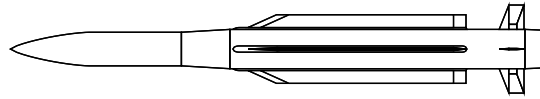
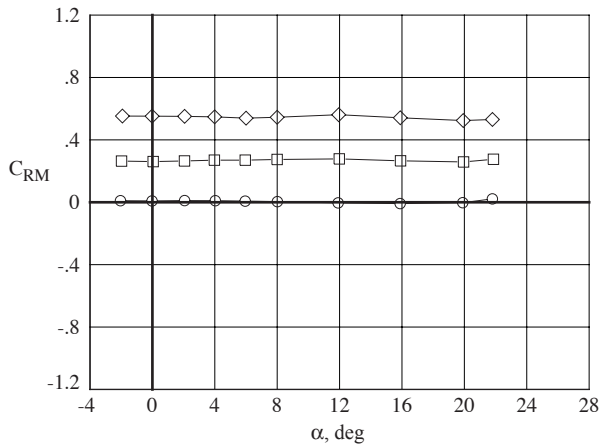
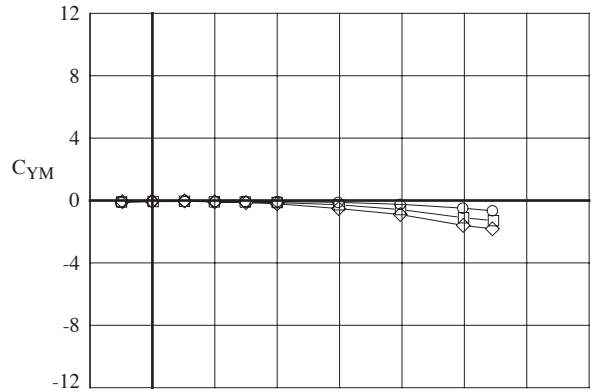


Run	Config	Mach	ϕ	δ_1	δ_2	δ_3	δ_4	$\delta_p/\delta_Y/\delta_R$
1005	SN-LS-T	1.18	0.0	0.0	0.0	0.0	0.0	0/0/0
1006	SN-LS-T	1.18	0.0	5.0	5.0	5.0	5.0	0/0/5
1015	SN-LS-T	1.19	0.0	10.0	10.0	10.0	10.0	0/0/10

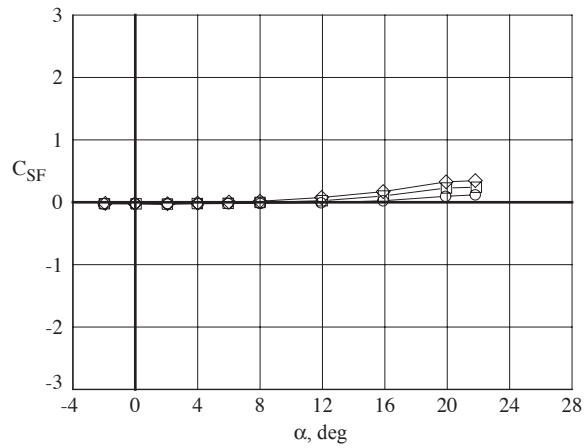


(a) Configuration longitudinal loads.

Figure 29. Effects of roll control deflections.

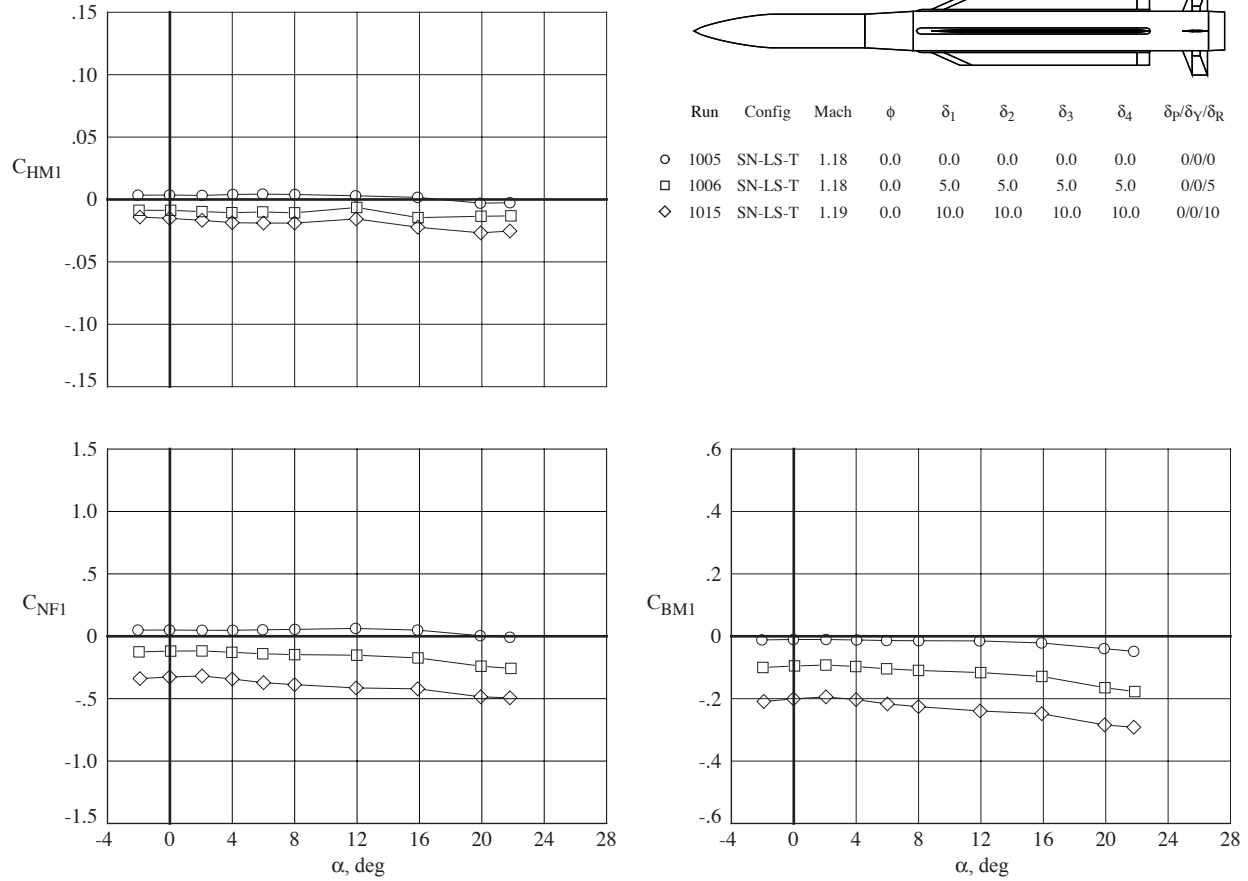


Run	Config	Mach	ϕ	δ_1	δ_2	δ_3	δ_4	$\delta_p/\delta_Y/\delta_R$
1005	SN-LS-T	1.18	0.0	0.0	0.0	0.0	0.0	0/0/0
1006	SN-LS-T	1.18	0.0	5.0	5.0	5.0	5.0	0/0/5
1015	SN-LS-T	1.19	0.0	10.0	10.0	10.0	10.0	0/0/10



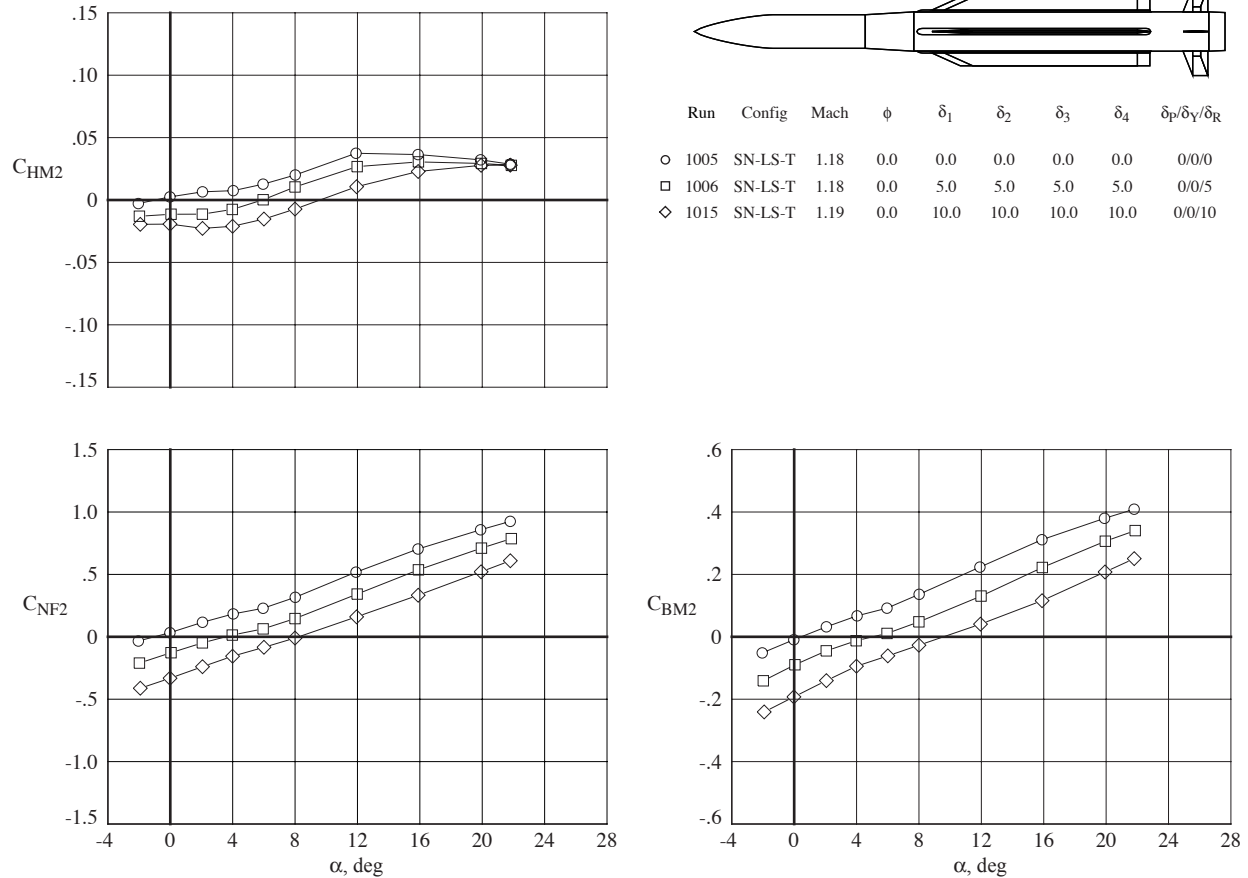
(b) Configuration lateral-directional loads.

Figure 29. Continued.



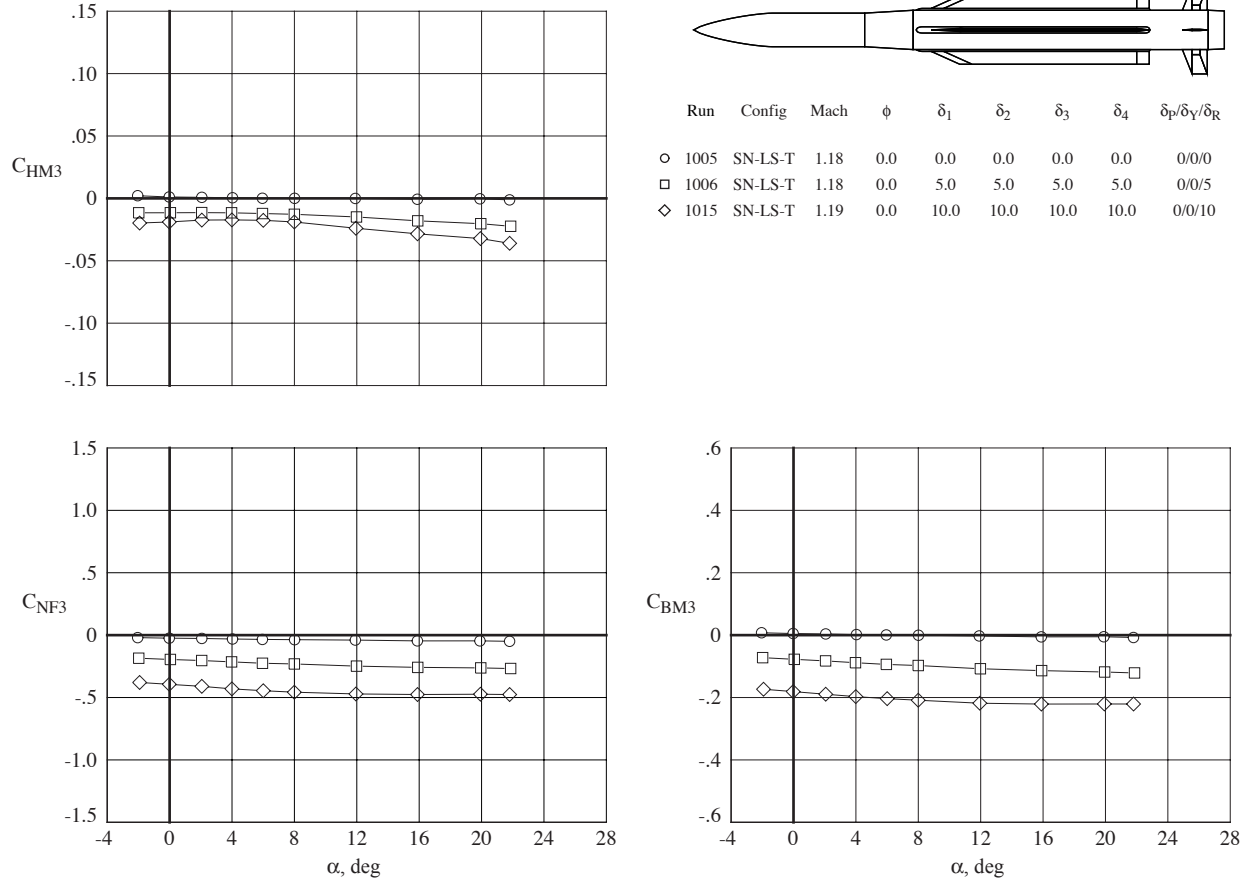
(c) Tail fin 1 loads.

Figure 29. Continued.



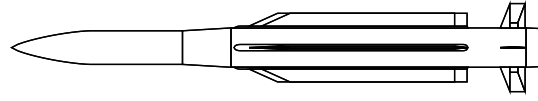
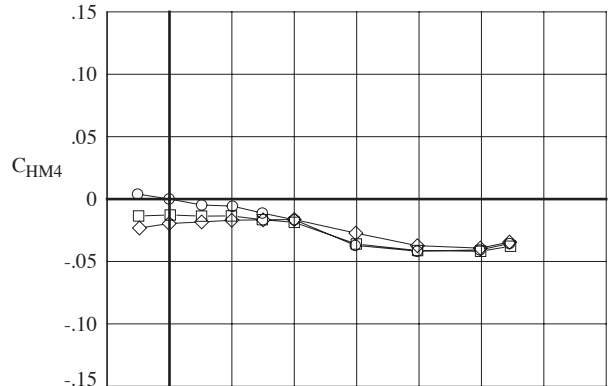
(d) Tail fin 2 loads.

Figure 29. Continued.

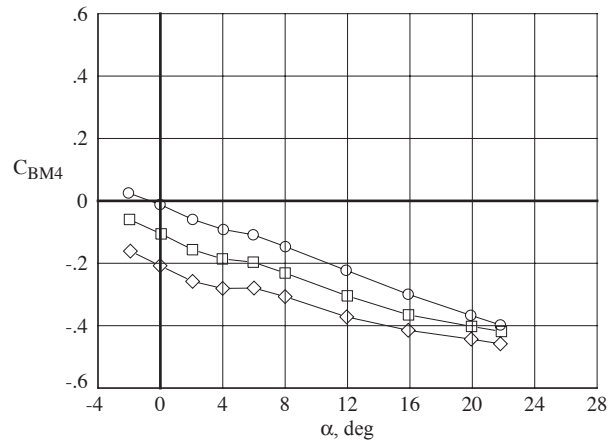
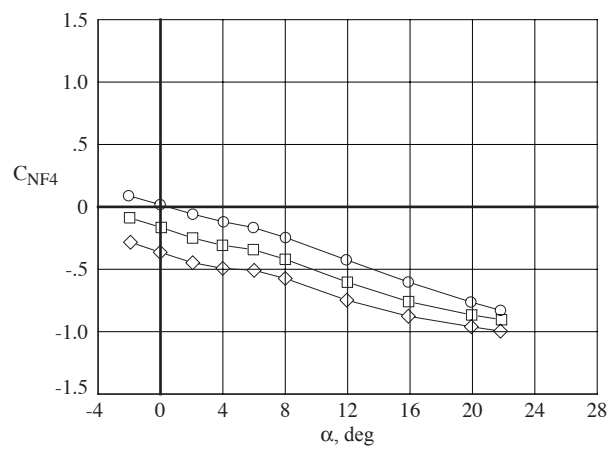


(e) Tail fin 3 loads.

Figure 29. Continued

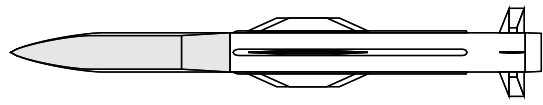
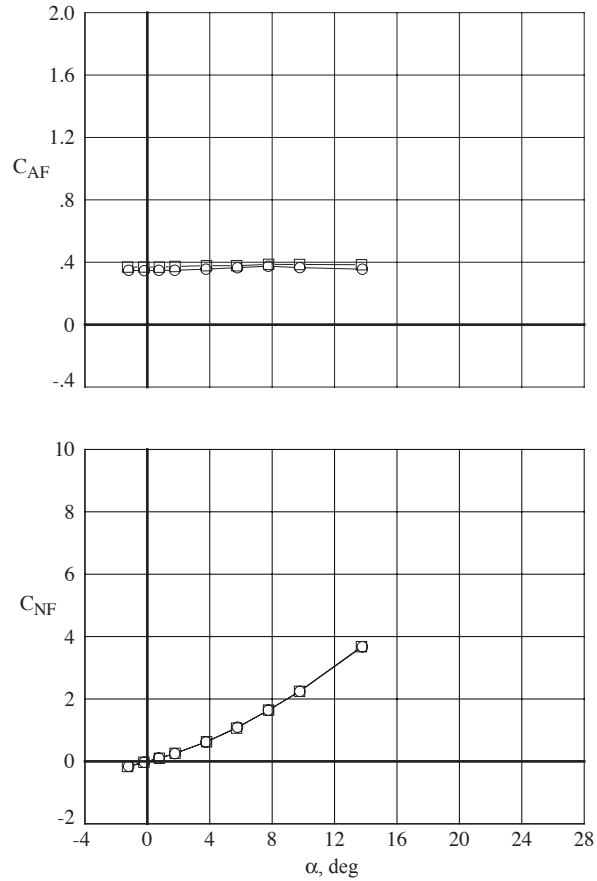


Run	Config	Mach	ϕ	δ_1	δ_2	δ_3	δ_4	$\delta_P/\delta_Y/\delta_R$
1005	SN-LS-T	1.18	0.0	0.0	0.0	0.0	0.0	0/0/0
1006	SN-LS-T	1.18	0.0	5.0	5.0	5.0	5.0	0/0/5
1015	SN-LS-T	1.19	0.0	10.0	10.0	10.0	10.0	0/0/10

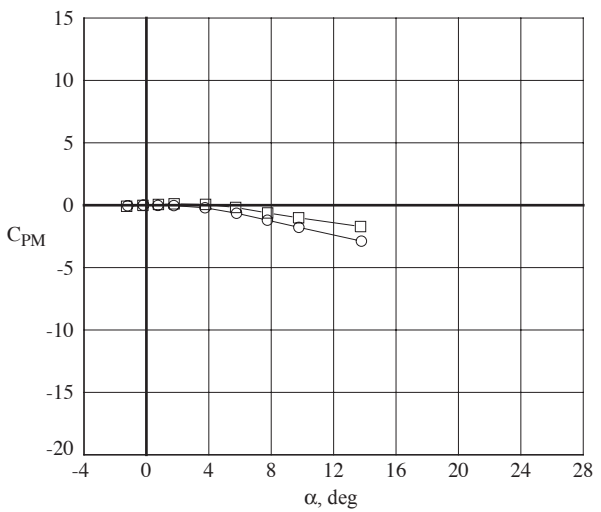


(f) Tail fin 4 loads.

Figure 29. Concluded.

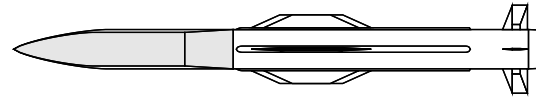
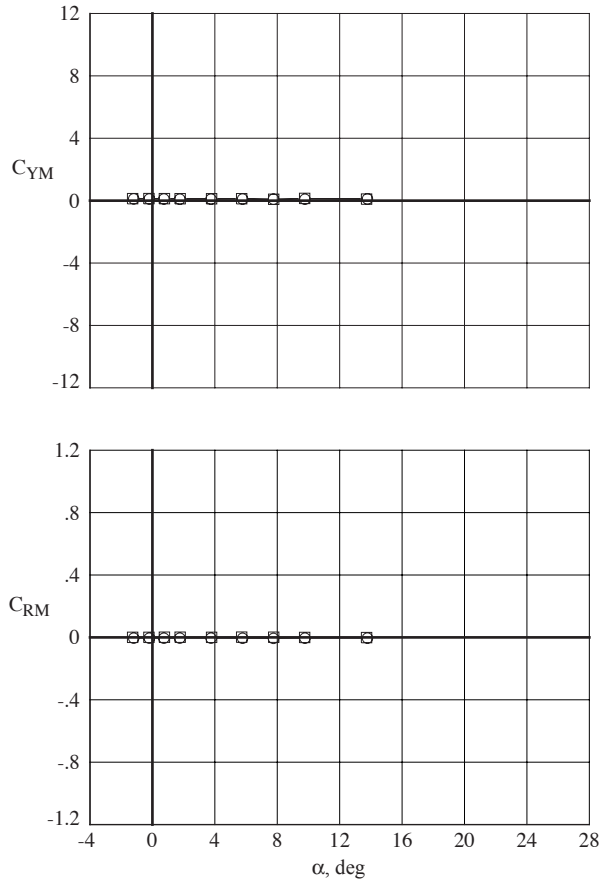


Run	Config	Mach	ϕ	δ_1	δ_2	δ_3	δ_4	$\delta_P/\delta_Y/\delta_R$
○ 585	SN-SS-T	1.70	0.0	0.0	0.0	0.0	0.0	0/0/0
□ 713	LN-SS-T	1.75	0.0	0.0	0.0	0.0	0.0	0/0/0

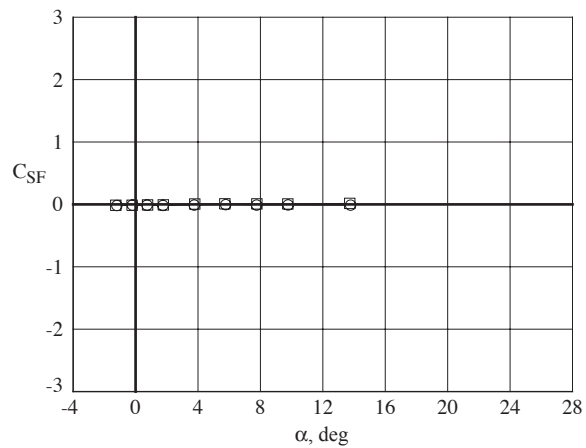


(a) Configuration longitudinal loads.

Figure 30. Effects of nose size.

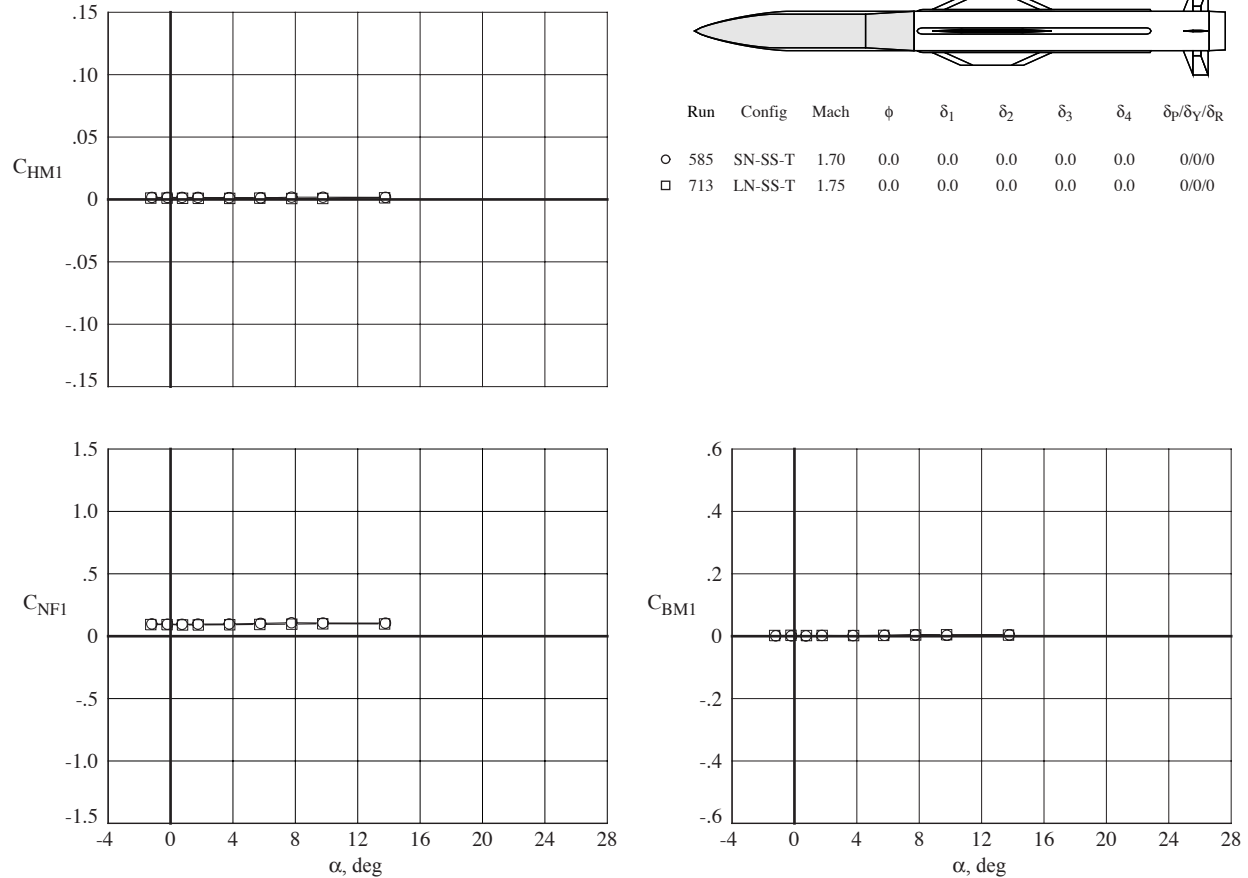


Run	Config	Mach	ϕ	δ_1	δ_2	δ_3	δ_4	$\delta_p/\delta_Y/\delta_R$
585	SN-SS-T	1.70	0.0	0.0	0.0	0.0	0.0	0/0/0
713	LN-SS-T	1.75	0.0	0.0	0.0	0.0	0.0	0/0/0



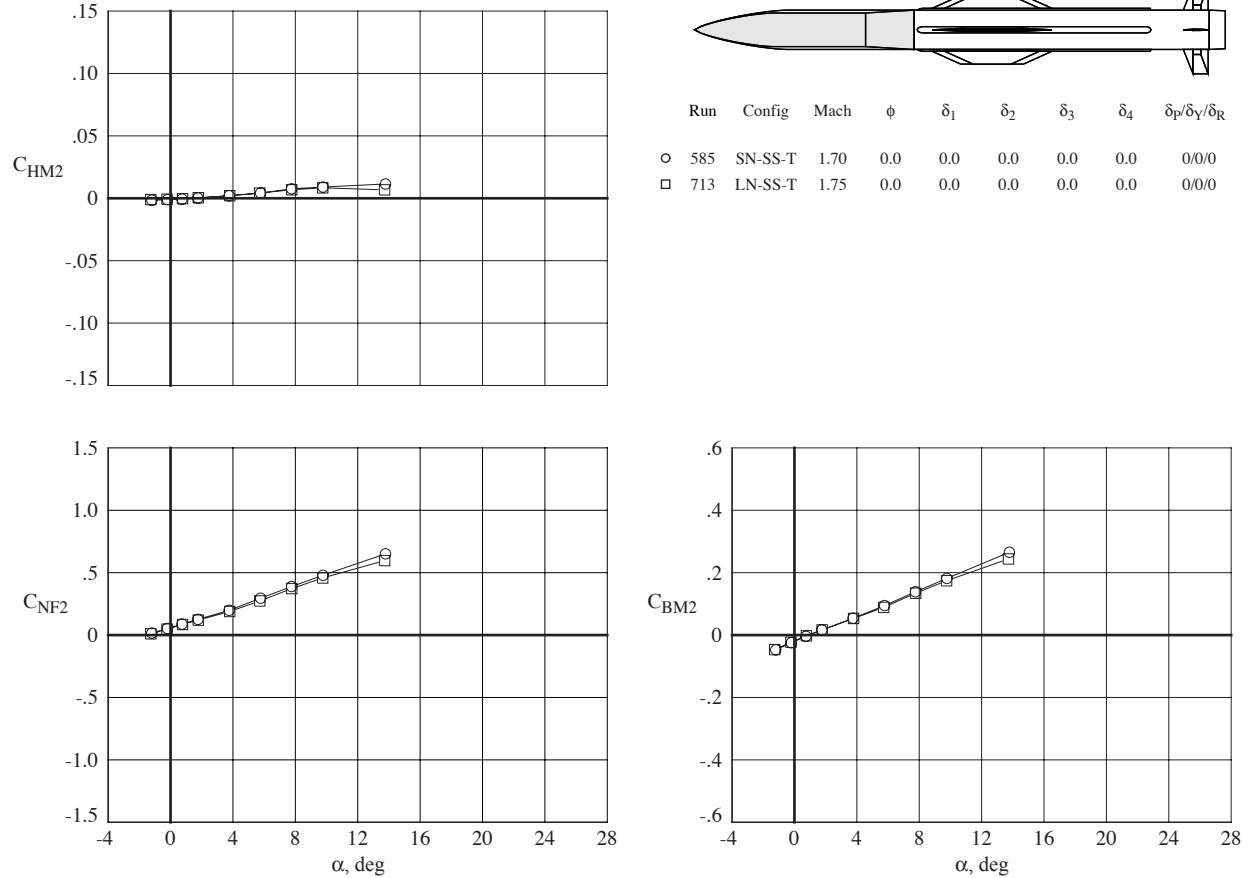
(b) Configuration lateral-directional loads.

Figure 30. Continued.



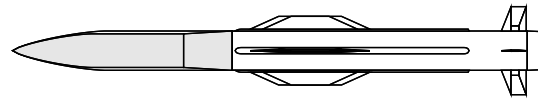
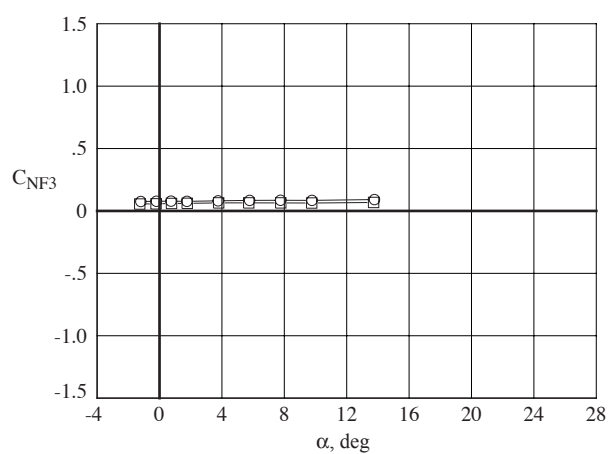
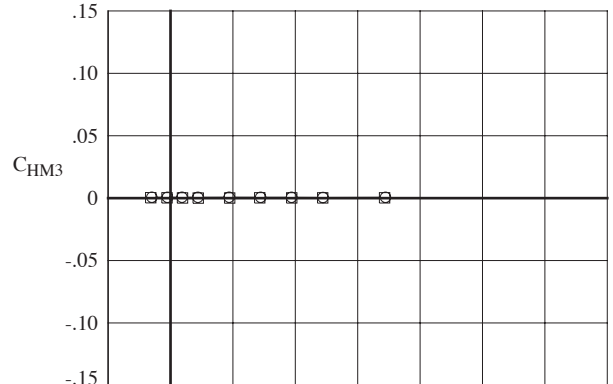
(c) Tail fin 1 loads.

Figure 30. Continued.

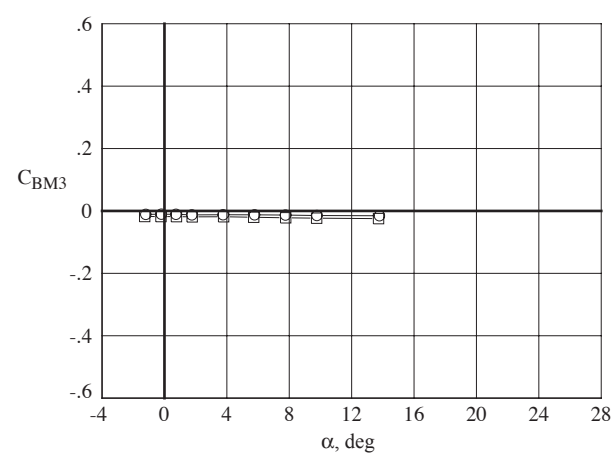


(d) Tail fin 2 loads.

Figure 30. Continued.

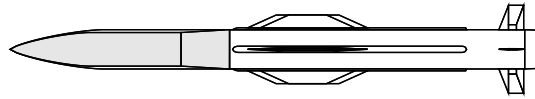
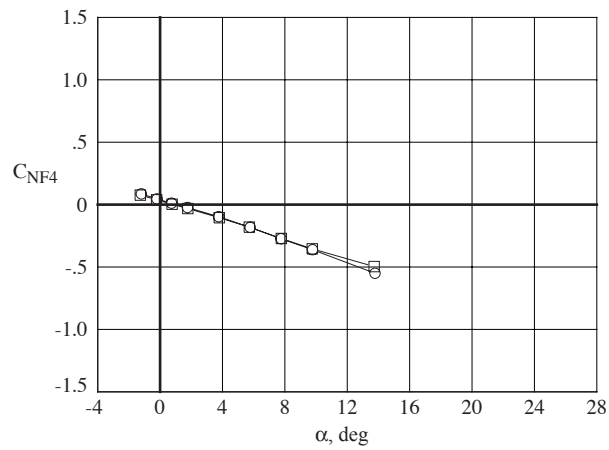
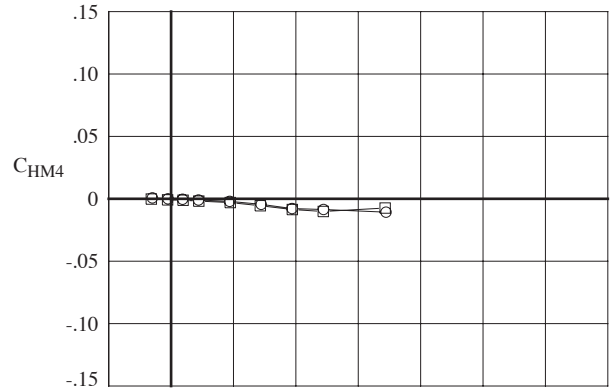


Run	Config	Mach	ϕ	δ_1	δ_2	δ_3	δ_4	$\delta_P/\delta_Y/\delta_R$
○ 585	SN-SS-T	1.70	0.0	0.0	0.0	0.0	0.0	0/0/0
□ 713	LN-SS-T	1.75	0.0	0.0	0.0	0.0	0.0	0/0/0

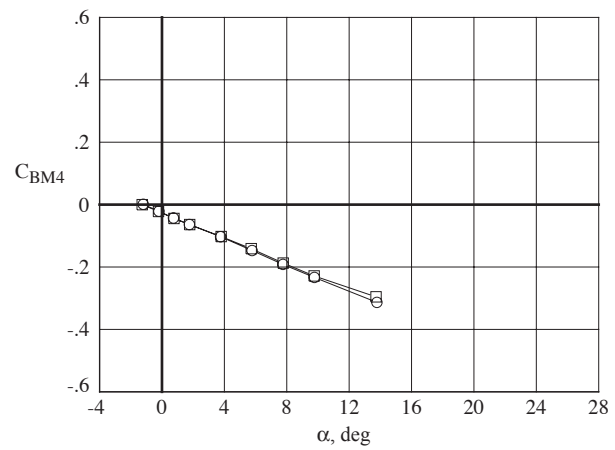


(e) Tail fin 3 loads.

Figure 30. Continued.



Run	Config	Mach	ϕ	δ ₁	δ ₂	δ ₃	δ ₄	δ _P /δ _Y /δ _R
○ 585	SN-SS-T	1.70	0.0	0.0	0.0	0.0	0.0	0/0/0
□ 713	LN-SS-T	1.75	0.0	0.0	0.0	0.0	0.0	0/0/0



(f) Tail fin 4 loads.

Figure 30. Concluded.

REPORT DOCUMENTATION PAGE				Form Approved OMB No. 0704-0188	
<p>The public reporting burden for this collection of information is estimated to average 1 hour per response, including the time for reviewing instructions, searching existing data sources, gathering and maintaining the data needed, and completing and reviewing the collection of information. Send comments regarding this burden estimate or any other aspect of this collection of information, including suggestions for reducing this burden, to Department of Defense, Washington Headquarters Services, Directorate for Information Operations and Reports (0704-0188), 1215 Jefferson Davis Highway, Suite 1204, Arlington, VA 22202-4302. Respondents should be aware that notwithstanding any other provision of law, no person shall be subject to any penalty for failing to comply with a collection of information if it does not display a currently valid OMB control number.</p> <p>PLEASE DO NOT RETURN YOUR FORM TO THE ABOVE ADDRESS.</p>					
1. REPORT DATE (DD-MM-YYYY)	2. REPORT TYPE			3. DATES COVERED (From - To)	
01-03-2005	Technical Memorandum				
4. TITLE AND SUBTITLE			5a. CONTRACT NUMBER		
Aerodynamics of an Axisymmetric Missile Concept Having Cruciform Strakes and In-Line Tail Fins From Mach 0.60 to 4.63			5b. GRANT NUMBER		
			5c. PROGRAM ELEMENT NUMBER		
6. AUTHOR(S)			5d. PROJECT NUMBER		
Allen, Jerry M.			5e. TASK NUMBER		
			5f. WORK UNIT NUMBER		
			23-090-20-35		
7. PERFORMING ORGANIZATION NAME(S) AND ADDRESS(ES)				8. PERFORMING ORGANIZATION REPORT NUMBER	
NASA Langley Research Center Hampton, VA 23681-2199				L-19027	
9. SPONSORING/MONITORING AGENCY NAME(S) AND ADDRESS(ES)				10. SPONSOR/MONITOR'S ACRONYM(S)	
National Aeronautics and Space Administration Washington, DC 20546-0001				NASA	
				11. SPONSOR/MONITOR'S REPORT NUMBER(S)	
				NASA/TM-2005-213541	
12. DISTRIBUTION/AVAILABILITY STATEMENT					
Unclassified - Unlimited Subject Category 02 Availability: NASA CASI (301) 621-0390					
13. SUPPLEMENTARY NOTES Allen, Langley Research Center, Hampton, VA. An electronic version can be found at http://ntrs.nasa.gov A CD-ROM supplement for TM-2005-213541 is available upon request.					
14. ABSTRACT					
An experimental study has been performed to develop a large force and moment aerodynamic data set on a slender axisymmetric missile configuration having cruciform strakes and in-line control tail fins. The data include six-component balance measurements of the configuration aerodynamics and three-component measurements on all four tail fins. The test variables include angle of attack, roll angle, Mach number, model buildup, stike length, nose size, and tail fin deflection angles to provide pitch, yaw, and roll control. Test Mach numbers ranged from 0.60 to 4.63. The entire data set is presented on a CD-ROM that is attached to this paper. The CD-ROM also includes extensive plots of both the six-component configuration data and the three-component tail fin data. Selected samples of these plots are presented in this paper to illustrate the features of the data and to investigate the effects of the test variables.					
15. SUBJECT TERMS Experimental aerodynamics; Missile control fins; Wind tunnel tests; Subsonic/Transonic; Supersonic					
16. SECURITY CLASSIFICATION OF:			17. LIMITATION OF ABSTRACT	18. NUMBER OF PAGES	19a. NAME OF RESPONSIBLE PERSON STI Help Desk (email: help@sti.nasa.gov)
a. REPORT	b. ABSTRACT	c. THIS PAGE	UU	115	19b. TELEPHONE NUMBER (Include area code) (301) 621-0390
U	U	U			